PACIFIC EARTHQUAKE ENGINEERING RESEARCH CENTER

Analytical and Experimental Study of Fiber-Reinforced Strip Isolators

James M. Kelly

and

Shakhzod M. Takhirov
Department of Civil and Environmental Engineering
University of California, Berkeley

PEER 2002/11
SEPTEMBER 2002

Analytical and Experimental Study of Fiber-Reinforced Strip Isolators

James M. Kelly
Professor Emeritus
Department of Civil and Environmental Engineering
University of California, Berkeley

and

Shakhzod M. Takhirov
Senior Development Engineer
Earthquake Engineering Research Center
University of California, Berkeley

PEER Report 2002/11
Pacific Earthquake Engineering Research Center
College of Engineering
University of California, Berkeley

September 2002

ABSTRACT

This report describes an experimental and theoretical study of the feasibility of using fiber reinforcement to produce lightweight, low-cost elastomeric isolators for application to housing, schools, and other public buildings in highly seismic areas of the developing world. The theoretical analysis covers the mechanical characteristics of multi-layer elastomeric isolation bearings in which the reinforcing elements, normally steel plates, are replaced by a fiber reinforcement. The fiber in the fiber-reinforced isolator, in contrast to the steel in the conventional isolator (which is assumed to be rigid both in extension and flexure), is assumed to be flexible in extension, but completely without flexure rigidity. The theoretical analysis on which the design of steel-reinforced isolators is based is then extended to accommodate the stretching of the fiber-reinforcement. Several examples of isolators in the form of long strips were made by Dongil Rubber Belt Company Ltd., of Pusan, Korea, and tested in the Structural Research Laboratory of the Earthquake Engineering Research Center, University of California, Berkeley. The tested isolators had significantly large shape factors, which for conventional isolators require accounting for the effects of material compressibility. The theoretical analysis is then extended to include compressibility, and the competing influences of reinforcement flexibility and compressibility are studied.

The theoretical analysis suggests, and the test results confirm, that it is possible to produce a fiber-reinforced strip isolator that matches the behavior of a steel-reinforced isolator. Furthermore, the fiber-reinforced isolator is significantly lighter and can be made by a much less labor-intensive manufacturing process. The advantage of the strip isolator is that it can easily be used in buildings with masonry walls. The intention of this research is to provide a low-cost lightweight isolation system for housing and public buildings in the developing countries.

ACKNOWLEDGMENTS

The sample isolators were made by Dongil Rubber Belt Company Ltd. of Pusan, Korea. The test program was conducted at the Structural Research Laboratory of the University of California, Berkeley, Richmond Field Station. This research work was partly supported by the Engineering Research Center for Met-Shape and Die Manufacturing of Pusan National University, Pusan, Korea, which are gratefully acknowledged.

CONTENTS

LIST OF FIGURES

LIST OF TABLES

1 Introduction

The recent earthquakes in India, Turkey, and South America have again demonstrated that major loss of life in earthquakes happens primarily in developing countries. Even in relatively moderate earthquakes many people are killed as the result of substandard construction, most typically by the collapse of brittle, heavy unreinforced masonry or poorly constructed concrete buildings. In these countries, many modern technologies, such as structural control technologies and energy-dissipation devices, can do little to alleviate this. Seismic isolation technology, however, may be an exception that is adaptable to poor construction and therefore a means for developing countries to improve the seismic resistance of buildings, particularly schools and hospitals.

The theoretical basis of seismic isolation shows that the reduction of seismic loading produced by the isolation systems depends primarily on the ratio of the isolation period to the fixed-base period. Since the fixed-base period of a masonry block or brick building may be of the order of 1/10 sec an isolation period of 1 sec or longer would provide a significant reduction in the seismic loads on the building and would not require a large isolation displacement. For example, the current UBC code for seismic isolation [1997] has a formula for minimum isolator displacement which, for a 1.5 sec system, would be around 15 cm (6 in.).

The problem with adapting isolation to developing countries is that conventional isolators are large, expensive, and heavy. An individual isolator can weight one ton or more. To extend this valuable earthquake-resistant strategy to housing and other public buildings, it is necessary to reduce the cost and weight of the isolators.

The primary weight in an isolator is due to the steel reinforcing plates, which are used to provide the vertical stiffness of the rubber-steel composite element. A typical rubber isolator has two large end-plates (25 mm) and 20 thin reinforcing plates (3 mm). The high cost of producing the isolators results from the labor involved in preparing the steel plates and laying-up of the rubber sheets and steel plates for vulcanization bonding in a mold. The steel plates are cut, sandblasted, acid cleaned, and then coated with bonding compound. Next, the compounded rubber sheets with the interleaved steel plates are put into a mold and heated under pressure for several hours to complete the manufacturing process. The purpose of this research is to suggest that both the weight and the cost of isolators can be reduced by eliminating the steel reinforcing plates and replacing them with a fiber reinforcement.

The weight reduction is possible because fiber materials are available with an elastic stiffness that is of the same order as steel. Thus the reinforcement needed to provide the vertical stiffness may be obtained by using a similar volume of very much lighter material. The cost savings may be possible if the use of fiber allows a simpler, less labor-intensive manufacturing process.

Another benefit to using fiber reinforcement is that it would then be possible to build isolators in long rectangular strips, whereby individual isolators could be cut to the required size. All isolators are currently manufactured as either circular or square. Rectangular isolators in the form of long strips would have distinct advantages over square or circular isolators when applied to buildings where the lateral resisting system is walls. When isolation is applied to buildings with structural walls, additional wall beams are needed to carry the wall from isolator to isolator. A strip isolator would have a distinct advantage for retrofitting masonry structures and for isolating residential housing constructed from concrete or masonry blocks.

To calculate the vertical stiffness of a steel-reinforced bearing, an approximate analysis is used that assumes that each individual pad in the bearing deforms in such **a** way that horizontal planes remain horizontal and points on a vertical line lie on a parabola after loading. The plates are assumed to constrain the displacement at the top and bottom of the pad. Linear elastic behavior with incompressibility is assumed, with the additional assumption that the normal stress components are approximated by the pressure. This leads to the well-known “pressure solution,” which is generally accepted as an adequate approximate approach for calculating the vertical stiffness. It will be shown that the extensional flexibility of the fiber reinforcement can be incorporated into this approach, and that predictions of the resulting vertical stiffness can be made.

The theoretical analysis of the fiber-reinforced isolator has been supplemented by experimental work at the EERC laboratory. A number of carbon fiber-reinforced rubber strip isolators were obtained and tested on a small isolator test machine. The tests show that the concept is viable. The vertical and horizontal stiffnesses of the strip isolator are less than that for the equivalent steel reinforced isolator but are still adequate and easy to cut with a standard saw, in contrast to steel-reinforced isolators, which are difficult to cut and need special saws. Additionally, the fiber-reinforced strips are light and can be placed without the use of lifting equipment.

Much recent discussion has focused on “smart” rubber bearings and “intelligent” base isolation systems as the new thrust in seismic isolation research. While there may be a role for these adaptive systems for large expensive buildings in advanced economies, the development of lightweight, low-cost isolators is crucial if this method of seismic protection is to be applied to a wide range of buildings, such as housing, schools, and medical centers, in earthquake-prone areas of the world.

2 Vertical Stiffness of Fiber-Reinforced Bearings

The essential characteristic of the elastomeric isolator is the very large ratio of the vertical stiffness relative to the horizontal stiffness. This is produced by the reinforcing plates, which in current industry standard are thin steel plates. These plates prevent lateral bulging of the rubber, but allow the rubber to shear freely. The vertical stiffness can be several hundred times the horizontal stiffness. The steel reinforcement has a similar effect on the resistance of the isolator to bending moments, usually referred to as the "bending stiffness." This important design quantity makes the isolator stable against large vertical loads.

2.1 Compression of Pad with Rigid Reinforcement

Before developing the solution for the flexible reinforcement, it is useful to review the theory for the rigid reinforcement. A linear elastic theory is the most common method used to predict the compression and the bending stiffness of a thin elastomeric pad. The first analysis of the compression stiffness was done using an energy approach by Rocard [1937]; further developments were made by Gent and Lindley [1959] and Gent and Meinecke [1970]. The theory given here is a simplified version of these analyses and is applicable to bearings with shape factors greater than around five.

The analysis is an approximate one based on a number of assumptions. The kinematic assumptions are as follows:

(i) points on a vertical line before deformation lie on a parabola after loading; and

(ii) horizontal planes remain horizontal.

We consider an arbitrarily shaped pad of thickness, *t,* and locate a rectangular Cartesian coordinate system, (x, y, z), in the middle surface of the pad, as shown in Fig. 2-1a. Figure 2-1b shows the displacements, (u, v, w), in the coordinate directions under assumptions (i) and (ii):

$$
\begin{aligned}
u(x, y, z) &= u_0(x, y)\left(1 - \frac{4z^2}{t^2}\right) \\
v(x, y, z) &= v_0(x, y)\left(1 - \frac{4z^2}{t^2}\right) \\
w(x, y, z) &= w(z)\ .
\end{aligned}
\tag{2.1}
$$

This displacement field satisfies the constraint that the top and bottom surfaces of the pad are bonded to rigid substrates. The assumption of incompressibility produces a further constraint on the three components of strain, $\varepsilon_{xx}, \varepsilon_{yy}, \varepsilon_{zz}$, in the form

$$\varepsilon_{xx} + \varepsilon_{yy} + \varepsilon_{zz} = 0 \tag{2.2}$$

and this leads to

$$(u_{0,x} + v_{0,y})\left(1 - \frac{4z^2}{t^2}\right) + w_{,z} = 0$$

where the commas imply partial differentiation with respect to the indicated coordinate. When integrated through the thickness this gives

$$u_{0,x} + v_{0,y} = \frac{3\Delta}{2t} \tag{2.3}$$

where the change of thickness of the pad is Δ ($\Delta > 0$ in compression).

The stress state is assumed to be dominated by the internal pressure, p, such that the normal stress components, $\tau_{xx}, \tau_{yy}, \tau_{zz}$, differ from $-p$ only by terms of order $(t^2/l^2)p$, i.e.,

$$\tau_{xx} \approx \tau_{yy} \approx \tau_{zz} \approx -p\left[1 + O\left(\frac{t^2}{l^2}\right)\right]$$

where l is a typical dimension of the pad. The shear stress components, τ_{xz} and τ_{yz}, which are generated by the constraints at the top and bottom of the pad, are assumed to be of order $(t/l)p$;

the in-plane shear stress, τ_{xy}, is assumed to be of order $(t^2/l^2)p$.

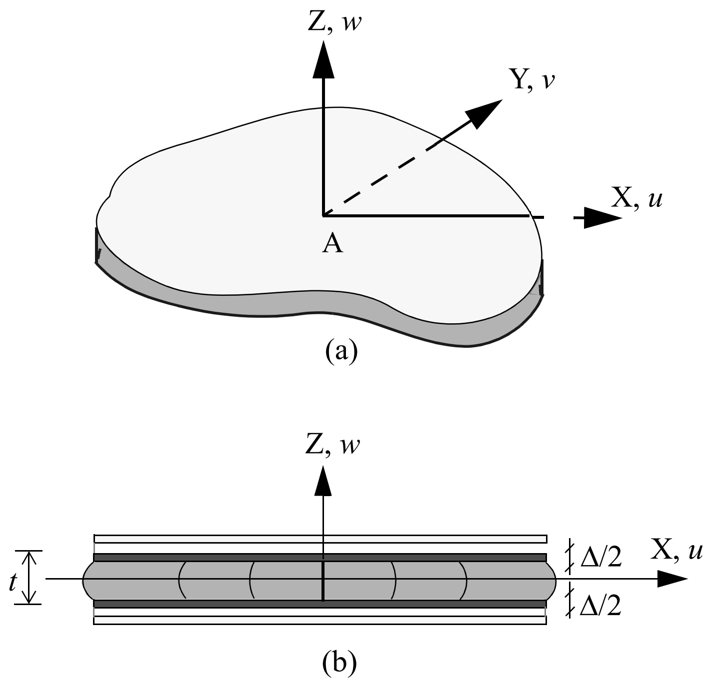

Figure 2-1 Constrained rubber pad and coordinate system

The equations of equilibrium for the stresses

$$
\begin{aligned}
\tau_{xx,x} + \tau_{xy,y} + \tau_{xz,z} &= 0 \\
\tau_{xy,x} + \tau_{yy,y} + \tau_{yz,z} &= 0 \\
\tau_{xz,x} + \tau_{yz,y} + \tau_{zz,z} &= 0
\end{aligned}
$$

reduce under these assumptions to

$$
\begin{aligned}
\tau_{xx,x} + \tau_{xz,z} &= 0 \\
\tau_{yy,y} + \tau_{yz,z} &= 0\ .
\end{aligned}
\tag{2.4}
$$

Assuming that the material is linearly elastic, the shear stresses τ_{xz} and τ_{yz} are related to the shear strains, γ_{xz} and γ_{yz}, by

$$\tau_{xz} = G\gamma_{xz} \qquad , \qquad \tau_{yz} = G\gamma_{yz}$$

with G being the shear modulus of the material; thus,

$$\tau_{xz} = -8Gu_0\frac{z}{t^2} \qquad , \qquad \tau_{yz} = -8Gv_0\frac{z}{t^2} \quad . \tag{2.5}$$

From the equilibrium equations, therefore,

$$\tau_{xx,x} = \frac{8Gu_0}{t^2} \qquad , \qquad \tau_{yy,y} = \frac{8Gv_0}{t^2} \tag{2.6}$$

which when inverted to give u_0, v_0 and inserted into the incompressibility condition Eq. (2.3) gives

$$\frac{t^2}{8G}(\tau_{xx,xx} + \tau_{yy,yy}) = \frac{3\Delta}{2t} \tag{2.7}$$

In turn, by identifying both τ_{xx} and τ_{yy} as $-p$, this reduces to

$$p_{,xx} + p_{,yy} = \nabla^2 p = -\frac{12G\Delta}{t^3} = -\frac{12G}{t^2}\varepsilon_c \tag{2.8}$$

where $\varepsilon_c = \Delta/t$ is the compression strain. The boundary condition, $p = 0$, on the perimeter, C, of the pad completes the system for $p(x, y)$.

The vertical stiffness of a rubber bearing is given by the formula

$$K_V = \frac{E_c A}{t_r}$$

where A is the area of the bearing, t_r is the total thickness of rubber in the bearing, and E_c is the instantaneous compression modulus of the rubber-steel composite under the specified level of vertical load. The value of E_c for a single rubber layer is controlled by the shape factor, S, defined as

$$S = \frac{\text{loaded area}}{\text{free area}}$$

which is a dimensionless measure of the aspect ratio of the single layer of the elastomer. For example, in an infinite strip of width 2*b*, and with a single layer thickness of *t*, $S = b/t$, and for a circular pad of diameter ϕ and thickness *t*,

$$S = \phi/(4t)$$

and for a square pad of side *a* and thickness *t*,

$$S = a/(4t)\ .$$

To determine the compression modulus, E_c, we solve Eq. (2.8) for *p* and integrate over *A* to determine the resultant normal load, *P*. E_c is then given by

$$E_c = \frac{P}{A\varepsilon_c}\ . \tag{2.9}$$

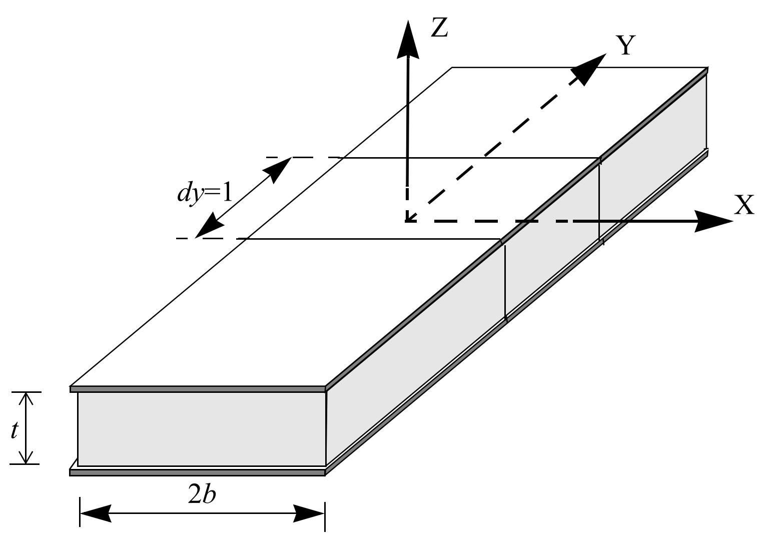

Figure 2-2   Infinitely long rectangular pad showing dimensions

For example, for an infinite strip of width $2b$ (see Fig. 2-2), Eq. (2.8) reduces to

$$\nabla^2 p = \frac{d^2 p}{dx^2} = -\frac{12G}{t^2}\varepsilon_c$$

which, with $p = 0$ at $x = \pm b$, gives

$$p = \frac{6G}{t^2}(b^2 - x^2)\varepsilon_c \ .$$

In this case the load per unit length of the strip, P, is given by

$$P = \int_{-b}^{b} p dx = \frac{8Gb^3}{t^2}\varepsilon_c \ .$$

Since the shape factor, $S = b/t$, and the area per unit length is $A = 2b$,

$$E_c = \frac{P}{A\varepsilon_c} = 4GS^2 \ . \tag{2.10}$$

2.2 Compression Stiffness with Flexible Reinforcement

Developing the solution for the compression of a pad with rigid reinforcement is algebraically simple enough to be treated in two dimensions and for an arbitrary shape. The problem for the pad with flexible reinforcement is more complicated, however; for simplicity, the derivation will be developed for a long, rectangular strip. As before, the rubber is assumed incompressible and the pressure is assumed to be the dominant stress component. The kinematic assumption of quadratically variable displacement is supplemented by an additional displacement that is constant through the thickness and is intended to accommodate the stretching of the reinforcement. Thus in this case of plain strain the displacement pattern is

$$\begin{aligned} u(x, z) &= u_0(x)\left(1 - \frac{4z^2}{t^2}\right) + u_1(x) \\ w(x, z) &= w(z) \ . \end{aligned} \tag{2.11}$$

The constraint of incompressibility means

$$\varepsilon_{xx} + \varepsilon_{zz} = 0$$

leading to

$$u_{0,x}\left(1 - \frac{4z^2}{t^2}\right) + u_{1,x} + w_{,z} = 0 .$$

Integration through the thickness with respect to z leads to

$$u_{0,x} + \frac{3}{2}u_{1,x} = \frac{3\Delta}{2t} \quad . \tag{2.12}$$

The only equation of stress equilibrium in this case is $\tau_{xx,x} + \tau_{xz,z} = 0$, and the assumption of elastic behavior means that

$$\tau_{xz} = G\gamma_{xz} \tag{2.13}$$

which with

$$\gamma_{xz} = -\frac{8z}{t^2}u_0 \tag{2.14}$$

from Eq. (2.11), gives

$$\tau_{xx,x} = \frac{8Gu_0}{t^2}$$

which with the assumption that $\tau_{xx} = \tau_{zz} = -p$ provides the sole equation of equilibrium as

$$p_{,x} = -\frac{8Gu_0}{t^2} \quad . \tag{2.15}$$

The individual fibers are replaced by an equivalent sheet of reinforcement of thickness t_f. The internal force, $F(x)$, per unit width of the equivalent reinforcing sheet is related to the shear stresses on the top and bottom of the pad by

$$\frac{dF}{dx} - \tau_{xz}\Big|_{z = \frac{t}{2}} + \tau_{xz}\Big|_{z = -\frac{t}{2}} = 0$$

as shown in Fig. 2-3.

From Eqs. (2.13) and (2.14) we have

$$\tau_{xz}\Big|_{z = \frac{t}{2}} = -\frac{8Gu_0}{2t}; \quad \tau_{xz}\Big|_{z = -\frac{t}{2}} = \frac{8Gu_0}{2t}$$

giving

$$\frac{dF}{dx} = -\frac{8Gu_0}{t} \quad . \tag{2.16}$$

The extensional strain in the reinforcement ε_f is related to the stretching force through the elastic modulus of the reinforcement, E_f , and the thickness, t_f , such that

$$\varepsilon_f = u_{1,x} = \frac{F}{E_f t_f} \tag{2.17}$$

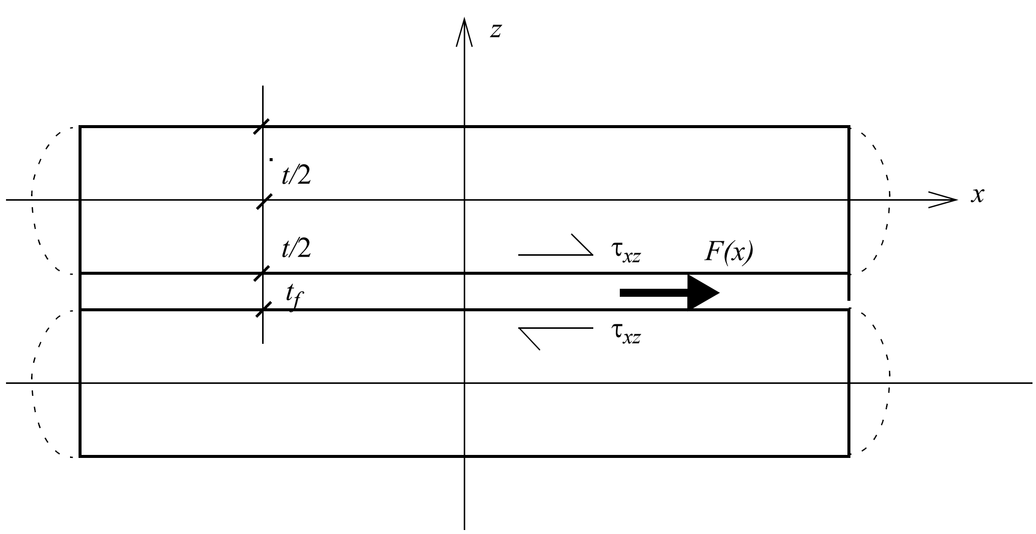

Figure 2-3   Force in equivalent sheet of reinforcement

which when combined with Eq. (2.16), gives

$$u_{1,xx} = -\frac{8G}{E_f t_f t} u_0 \quad .$$

The complete system of equations is

$$p_{,x} = -\frac{8Gu_0}{t^2} \tag{2.18}$$

$$u_{0,x} + \frac{3}{2} u_{1,x} = \frac{3\Delta}{2t} \tag{2.19}$$

$$u_{1,xx} = -\frac{8G}{E_f t_f t} u_0 \tag{2.20}$$

with boundary conditions or symmetric conditions as follows:

$$\begin{aligned} u_0(0) &= 0 \\ u_1(0) &= 0 \\ \tau_{xx}(\pm b) &= 0 \\ F(\pm b) &= 0 \, . \end{aligned}$$

Combining Eqs. (2.19) and (2.20) to eliminate u_0, gives

$$u_{1,xxx} - \frac{12G}{E_f t_f t} u_{1,x} = -\frac{12G}{E_f t_f t} \cdot \frac{\Delta}{t} \quad . \tag{2.21}$$

We define $\alpha^2 = 12Gb^2 / E_f t_f t$, leading to

$$u_1 = A + B\cosh\alpha x/b + C\sinh\alpha x/b + \frac{\Delta}{t}x \quad .$$

Symmetry suggests that $A = 0$, $B = 0$, giving

$$u_1 = C\sinh\alpha x/b + \frac{\Delta}{t}x \quad .$$

From Eq. (2.17) we have

$$F = E_f t_f u_{1,x} = E_f t_f \left(\frac{\alpha}{b} C \cosh \alpha x / b + \frac{\Delta}{t}\right)$$

which with $F = 0$ on $x = \pm b$ leads to

$$F(x) = \frac{\Delta}{t} E_f t_f \left(1 - \frac{\cosh \alpha x / b}{\cosh \alpha}\right)$$

$$u_1(x) = \frac{\Delta}{t} \left(x - \frac{b \sinh \alpha x / b}{\alpha \cosh \alpha}\right)$$

$$u_0(x) = \frac{3}{2} \frac{\Delta}{t} \frac{b \sinh \alpha x / b}{\alpha \cosh \alpha} \ .$$

Also, using Eq. (2.18) and the boundary condition $\tau_{xx} = 0$ at $x = \pm b$ gives

$$p = \frac{\Delta}{t} \frac{E_f t_f}{t} \left(1 - \frac{\cosh \alpha x / b}{\cosh \alpha}\right) \ .$$

The load per unit length of the strip, *P*, is given by

$$P = \frac{E_f t_f}{t} 2 \int_0^b \left(1 - \frac{\cosh \alpha x / b}{\cosh \alpha}\right) dx \cdot \frac{\Delta}{t}$$

$$= \frac{2 E_f t_f}{\alpha t} b (\alpha - \tanh \alpha) \frac{\Delta}{t} \ .$$

This result can be interpreted as an effective compression modulus, E_c, given by

$$E_c = \frac{P}{A} \cdot \frac{t}{\Delta} = \frac{E_f t_f}{t} \left(1 - \frac{\tanh \alpha}{\alpha}\right) \ . \qquad (2.22)$$

We note that when $\alpha \to 0$, i.e., $E_f \to \infty$, we have $E_c \to 4 G S^2$ as before. The formula also shows that

$$E_c < 4GS^2$$

for all finite values of E_f.

The effect of the elasticity of the reinforcement on the various quantities of interest can be illustrated by a few examples. We normalize the compression modulus, E_c, by dividing by $4GS^2$, giving from Eq. (2.22)

$$\frac{E_c}{4GS^2} = \frac{3}{\alpha^2}\left(1 - \frac{\tanh\alpha}{\alpha}\right)$$

which is shown in Fig. 2-4 for $0 \le \alpha \le 5$; note how the stiffness decreases with decreasing E_f. The distribution of the pressure for various values of α from $\alpha = 0$, corresponding to $E_f = \infty$ (the steel pressure solution), to $\alpha = 3$, corresponding to very flexible reinforcement is shown in Fig. 2-5. The displacements pattern for the reinforcement and for the force in the reinforcement for these values of α are shown in Fig. 2-6 and Fig. 2-7. As the reinforcement becomes more flexible, the displacement tends to almost linear in x and the force is almost constant. Figure 2-8 presents normalized compression modulus as a function of normalized reinforcement modulus.

2.3 Flexible Reinforcement and Compressibility

The previous analyses for rigid reinforcement and flexible reinforcement made use of the assumption that the elastomer is incompressible. This is a reasonable approximation in cases where the shape factor S is not large (say <20). In cases of larger shape factors the estimate of E_c can be comparable to the value of the bulk modulus of the material, for natural rubber approximately 2000 MPa (300,000psi), so that neglect of compressibility is not justified. To include the influence of compressibility on the behavior of a pad in compression in a way that is consistent with the assumptions of the analysis, it is possible to replace the equation of incompressibility Eq. (2.19) by

$$\varepsilon_{xx} + \varepsilon_{zz} = -\frac{p}{K} \tag{2.23}$$

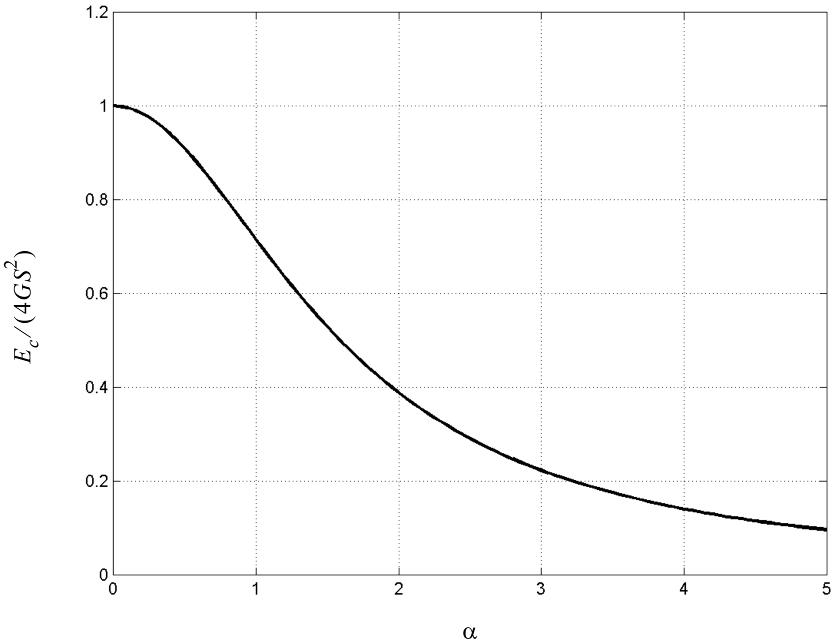

Figure 2-4 Normalized effective compression modulus as a function of $\alpha = (12Gb^2/E_f t_f t)^{1/2}$

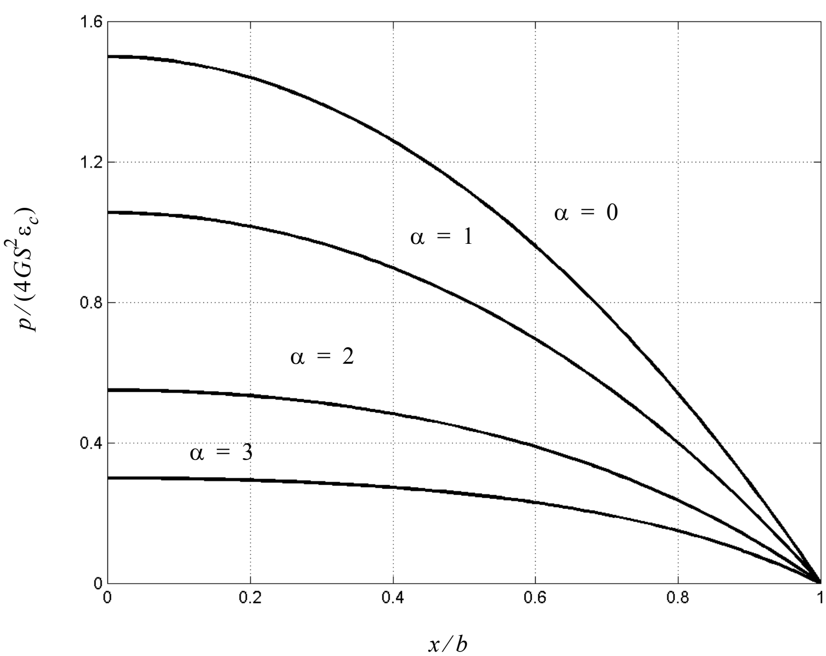

Figure 2-5 Pressure distributions for various values of α

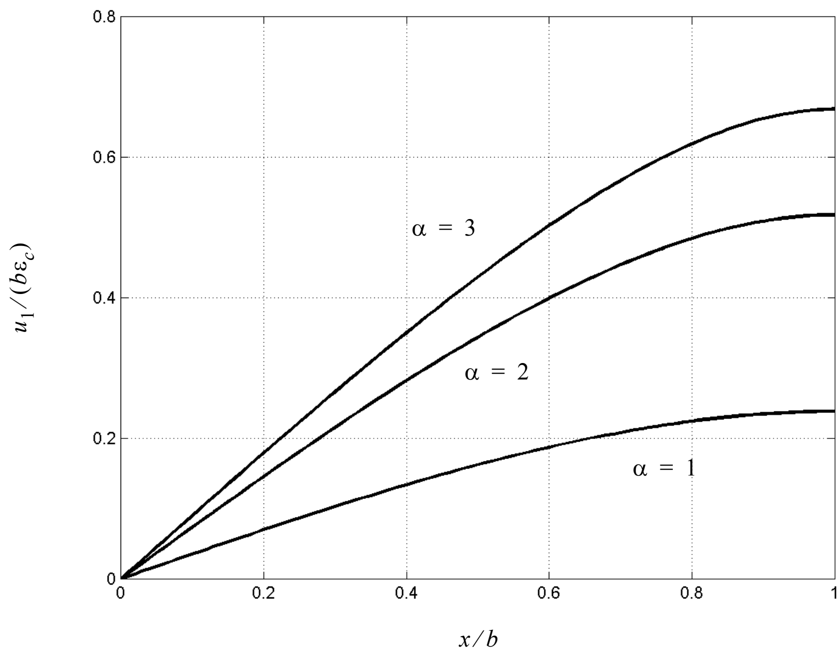

Figure 2-6 Displacement pattern for fiber reinforcement for various values of α

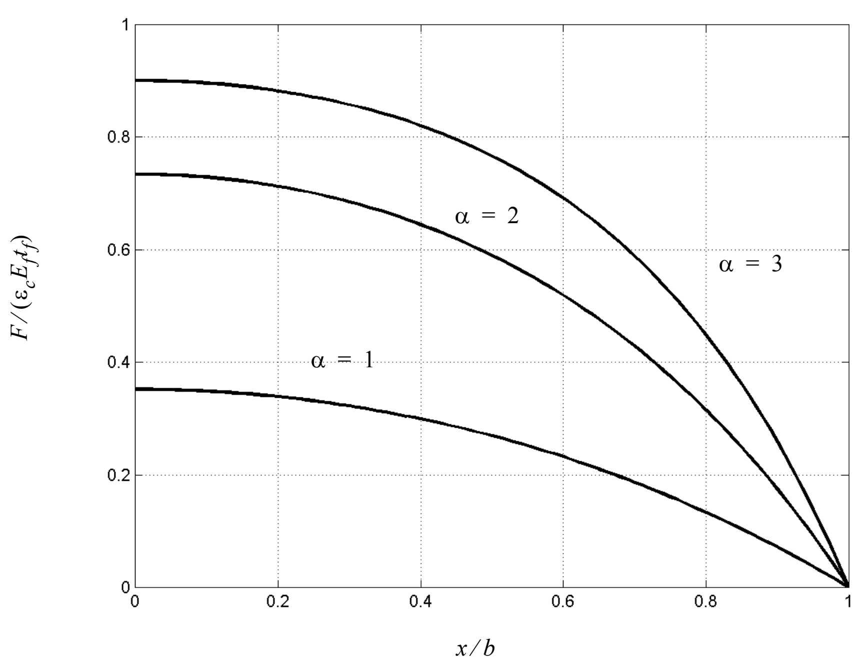

Figure 2-7 Normalized force pattern in reinforcement

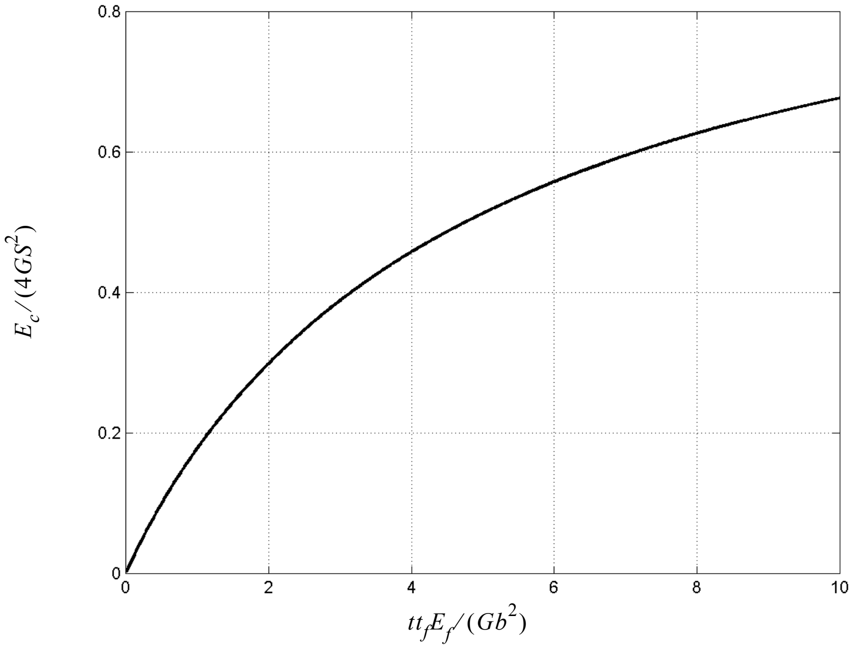

Figure 2-8 Normalized compression modulus as a function of normalized reinforcement modulus

where K is the bulk modulus. Integration through the thickness leads to the amended form of Eq. (2.19)

$$\frac{2}{3}u_{0,x} + u_{1,x} + \frac{p}{K} = \frac{\Delta}{t} \quad . \tag{2.24}$$

This is then supplemented by the equation of equilibrium Eq. (2.18) which is unchanged and by the equation for the forces in the reinforcement Eq. (2.20). The system of equations for the combined effects of reinforcement flexibility and compressibility is now

$$p_{,x} = -\frac{8Gu_0}{t^2} \tag{2.25}$$

$$u_{1,xx} = -\frac{8Gu_0}{E_f t_f t} \tag{2.26}$$

$$\frac{2}{3}u_{o,x} + u_{1,x} + \frac{p}{K} = \frac{\Delta}{t} \quad . \tag{2.27}$$

It is convenient now to define two dimensionless parameters, λ and μ, that determine the comparative significance of flexibility in the reinforcement and compressibility in the elastomer, using

$$\lambda = \frac{12Gb^2}{Kt^2} \quad \text{and} \quad \mu = \frac{12Gb^2}{E_f t_f t}$$

which can also be expressed in terms of the shape factor S which for the long strip is

$$S = b/t$$

giving

$$\lambda = \frac{12GS^2}{K} \quad \text{and} \quad \mu = \frac{12Gt}{E_f t_f}S^2 \quad .$$

In terms of these, Eqs. (2.25) and (2.26) become

$$(p/K)_{,x} = \frac{2}{3}\lambda u_o/b^2 \tag{2.28}$$

$$u_{1,xx} = -\frac{2}{3}\mu u_0/b^2 \quad . \tag{2.29}$$

Differentiation of Eq. (2.27) once and substitution of p and u_1 from Eqs. (2.25) and (2.26) give

$$u_{0,xx} - \frac{(\lambda + \mu)}{b^2}u_0 = 0$$

from which we have

$$u_0 = A\cosh\beta x/b + B\sinh\beta x/b$$

where

$$\beta^2 = \lambda + \mu \ .$$

In turn using Eq. (2.25) and (2.26) gives solutions for p and u_1 in the forms

$$u_1 = -\frac{2}{3}\frac{\mu}{\beta^2} A \cosh \beta x/b - \frac{2}{3}\frac{\mu}{\beta^2} B \sinh \beta x/b + C_1 x + D$$

and

$$p/K = -\frac{2}{3}\frac{\lambda}{\beta b} A \sinh \beta x/b - \frac{2}{3}\frac{\lambda}{\beta b} B \cosh \beta x/b + C_2 \ .$$

The constants of integration, of course, are not independent of each other but are related through the basic equations. Substitution of the three solutions into Eq. (2.27) gives

$$\frac{2\beta}{3b}(A \sinh \beta x/b + B \cosh \beta x/b) - \frac{2}{3}\frac{\mu}{\beta b}(A \sinh \beta x/b + B \cosh \beta x/b) + C_1$$

$$-\frac{2\lambda}{3\beta}(A \sinh \beta x/b + B \cosh \beta x/b) + C_2 = \frac{\Delta}{t} \ .$$

Since $\beta^2 = \lambda + \mu$ the coefficients of $\sinh \beta x/b$ and $\cosh \beta x/b$ vanish and the result is

$$C_1 + C_2 = \frac{\Delta}{t} \ .$$

For the particular problem of the compression of the strip it is useful to consider the obvious symmetries in the solutions. Thus u_0 and u_1 are antisymmetric and p is symmetric on $-b \le x \le +b$. It follows that $A = 0$ and $D = 0$ giving

$$u_0 = B \sinh \beta x/b$$

$$u_1 = -\frac{2}{3}\frac{\mu}{\beta^2} B \sin \beta x/b + C_1 x$$

$$\frac{p}{K} = -\frac{2}{3}\frac{\lambda}{\beta b} B \cosh \beta x/b + \frac{\Delta}{t} - C_1 \ .$$

The boundary conditions that fix B and C_1 are given by the fact that the pressure p at the edges $x = \pm b$ is zero and that the stress in the reinforcement $E_f u_{1,x}$ also vanishes at the edges. Thus

$$-\frac{2}{3}\frac{\mu}{\beta b}B\cos\beta + C_1 = 0$$

$$-\frac{2}{3}\frac{\lambda}{\beta b}B\cosh\beta - C_1 = -\frac{\Delta}{t}$$

giving

$$B = \frac{3}{2}\frac{\beta}{\lambda+\mu}b\frac{1}{\cosh\beta}\frac{\Delta}{t}$$

$$C_1 = \frac{\mu}{\lambda+\mu}\frac{\Delta}{t}$$

and the final solution becomes

$$u_0 = \frac{3}{2}b\frac{\sinh\beta x/b}{\alpha\cosh\beta}\frac{\Delta}{t}$$

$$u_1 = b\frac{\mu}{\lambda+\mu}\left(\frac{x}{b} - \frac{\sinh\beta x/b}{\beta\cosh\beta}\right)\frac{\Delta}{t}$$

and

$$\frac{p}{K} = \frac{\lambda}{\lambda+\mu}\left(1 - \frac{\cosh\beta x/b}{\cosh\beta}\right)\frac{\Delta}{t} \ . \tag{2.30}$$

The quantity of immediate interest is the effective compression modulus E_c given by

$$P = E_c A\frac{\Delta}{t}$$

where

$$P = \int_{-b}^{b} p(x)dx \text{ and } A = 2b \ .$$

Substitution of p from Eq. (2.30) above and integration gives

$$E_c = K\frac{\lambda}{\lambda+\mu}\left(1 - \frac{\tanh\beta}{\beta}\right) . \tag{2.31}$$

It is worth noting that if the effect of compressibility is negligible, then $\lambda \to 0$ $\beta^2 \to \mu$ and we have

$$K\lambda = \frac{12Gb^2}{t^2}$$

giving

$$E_c = \frac{12Gb^2}{t^2}\frac{1}{\beta^2}\left(1 - \frac{\tanh\beta}{\beta}\right) = \frac{E_f t_f}{t}\left(1 - \frac{\tanh\beta}{\beta}\right) \tag{2.32}$$

which is the same as the result in section 2.2. On the other hand if the flexibility of the reinforcement is negligible, then $\mu \to 0$ and $\beta^2 \to \lambda$ giving

$$E_c = K\left(1 - \frac{\tanh\beta}{\beta}\right) . \tag{2.33}$$

If the compression modulus is normalized by $4GS^2$ then from Eq. (2.31) we have

$$\frac{E_c}{4GS^2} = \frac{3}{\lambda+\mu}\left(1 - \frac{\tanh(\lambda+\mu)^{1/2}}{(\lambda+\mu)^{1/2}}\right) \tag{2.34}$$

which demonstrates how the vertical stiffness is reduced by both compressibility in the elastomer and flexibility in the reinforcement.

The experimental results described later suggest that both the fiber flexibility and the compressibility of the elastomer have an effect in reducing the stiffness of the bearings and that the effect of compressibility in the elastomer cannot be ignored. A more detailed analysis will be provided in the later section on experimental results.

3 Bending Stiffness of a Single Pad

The response of a single pad to an applied bending moment is also an important aspect of isolation bearings, since the bending stiffness of a pad plays an important role in providing the resistance of the whole bearing to buckling under a compressive load. In the case of the strip isolator the buckling is in the short direction and the buckling problem is complicated in the case of the unbonded bearings by the fact that the boundary conditions involve a possible uplift. Nevertheless an adequate bending stiffness is essential to prevent lateral instability.

3.1 Bending Stiffness with Rigid Reinforcement

The bending stiffness is computed using a similar argument as before. The displaced configuration, however, is obtained in two stages. First we visualize a deformation, shown dotted in Fig. 3-1, which is what would occur if the bending conformed to elementary beam theory. Since this cannot satisfy the incompressibility constraint, a further pure shear deformation is superimposed. The displacement field is given by

$$\begin{aligned} u(x, y, z) &= u_0(x, y)\left(1 - \frac{4z^2}{t^2}\right) - \theta\frac{z^2}{2t} \\ v(x, y, z) &= v_0(x, y)\left(1 - \frac{4z^2}{t^2}\right) \\ w(x, y, z) &= \frac{\theta z x}{t} \quad . \end{aligned} \tag{3.1}$$

Here, θ is the angle between the rigid plates in the deformed configuration and the bending is about the y-axis. The radius of curvature, ρ, generated by the deformation is related to θ by

$$\frac{1}{\rho} = \frac{\theta}{t} .$$

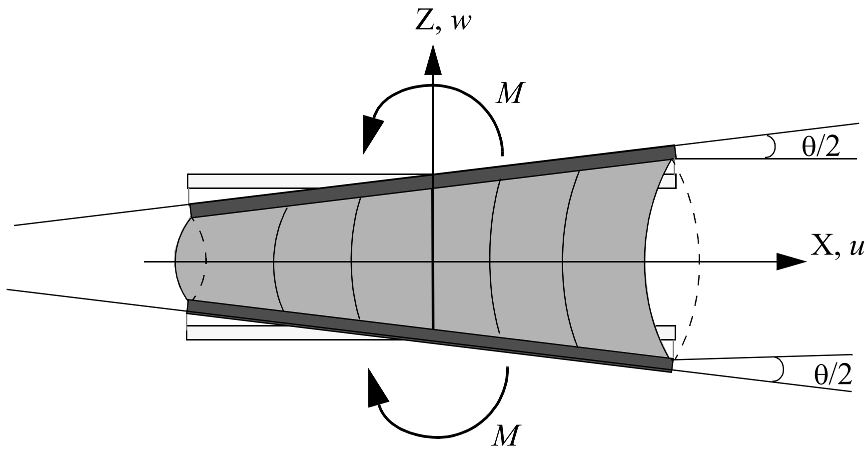

Figure 3-1 Pad in pure flexure

The incompressibility condition Eq. (2.2) when integrated through the thickness becomes

$$u_{0,x} + v_{0,y} + \frac{3}{2}\frac{\theta}{t}x = 0 .$$

The shear stresses, τ_{xz}, τ_{yz}, are given by

$$\tau_{xz} = -\frac{8Gz}{t^2}u_0 \qquad , \qquad \tau_{yz} = -\frac{8Gz}{t^2}v_0$$

and substitution into the equations of equilibrium gives

$$u_0 = -\frac{t^2}{8G}p_{,x} \qquad , \qquad v_0 = -\frac{t^2}{8G}p_{,y}$$

which with the incompressibility condition leads to

$$\nabla^2 p = p_{,xx} + p_{,yy} = \frac{12\theta G}{t^3}x \tag{3.2}$$

with $p = 0$ on the edges.

For the example of the infinite strip $2b$ wide, shown in Fig. 3-1, we have

$$p_{,xx} = \frac{12\theta G x}{t^3}$$

or

$$p = \frac{12\theta G}{t^3}(x^2 - b^2)x \quad . \tag{3.3}$$

The resultant moment, M, is given by

$$M = -\int_{-b}^{b} pxdx = \frac{8\theta G b^5}{15t^3} \quad . \tag{3.4}$$

If we compare this with the usual bending equation for a beam, namely, $M = EI/\rho$, where I is the moment of inertia of a beam cross section with the shape of the pad, and identify E by $E_c = 4GS^2$, where $S = b/t$, then $EI = 2E_c b^3/15$. Thus the effective I for the strip is $2b^3/15$. This reduction is due to the pressure distribution varying cubically across the width of the strip, whereas in a beam, the stress distribution is linear.

3.2 Bending Stiffness with Flexible Reinforcement

The derivation of the bending stiffness starts with the addition of the stretching term $u_1(x)$ to the displacement assumption of Eq. (3.1), giving

$$\begin{aligned} u(x,z) &= u_0(x)\left(1 - \frac{4z^2}{t^2}\right) + u_1(x) - \theta\frac{z^2}{2t} \\ w(x,z) &= \frac{\theta z x}{t} \quad . \end{aligned} \tag{3.5}$$

As before, the curvature $1/\rho = \theta/t$.

Incompressibility and integration across the thickness leads to

$$u_{0,x} + \frac{3}{2}u_{1,x} = \frac{3\theta x}{2t} \quad .$$

Combining the shear stress-strain relation with the single equation of equilibrium gives $p_{,x} = -\frac{8G}{t^2}u_0$, and, as before, the force in the reinforcement is given by

$$\frac{dF}{dx} = -\frac{8Gu_0}{t}$$

leading to

$$u_{1,xx} = -\frac{8G}{E_f t_f t}u_0 \quad .$$

The complete system of equations is

$$p_{,x} = -\frac{8Gu_0}{t^2} \quad ; \quad p(\pm b) = 0 \tag{3.6}$$

$$u_{0,x} + \frac{3}{2}u_{1,x} = -\frac{3\theta}{2t}x \tag{3.7}$$

$$u_{1,xx} = -\frac{8G}{E_f t_f t}u_0 \tag{3.8}$$

$$F(x) = E_f t_f u_{1,x} \quad ; \quad F(\pm b) = 0 \quad . \tag{3.9}$$

Eliminating u_0 as before, we get

$$u_{1,xxx} - \frac{12G}{E_f t_f t}u_{1,x} = -\frac{12G}{E_f t_f t}\frac{\theta x}{t} \tag{3.10}$$

and the resulting solutions with $\alpha^2 = \frac{12Gb^2}{E_f t_f t}$ are

$$u_1 = A\cosh\alpha x/b + B\sinh\alpha x/b + \frac{\theta x^2}{2t} + C \quad . \tag{3.11}$$

Now by Eq. (3.8)

$$u_0 = -\frac{E_f t_f t}{8G} u_{1,\mathrm{xx}}$$

thus

$$u_0 = -\frac{E_f t_f t}{8G}\left(\frac{\alpha^2}{b^2} A \cosh\frac{\alpha x}{b} + \frac{\theta}{t}\right)$$

and in turn from Eq. (3.6) we have

$$p_{,\mathrm{x}} = -\frac{8G}{t^2} u_0$$

giving

$$p = \frac{E_f t_f}{t}\left(\frac{\alpha}{b} A \sinh\frac{\alpha x}{b} + \frac{\theta x}{t}\right) + D \quad .$$

Since we expect p to be antisymmetric, $D = 0$.

The two boundary conditions $p(b) = 0$ and $u_{1,\mathrm{x}}(b) = 0$ turn out to give the same result for A in the form

$$A = -\frac{\theta}{t}\frac{b^2}{\alpha}\frac{1}{\sinh\alpha}$$

so that

$$p(x) = \frac{E_f t_f}{t}\frac{\theta b}{t}\left(\frac{x}{b} - \frac{\sinh\alpha x / b}{\sinh\alpha}\right)$$

and

$$u_1(x) = \frac{\theta b^2}{t}\left(\frac{x^2}{t^2} - \frac{\cosh\alpha x / b}{\alpha \sinh\alpha}\right) \quad . \qquad \textit{(3.12)}$$

The resulting moment, *M,* is computed from the pressure distribution using Eq. (3.4) and is

$$M = \frac{E_f^2 t_f^2}{6Gt} \theta b \left(1 + \frac{\alpha^2}{3} - \frac{\alpha}{\tanh\alpha}\right)$$

giving for the effective bending stiffness $(EI)_{eff}$,

$$(EI)_{eff} = \frac{M}{\theta/t} = \frac{E_f^2 t_f^2 b}{6G} \left(1 + \frac{\alpha^2}{3} - \frac{\alpha}{\tanh\alpha}\right) \quad . \tag{3.13}$$

When $E_f \to \infty$, we have $\alpha \to 0$, and using

$$\coth x = \frac{1}{x} + \frac{x}{3} - \frac{x^3}{45} + \ldots$$

As expected, we have

$$\begin{aligned} (EI)_{eff} &\to \left(\frac{E_f^2 t_f^2 b}{6G}\right)\left(1 + \frac{\alpha^2}{3} - 1 + \frac{\alpha^2}{3} + \frac{\alpha^4}{45} + \ldots\right) \\ &= \frac{1}{5}(E_c)I \end{aligned}$$

Including a further term in the series for $\coth x$ shows that, as expected, the bending stiffness is reduced by the flexibility in the reinforcement.

The forces in the reinforcement which can be obtained from Eq. (3.12) can be negative in this case and of course this is physically impossible in that the sheet without bending rigidity cannot be expected to sustain compression. The solution is valid only so long as the tension forces in the reinforcement due to the compressive load exceed the compressive stresses generated by the bending moment.

3.3 Bending Stiffness with Inclusion of Compressibility

To include both effects into the calculation of the bending stiffness it is only necessary to add the volumetric strain p/K to the integrated equation of compressibility Eq. (3.7) giving

$$\frac{2}{3}u_{o,x} + u_{1,x} + \frac{p}{K} = \frac{\theta}{t}x \quad . \tag{3.14}$$

All other equations remain the same but we modify Eq. (3.6) to read

$$\left(\frac{p}{K}\right)_{,x} = -\frac{8Gb^2}{Kt^2}\frac{u_0}{b^2} = \frac{-2\lambda u_0}{3b^2} \quad ,$$

whereas in section 3.2 we have

$$\lambda = \frac{12Gb^2}{Kt^2} \quad .$$

The resulting solutions follow the same procedure as in the previous section leading to the expression for the effective bending stiffness

$$(EI)_{eff} = \frac{2K\lambda b^2}{(\lambda+\mu)^2}\left[1 + \frac{\lambda+\mu}{3} - (\lambda+\mu)^{1/2}\coth(\lambda+\mu)^{1/2}\right] \quad .$$

Since $K\lambda = \dfrac{12Gb^2}{t^2}$ this can be written as

$$(EI)_{eff} = \frac{24Gb^4}{(\lambda+\mu)^2 t^2}\left[1 + \frac{\lambda+\mu}{3} - (\lambda+\mu)^{1/2}\coth(\lambda+\mu)^{1/2}\right] \quad .$$

The two limiting cases of incompressibility, i.e., $\lambda = 0$, and rigid reinforcement, $\mu = 0$, are

$$(EI)_{eff} = \frac{6E_f^2 t_f^2 t^2 b^2}{G}\left[1 + \frac{\alpha^2}{3} - \alpha\coth\alpha\right]$$

as in section 3.2 and

$$(EI)_{eff} = \frac{2Kb^2}{\lambda}\left[1 + \frac{\alpha^2}{3} - \alpha\coth\alpha\right]$$

where in the first $\alpha^2 = \dfrac{12Gb^2}{E_f t_f t}$ and in the second $\alpha^2 = \dfrac{12Gb^2}{Kt^2}$.

The relative importance of the two effects appears in the same form as before in section 2.3.

4 Experimental Results

Several samples of fiber-reinforced bearings were constructed and tested in compression and shear to verify if the approach was practical. All bearings were manufactured by Dongil Rubber Belt Co., Ltd. (Pusan, Korea). The six specimens shipped were in the form of strips with slightly different geometric dimensions (Table 4.1). The width to height ratio was very close to 2 and

Table 4-1 Fiber-reinforced test specimens

Name	Length [mm]	Width [mm]	Height [mm]	Area [sq.mm]	Comments	Presence of rubber cover			
						East	West	North	South
DRB1	735	183	105	134505	originally shipped	Yes	No	No	No
DRB2	750	190	105	142500	originally shipped	Yes	No	Yes	No
DRB3	740	190	105	140600	originally shipped	No	Yes	Yes	No
DRB4	365	190	105	69350	cut from 190x755x105	No	No	Yes	No
DRB5	390	190	105	74100	cut from 190x755x105	Yes	No	Yes	No
DBB6	377	183	105	68991	cut from 183x755x105	No	Yes	No	No
DBB7	377	183	105	68991	cut from 183x755x105	No	No	No	No
DRB8	730	185	105	135050	keep as sample				

Notes:
(1) All test specimens were composed of 33 layers of 3 mm rubber and 30 layers of 0.27 mm fiber; there were two double rubber layers on the bearing top and bottom.
(2) The in-plane test machine imposed shear in the east-west direction (corresponds to the 0 degrees direction).
(3) The location angle of the specimen was measured from the west direction counter-clockwise, (so at 90 degrees the former west side points south).
(4) The rubber cover of the bearing sides reduces the effective work area of the bearing in the vertical direction. The thickness of the rubber cover varied from 5 mm to 9 mm on a long side of the bearing (north or south) and varied from 1 mm to 3 mm on a short side of the bearing (east or west).

length to height ratio was around 7.5. To reach a desired level of vertical pressure within the capacity of the testing machine, two of the strips were cut in half and used as test specimens. In each bearing the total thickness of rubber was 99 mm and was reinforced by 30 plane sheets of carbon fiber 0.27 mm thick. The experimental research was conducted to study the behavior of the fiber-reinforced strips in compression and shear at various levels of vertical pre-load. The test program and a summary of the obtained results are presented in Tables 4.2–4.9 . The average ver-

Table 4-2 Test program and results for DBR1

Test No.	Rotation degree	Test name	Axial load [kN]	Axial stress [MPa]	Shear strains: [%]	Average stiffness [kN/m]
1	0	vertical	233.6	1.73	0	550853.9
2	0	vertical	467.3	3.45	0	791048.8
3	0	horizontal	233.6	1.73	25, 50, 75, 100	1408.6
4	0	horizontal	467.3	3.45	25, 50, 75, 100	1354.3
5	0	horizontal	233.6	1.73	37.5, 75, 112.5, 150	1228.1
6	0	horizontal	467.3	3.45	37.5, 75, 112.5, 150	1173.8
7	90	horizontal	233.6	1.73	25, 50, 75, 100	856.7
8	90	horizontal	467.3	3.45	25, 50, 75, 100	839.2
9	90	horizontal	233.6	1.73	37.5, 75, 112.5, 150	571.1
10	90	horizontal	467.3	3.45	37.5, 75, 112.5, 150	609.7
11	45	horizontal	233.6	1.73	25, 50, 75, 100	1066.9
12	45	horizontal	467.3	3.45	25, 50, 75, 100	1116.0
13	45	horizontal	233.6	1.73	37.5, 75, 112.5, 150	842.7
14	45	horizontal	467.3	3.45	37.5, 75, 112.5, 150	947.8

tical stiffness of the bearing was obtained from a compression test conducted in the following way. The specimen was monotonically loaded up to the target value of vertical pressure and then three cycles of vertical loading with small amplitude about this target value were performed. The shear stiffness of the specimens was obtained from a shear test, in which sets of shear cycles with step-wise increasing amplitude were applied. These shear tests were conducted for various values of vertical pressure and for three angles between the testing direction and the longitudinal direction of the strip. All tests were conducted on bearings not bonded to the test machine. The residual slip of the specimens after cyclic tests was negligibly small. An extra set of tests to measure the possible slip of the bearing was conducted in monotonic shear loading and unloading. The behavior of the specimens for low vertical pressure was also studied in this last set of tests.

Table 4-3 Test program and results for DRB2

Test No.	Rotation degree	Test name	Axial load [kN]	Axial stress [MPa]	Shear strains: [%]	Average stiffness [kN/m]
1	0	vertical	233.6	1.73	0	602975.0
2	0	vertical	467.3	3.45	0	849319.3
3	45	horizontal	233.6	1.73	25, 50, 75, 100	1107.2
4	45	horizontal	467.3	3.45	25, 50, 75, 100	1103.7
5	45	horizontal	233.6	1.73	37.5, 75, 112.5, 150	855.0
6	45	horizontal	467.3	3.45	37.5, 75, 112.5, 150	856.7
7	0	horizontal	233.6	1.73	25, 50, 75, 100	1180.8
8	0	horizontal	467.3	3.45	25, 50, 75, 100	1189.6
9	0	horizontal	233.6	1.73	37.5, 75, 112.5, 150	1066.9
10	0	horizontal	467.3	3.45	37.5, 75, 112.5, 150	1052.9
11	90	horizontal	233.6	1.73	25, 50, 75, 100	763.9
12	90	horizontal	467.3	3.45	25, 50, 75, 100	788.4
13	90	horizontal	233.6	1.73	37.5, 75, 112.5, 150	529.1
14	90	horizontal	467.3	3.45	37.5, 75, 112.5, 150	578.1

Table 4-4 Test program and results for DRB3

Test No.	Rotation degree	Test name	Axial load [kN]	Axial stress [MPa]	Shear strains: [%]	Average stiffness [kN/m]
1	0	vertical	233.6	1.73	0	597053.3
2	0	vertical	467.3	3.45	0	752785.8
3	90	horizontal	233.6	1.73	25, 50, 75, 100	977.6
4	90	horizontal	467.3	3.45	25, 50, 75, 100	949.6
5	90	horizontal	233.6	1.73	37.5, 75, 112.5, 150	651.7
6	90	horizontal	467.3	3.45	37.5, 75, 112.5, 150	695.5
7	45	horizontal	233.6	1.73	25, 50, 75, 100	1161.6
8	45	horizontal	467.3	3.45	25, 50, 75, 100	1168.6
9	45	horizontal	233.6	1.73	37.5, 75, 112.5, 150	951.3
10	45	horizontal	467.3	3.45	37.5, 75, 112.5, 150	993.4
11	0	horizontal	233.6	1.73	25, 50, 75, 100	1263.2
12	0	horizontal	467.3	3.45	25, 50, 75, 100	1291.2
13	0	horizontal	233.6	1.73	37.5, 75, 112.5, 150	1137.0
14	0	horizontal	467.3	3.45	37.5, 75, 112.5, 150	1156.3

Table 4-5 Test program and results for DRB4

Test No.	Rotation degree	Test name	Axial load [kN]	Axial stress [MPa]	Shear strains: [%]	Average stiffness [kN/m]
1	0	vertical	253.7	3.45	0	349938.19
2	0	vertical	507.3	6.90	0	467372.64
3	0	horizontal	253.7	3.45	25, 50, 75, 100	604.43
4	0	horizontal	253.7	3.45	50,100,150, 200	478.29
5	0	horizontal	507.3	6.90	25, 50, 75, 100	569.39
6	0	horizontal	507.3	6.90	50,100,150, 200	550.12

Table 4-6 Test program and results for DRB5

Test No.	Rotation degree	Test name	Axial load [kN]	Axial stress [MPa]	Shear strains: [%]	Average stiffness [kN/m]
1	0	vertical	253.7	3.45	0	352040.6
2	0	vertical	507.3	6.90	0	445858.5
3	90	horizontal	253.7	3.45	25, 50, 75, 100	425.7
4	90	horizontal	253.7	3.45	50,100,150, 200	250.5
5	90	horizontal	507.3	6.90	25, 50, 75, 100	411.7
6	90	horizontal	507.3	6.90	50,100,150, 200	481.8

Table 4-7 Test program and results of stacked bearings (specimen 183mm x 75mm x 105mm and DRB8)

Test No.	Rotation degree	Test name	Axial load [kN]	Axial stress [MPa]	Shear strains: [%]	Effective stiffness [kN/m]
1	0	vertical	456.1	3.45	0	208309.1
2	0	horizontal	458.4	3.45	50,100,150, 200	588.7

Table 4-8 Test program and results for DRB6

Test No.	Rotation degree	Test name	Axial load [kN]	Axial stress [MPa]	Shear strains: [%]	Average stiffness [kN/m]	Residual slip [mm]
1	0	vertical	60.1	0.86	0	175617.3	
2	0	vertical	120.2	1.73	0	251687.8	
3	0	vertical	240.3	3.45	0	328721.9	
4	90	horizontal ramp	60.1	0.86	0,100,0	385.4	
5	90	manual unload	60.1	0.86	to 0		8
6	90	horizontal ramp	120.2	1.73	0,100,0	369.7	
7	90	manual unload	120.2	1.73	to 0		7
8	90	horizontal ramp	240.3	3.45	0,100,0	359.2	
9	90	manual unload	240.3	3.45	to 0		6
10	90	horizontal cycles	60.1	0.86	25, 50, 75, 100	373.2	
11	90	horizontal cycles	120.2	1.73	25, 50, 75, 100	378.4	
12	45	horizontal ramp	60.1	0.86	0,100,0	499.3	
13	45	manual unload	60.1	0.86	to 0		18
14	45	horizontal ramp	120.2	1.73	0,100,0	474.8	
15	45	manual unload	120.2	1.73	to 0		13
16	45	horizontal ramp	240.3	3.45	0,100,0	473.0	
17	45	manual unload	240.3	3.45	to 0		10
18	45	horizontal cycles	60.1	0.86	25, 50, 75, 100	459.0	
19	45	horizontal cycles	120.2	1.73	25, 50, 75, 100	473.0	
20	0	horizontal ramp	60.1	0.86	0,100,0	513.3	
21	0	manual unload	60.1	0.86	to 0		10
22	0	horizontal ramp	120.2	1.73	0,100,0	509.8	
23	0	manual unload	120.2	1.73	to 0		6
24	0	horizontal ramp	240.3	3.45	0,100,0	497.6	
25	0	manual unload	240.3	3.45	to 0		5
26	0	horizontal cycles	60.1	0.86	25, 50, 75, 100	485.3	
27	0	horizontal cycles	120.2	1.73	25, 50, 75, 100	502.8	

Table 4-9 Test program and results for DRB7

Test No.	Rotation degree	Test name	Axial load [kN]	Axial stress [MPa]	Shear strains: [%]	Average stiffness [kN/m]	Residual slip [mm]
1	0	vertical	60.1	0.86	0	167190.4	
2	0	vertical	120.2	1.73	0	278983.5	
3	0	vertical	240.3	3.45	0	351392.3	
4	90	horizontal ramp	60.1	0.86	0,100,0	417.0	
5	90	manual unload	60.1	0.86	to 0		16
6	90	horizontal ramp	120.2	1.73	0,100,0	401.2	
7	90	manual unload	120.2	1.73	to 0		9
8	90	horizontal ramp	240.3	3.45	0,100,0	380.2	
9	90	manual unload	240.3	3.45	to 0		6
10	90	horizontal cycles	60.1	0.86	25, 50, 75, 100	381.9	
11	90	horizontal cycles	120.2	1.73	25, 50, 75, 100	387.2	
12	45	horizontal ramp	60.1	0.86	0,100,0	446.8	
13	45	manual unload	60.1	0.86	to 0		19
14	45	horizontal ramp	120.2	1.73	0,100,0	495.8	
15	45	manual unload	120.2	1.73	to 0		17
16	45	horizontal ramp	240.3	3.45	0,100,0	469.5	
17	45	manual unload	240.3	3.45	to 0		15
18	45	horizontal cycles	60.1	0.86	25, 50, 75, 100	473.0	
19	45	horizontal cycles	120.2	1.73	25, 50, 75, 100	487.0	
20	0	horizontal ramp	60.1	0.86	0,100,0	508.1	
21	0	manual unload	60.1	0.86	to 0		11
22	0	horizontal ramp	120.2	1.73	0,100,0	509.8	
23	0	manual unload	120.2	1.73	to 0		8
24	0	horizontal ramp	240.3	3.45	0,100,0	520.3	
25	0	manual unload	240.3	3.45	to 0		7
26	0	horizontal cycles	60.1	0.86	25, 50, 75, 100	518.6	
27	0	horizontal cycles	120.2	1.73	25, 50, 75, 100	527.3	

4.1 Performance Parameters of Fiber-Reinforced Bearings

The hysteresis loops obtained during the tests were analyzed to obtain a number of different performance parameters for the fiber-reinforced bearings.

Depending on the loading conditions (axial load and shear strain), the bearing stiffness as revealed by the test hysteresis loops was nonlinear. It is clear that the bearing undergoes a substantial change of stiffness from the small strain to the large strain portions of the test. The average shear stiffness was defined for the test bearings and computed as the slope of a straight line interpolating the hysteresis loops obtained during cyclic tests. The least-squares method used to calculate this horizontal stiffness is referred to here as "the average stiffness of the specimens during cyclic reversals." The average compression stiffness was computed in the same way but using only the cyclic portion of the vertical test procedure.

4.2 Experimental Study Setup and Data Reduction Procedure

This section summarizes the experimental results of fiber-reinforced rubber bearings tested without bonding to the end plates. The tests were carried out in the Structural Research Laboratory of the Pacific Earthquake Engineering Research Center, University of California at Berkeley.

4.2.1 In-plane Test Machine

The test machine was designed to conduct in-plane vertical and horizontal cyclic loading tests, as shown in Fig. 4.1. The vertical load was applied to the specimen by two 570 kN hydraulic actuators, through a stiff frame. The horizontal load was applied to the same frame by a 450 kN hydraulic actuator. The test machine had a displacement capacity of ±254 mm in the horizontal direction and a load capacity of ±1,140 kN in the vertical direction. Two sets of tests were conducted. The vertical test was conducted using a vertical load control, and the horizontal test was performed using a horizontal displacement control. The photograph in Fig. 4.2 shows a global view of a test in progress.

4.2.2 Instrumentation

Many sensors were used to monitor the response of the specimen during the test in order to understand the specimen behavior. The instrumentation allocation was slightly different for the vertical and horizontal tests. Tables 4.10 and 4.11 present information on the instrumentation, with the

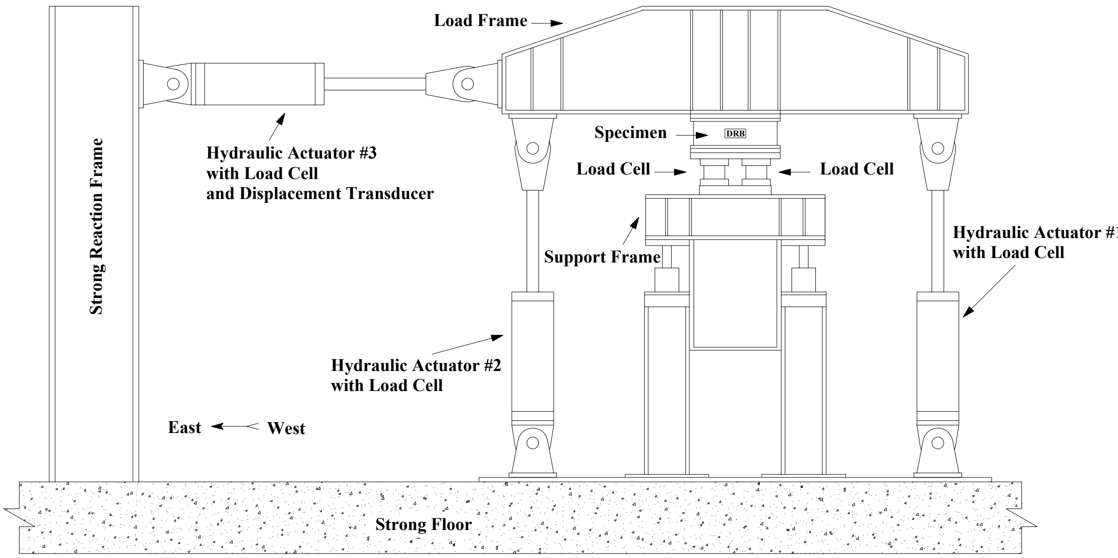

Figure 4-1 Testing setup

Figure 4-2 Test in progress

Table 4-10 Instrumentation setup for vertical test

Channel No.	Device	Measuring Response	Location	Notations
0	LVDT	Horizontal displacement	Horizontal actuator #3	δ
1	LC	Horizontal load	Horizontal actuator #3	$\boldsymbol{H}$
2	LC	Vertical load	Vertical actuator #1	V_1
3	LC	Vertical load	Vertical actuator #2	V_2
4	WP	Vertical displacement	Vertical actuator #1	
5	WP	Vertical displacement	Vertical actuator #2	
6	DCDT	Vertical displacement	Vertical actuator #1	
7	DCDT	Vertical displacement	Vertical actuator #2	
8	LC	Shear force	Load cell on support frame (left)	S_1
9	LC	Shear force	Load cell on support frame (right)	S_2
10	LC	Axial load	Load cell on support frame (left)	A_1
11	LC	Axial load	Load cell on support frame (right)	A_2
12	DCDT	Vertical displacement	Between isolator's base plates	δ_1
13	DCDT	Vertical displacement	Between isolator's base plates	δ_2
14	DCDT	Vertical displacement	Between isolator's base plates	δ_3
15	DCDT	Vertical displacement	Between isolator's base plates	δ_4

channel number, name of the measuring device, and the device location. Figure 4.3 shows the location of displacement and load measuring instruments for the vertical testing setup. The V_1 imposed vertical loads were measured by load cells built into the hydraulic actuators #1 and #2 and V_2. The vertical displacement between the base plates of the specimen was averaged from the data of four DCDTs (δ_1, δ_2, δ_3, and δ_4) located at four different corners of the bearing base-plates. The horizontal displacement was measured by an LVDT (Linear Variable Differential Transformer) built into hydraulic actuator #3. This displacement is denoted by δ, and a load cell in-line with the actuator measured the axial horizontal force $\boldsymbol{H}$. The shear (S_1, S_2) and axial loads (A_1, A_2) were measured by two load cells located under the test specimen. The vertical displacement of the top moving frame was measured at two vertical actuator locations.

The instrumentation for the horizontal test is presented in Fig. 4.4 with the channel description in Table 4.11, and differs from the previous one. Four channels for measuring the vertical displacement between base plates were exchanged in the following way. Two DCDTs were assigned to measure out-of-plane rotation of the top loading frame (δ_5 and δ_6). One channel was used to

Table 4-11 Instrumentation setup for horizontal test

Channel No.	Device	Measuring Response	Location	Notations
0	LVDT	Horizontal displacement	Horizontal actuator #3	δ
1	LC	Horizontal load	Horizontal actuator #3	$\boldsymbol{H}$
2	LC	Vertical load	Vertical actuator #1	$\boldsymbol{V_1}$
3	LC	Vertical load	Vertical actuator #2	$\boldsymbol{V_2}$
4	WP	Vertical displacement	Vertical actuator #1	
5	WP	Vertical displacement	Vertical actuator #2	
6	DCDT	Vertical displacement	Vertical actuator #1	
7	DCDT	Vertical displacement	Vertical actuator #2	
8	LC	Shear force	Load cell on support frame (left)	$\boldsymbol{S_1}$
9	LC	Shear force	Load cell on support frame (right)	$\boldsymbol{S_2}$
10	LC	Axial load	Load cell on support frame (left)	$\boldsymbol{A_1}$
11	LC	Axial load	Load cell on support frame (right)	$\boldsymbol{A_2}$
12	DCDT	Vertical displacement	Support frame flexibility	δ_8
13	WP	Vertical displacement	Back up	δ_7
14	DCDT	Vertical displacement	Used in out-of-plane rotation calc.	δ_6
15	DCDT	Vertical displacement	Used in out-of-plane rotation calc.	δ_5

measure the horizontal displacement of this frame as a back-up channel, δ_7. One DCDT was used to measure the horizontal flexibility of the bottom support frame, δ_8.

4.2.3 Data Acquisition

The test control and the data acquisition system were run by a PC Windows-based control and acquisition program called Automated Testing System (ATS) developed by SHRP Equipment Corporation of Walnut Creek, California. This program is capable of signal generation, four-channel servo-actuator command, and 16-channel data acquisition. For the tests the ATS system was used to monitor and control the displacement and force-feedback signals.

4.2.4 Loading History

The loading history varied from test to test. The experimental program is presented in Tables 4.2–4.9 and describes the entire test program for each specimen.

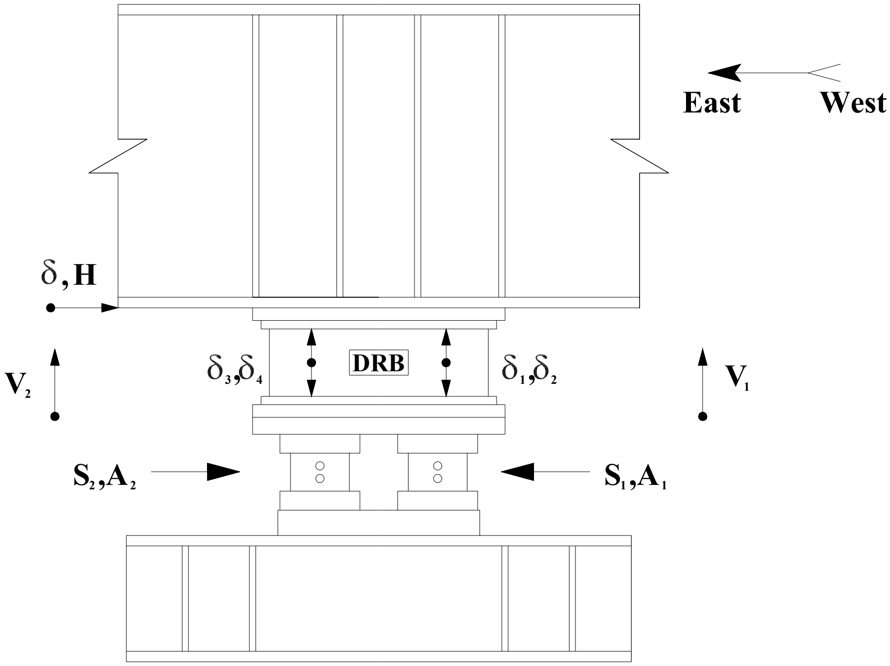

Figure 4-3 Instrumentation setup for vertical test

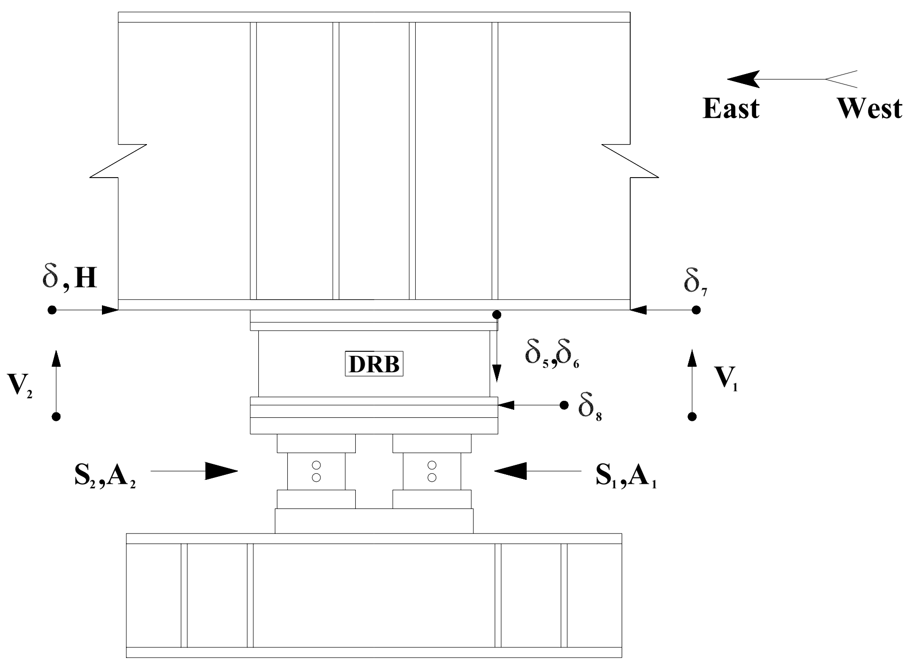

Figure 4-4 Instrumentation setup for horizontal test

Specimen DRB1 was tested under vertical load control. The specimen was monotonically loaded to 1.73 MPa of vertical pressure and three fully reversed cycles with ±0.35 MPa amplitude were performed. In the final stage of the vertical testing the specimen was monotonically unloaded. The loading history of the vertical test is presented in Fig. 4.5. A similar test at 3.45

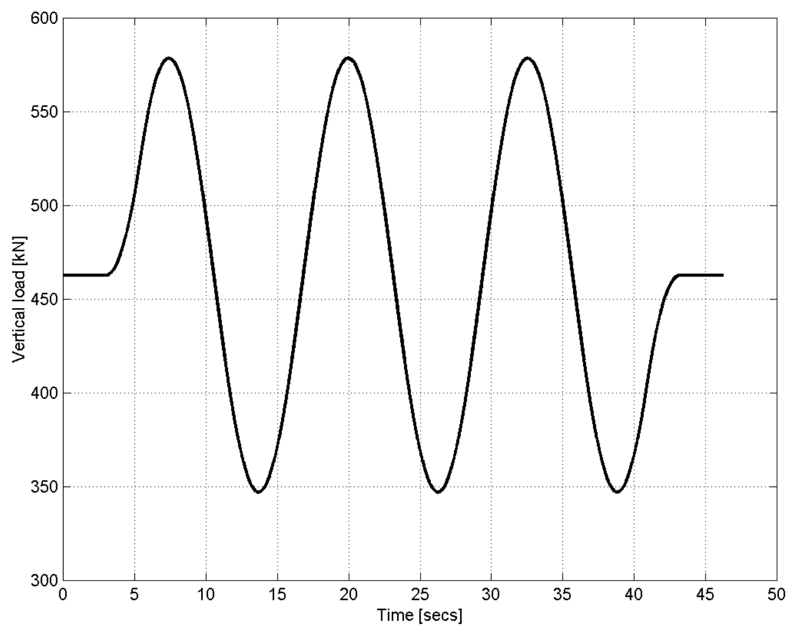

Figure 4-5 Input signal for vertical cyclic test results with 463 kN vertical pre-load

MPa of the original vertical pressure with ±0.35 MPa amplitude was performed also to study the vertical stiffness at higher values of vertical load.

The horizontal test was performed under horizontal displacement control. The specimen DRB1 was tested in cyclic shear, with three fully reversed cycles at four maximum strain levels of 25%, 50%, 75%, and 100% (based on 99 mm rubber thickness). The loading history in the horizontal test is presented in Fig. 4.6. These cycles were applied at a vertical pressure of 1.73 MPa. The value of the vertical pressure was increased to 3.45 MPa and the same shear test was performed. The degree of shear deformation was increased to 1.5 times in the next stage of testing and the same test set was repeated. The shear test was conducted for the following sequence of the angle between the testing direction and the longitudinal direction of the strip: 0°, 90°, and 45°. Table 4.2 presents the testing program for specimen DRB1 in the vertical and horizontal tests.

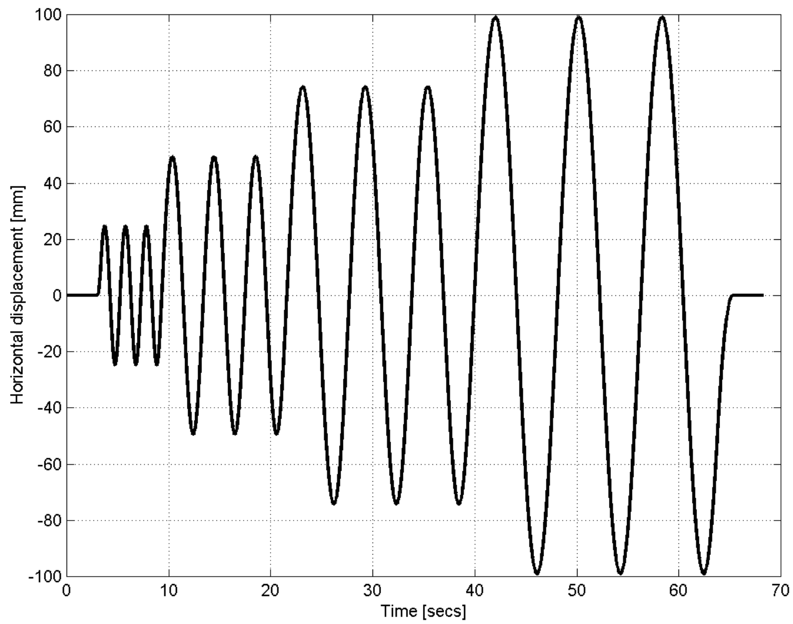

Figure 4-6 Input signal for horizontal cyclic test

Specimens DRB2 and DRB3 were tested under the same test program, but with different angle sequences between the testing direction and the longitudinal direction of the strip. For specimen DB2 this sequence was 45°, 0°, and 90°, and for specimen DRB3 it was 90°, 45°, and 0°. Tables 4.3 and 4.4 present the testing program for specimens DRB2 and DRB3 in the vertical and horizontal tests.

The test program for specimens DRB4 and DRB5 studied the fiber-reinforced bearing behavior at extreme levels of vertical load and horizontal shear deformation. In order not to exceed the capacity of the testing machine the originally shipped specimen was cut into two halves, DRB4 and DRB5. The value of vertical pre-load was increased to 6.90 MPa. The degree of shear deformation was increased by two times to study the behavior at a higher level of shear strain. The angle between the testing direction in shear and the longitudinal direction of the strip was 0° for specimen DRB4 and 90° for specimen DRB5. Tables 4.5 and 4.6 present the testing programs for specimens DRB4 and DRB5 in the vertical and horizontal tests.

The possibility of increasing the shear capacity of the bearings by stacking them (one on top of the other) was studied in tests using one of the original specimens (183mm x 755mm x

105mm) by stacking it on top of specimen DRB8. The joint specimen was vertically loaded up to 3.45 MPa vertical pressure and then was tested in shear with 50%, 100%, 150%, and 200% shear strain amplitudes. Table 4.7 presents the testing program for the joint specimen in the vertical and horizontal tests.

For the final test, this same original specimen was cut into two equal halves, designated specimens DRB6 and DRB7. They differed in that DRB6 had a rubber cover at one end, whereas specimen DRB7 had no side rubber cover. Both were tested under the same test program (Tables 4.8 and 4.9) at low levels of vertical pressure with up to 100% shear strain. The vertical and horizontal behavior of the bearings was tested at three levels of vertical pressure: 0.87 MPa, 1.73 MPa, and 3.45 MPa. The residual slip of the bearing after the shear cyclic tests was very small. A special test signal for horizontal displacement with one-way shear loading and unloading was imposed to study the residual slip for various vertical pressures. The time history of the imposed horizontal displacement is presented in Fig. 4.7.

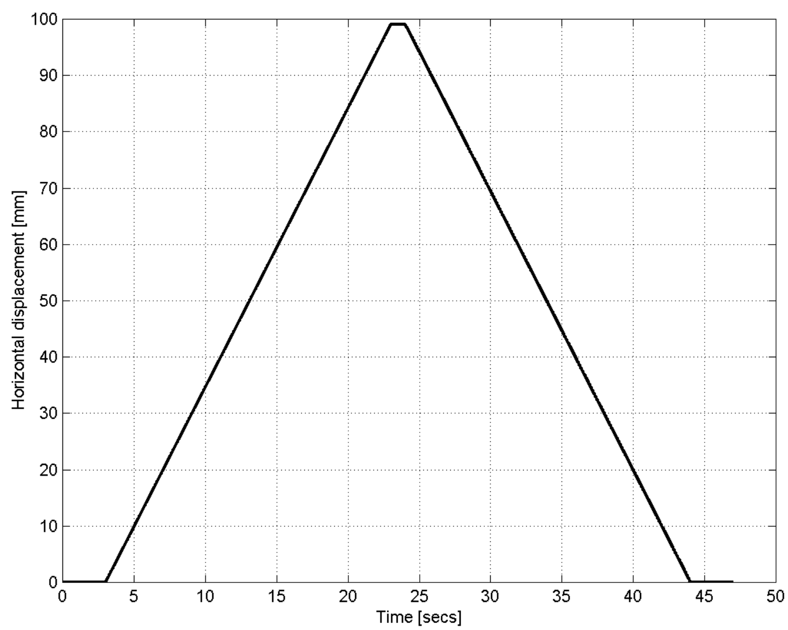

Figure 4-7   Input signal for horizontal monotonic test

To show an example of global behavior of the specimens during these tests photos of specimen DRB6 under deformation are included. Figure 4.8 is a photo of specimen DRB6 under 100%

Figure 4-8 Specimen DRB6 at 100% shear deformation (90°)

shear deformation tested at 90° to the longitudinal direction. The view of the deformation with the same magnitude at 45° to the longitudinal direction is presented in Fig. 4.9. The same specimen under 100% shear deformation tested in the longitudinal direction is presented in Fig. 4.10. Figure 4.11 shows the residual slip of specimen DRB6 after monotonic shear deformation with 100% shear deformation magnitude. The photo was taken during the test conducted at 90° to the longitudinal direction.

4.2.5 Data Processing

The specimen behavior was characterized by the following parameters during the vertical test: applied load and vertical displacement between top and bottom end plates. The applied vertical load was averaged from the two load cells located under the specimen (A_1, A_2). The relative vertical displacement between the end plates of the specimen was averaged from four DCDT data (δ_1, δ_2, δ_3, and δ_4) located at the four corners of the end plates.

During the horizontal test the specimen behavior was characterized by the applied horizontal load and the horizontal displacement of the top frame. The imposed horizontal load was

Figure 4-9 Specimen DRB6 at 100% shear deformation (45°)

Figure 4-10 Specimen DRB6 at 100% shear deformation (0°)

Figure 4-11 Residual slip of DRB6 after 100% monotonic shear deformation (90°)

computed as a sum of two shear loads measured by two load cells located under the test specimen (***S_1, S_2***). The relative horizontal displacement of the top loading frame was obtained from the horizontal displacement (δ_7) of the frame minus the horizontal displacement of the loading table (δ_8).

The least-squares method was used to calculate the average stiffness of the specimen during cyclic reversals. The average stiffness was calculated for the vertical and horizontal directions. For both directions the data from the corresponding cyclic test were used.

A set of programs for the MATLAB 5.3 environment was created to process the data and to plot results in accordance with the procedure described above.

4.3 Discussion of Experimental Results

4.3.1 Horizontal Test Results

The manufacturer of the test isolators gave the nominal shear modulus of this natural rubber compound as 0.690 MPa (100 psi). The three full-length uncut specimens had an average area of 0.140 m^2 and a total rubber thickness of 0.099 m. The horizontal stiffness, K_H, of a conventional isolator is given by

$$K_H = GA/t_r$$

and for these values K_H is

$$K_H = 970 kN/m \ .$$

At 100% shear strain and a pressure of 1.73 MPa (250 psi) the average horizontal stiffness in the longitudinal loading direction is 1280 kN/m, in the lateral loading direction 863 kN/m, and at 45º 1120 kN/m.

The hysteresis loops for the longitudinal loading direction tend to stiffen when the shear strain is increased from 100% to 150%, whereas in the lateral loading direction the loops turn over so that the instantaneous tangent stiffness is negative at the larger strains. However, the effect is reduced at higher pressure levels. The 45º loading does not produce either stiffening or softening but gives values intermediate between the 0º and 90º loadings.

The value of the stiffness at 100% shear strain in the longitudinal direction is slightly higher than would be expected from the nominal value of the shear modulus but in the transverse loading direction the stiffness is lower. At 45º the stiffness is intermediate between the other two. If we assume that the layout of the strip isolator is orthogonal with roughly the same number in each direction, the average between 0º and 90º is close to the value at 45º, so the system will have the same period in any direction of movement.

The period can be roughly estimated using the pressure and the effective shear modulus. The period T is given by

$$T = 2\pi\sqrt{\frac{pt_r}{Gg}} \ .$$

If the average pressure over the system is 3.45 MPa as in the tests and the modulus is 0.690 MPa with 99 mm of rubber, we have a period of 1.4 sec. From the code formula this would produce a displacement of 143 mm (5.64 in.) and a shear strain of 1.41. Adjusting the values to correspond to the measured stiffness at γ=1.5, we find that the period increases to 1.5 sec and the displacement to 150 mm (6 in.).

This suggests that if the period of 1.5 sec is acceptable as the target value for the design of the building, the strip isolators as tested would be adequate providing that the average pressure is at least 3.45 MPa (500 psi). A longer period can be obtained by having one isolator on top of another, as shown in Fig. 4.12 and in the test results of Table 4.7. This leads to a period of 2 sec

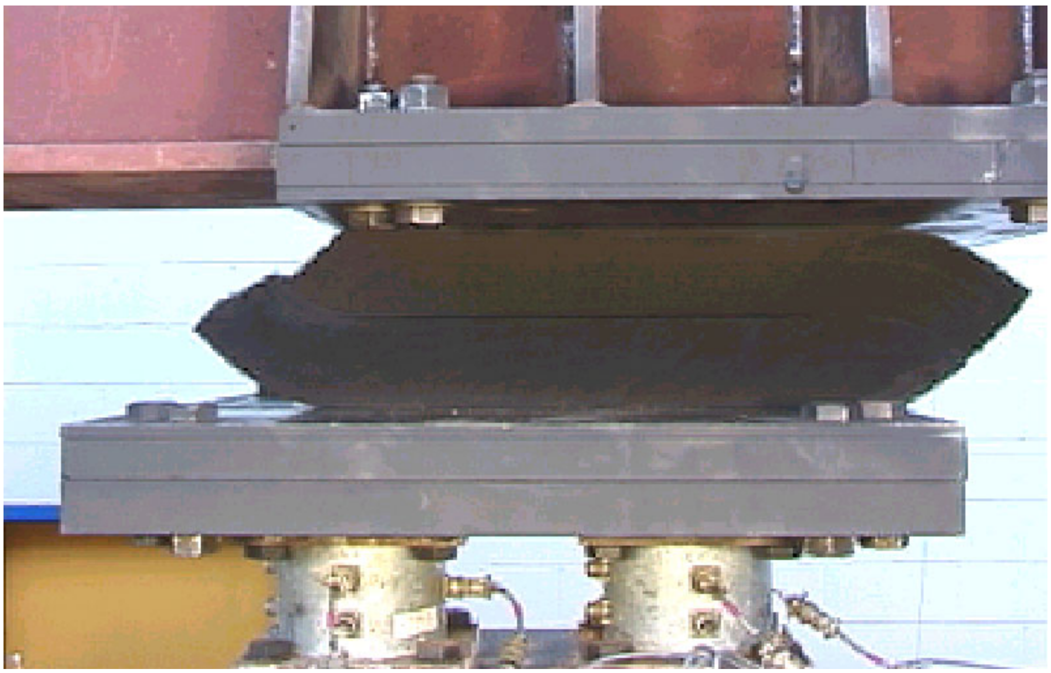

Figure 4-12 Joint test of two unbonded bearings at 200 mm total displacement (0°)

and a code displacement of 8 in. and a γ=1.0. It is clear that a wide range of practical objectives is possible. If it is necessary to have an average pressure of less than 3.45 MPa (500 psi) it is possible to use a softer compound. Compounds with shear moduli, at 100% strain, down to 0.40 MPa (60 psi) are available.

4.3.2 Vertical Test Results

The vertical test results are shown in Tables 4.12, 4.13, and 4.14. Since the dimensions of the bearings are slightly different in each case, it is useful to tabulate the vertical stiffness in terms of the effective compression modulus, E_c, as defined by Eq. (2.9). The first point to note is that there is considerable variation in this value. The full-length bearings of DRB1/2/3 are quite

Table 4-12 Vertical test results for 1.73 MPa vertical pressure

Specimen No.	Area $[m^2]$	Imposed Load [kN]	Average Pressure [MPa]	Average Stiffness K_{av} [kN/m]	Compression Modulus E_c [MPa]
DRB1	0.135	233.6	1.73	550853.9	404
DRB2	0.143	233.6	1.63	602975.0	417
DRB3	0.141	233.6	1.66	597053.3	419
DRB4	0.069	N/A	N/A	N/A	N/A
DRB5	0.074	N/A	N/A	N/A	N/A
DRB6	0.069	120.2	1.74	251687.8	361
DRB7	0.069	120.2	1.74	278983.5	400

Table 4-13 Vertical test results for 3.45 MPa vertical pressure

Specimen No.	Area $[m^2]$	Imposed Load [kN]	Average Pressure [MPa]	Average Stiffness K_{av} [kN/m]	Compression Modulus E_c [MPa]
DRB1	0.135	467.3	3.46	791048.8	580
DRB2	0.143	467.3	3.27	849319.3	588
DRB3	0.141	467.3	3.31	752785.8	529
DRB4	0.069	253.7	3.68	349938.19	502
DRB5	0.074	253.7	3.43	352040.6	471
DRB6	0.069	240.3	3.48	328721.9	472
DRB7	0.069	240.3	3.48	351392.3	504

Table 4-14 Vertical test results for extreme values of vertical pressure

Specimen No.	Area $[m^2]$	Imposed Load [kN]	Average Pressure [MPa]	Average Stiffness K_{av} [kN/m]	Compression Modulus E_c [MPa]
DRB1	0.135	N/A	N/A	N/A	N/A
DRB2	0.143	N/A	N/A	N/A	N/A
DRB3	0.141	N/A	N/A	N/A	N/A
DRB4	0.069	507.3	7.35	467372.6	671
DRB5	0.074	507.3	6.86	445858.5	596
DRB6	0.069	60.1	0.87	175617.3	252
DRB7	0.069	60.1	0.87	167190.4	240

consistent at around $414 MN/m^2$. The two sets of half-length bearings have consistently lower values of E_c at the same vertical pressures of testing. The pair denoted by DBR4/5 was not tested at 1.73 Mpa but at 3.45 Mpa and 6.90 Mpa, respectively. The set denoted by DBR6/7 was tested at 0.87 Mpa, 1.73 Mpa, and 3.45 Mpa. At the common test pressure of 3.45 Mpa the average of the two values of E_c of DBR4/5 was the same as that of DBR6/7, so that we can interpret the effect of variation of the target pressure over a eight-fold range of value. The fact that at the same pressures the E_c values for the full length bearings are higher than for the half-length bearings is most likely due to the longer influence of free ends in the latter case. The theoretical analysis was developed for the infinite length strip, and for the full-length bearings the length to height ratio of 7.5 is large enough that this assumption is still valid. At half this value the end effects can be expected to have some influence. The vertical stiffness of an elastomeric isolation bearing is always a difficult measurement to make, since the displacements at the vertical loads corresponding to practical use are extremely small and a great deal of scatter is to be expected.

It is clear, however, that there is for all test specimens a systematic increase in stiffness and E_c when the central value of the pressure around which the load is cycled is doubled from 1.73 MPa–3.45 MPa (250 psi–500 psi). At the higher pressure the average of the first three full-length isolators increases by 37% to $565 MN/m^2$. The half length bearing tests show a systematic increase in E_c over the complete range of pressure, the increase is not linear in pressure but tends to decrease with increasing pressure from 55% at the lowest level to 15% at the highest. This is consistent with the type of carbon fiber used in the bearings. The fiber is woven, two-directional, and epoxied into a thin sheet. As the pressure increases the in-plane fiber sheet tension increases and tends to straighten out the fiber strands, thus increasing the effective fiber modulus.

To assess the effect of the various parameters on the vertical stiffness it is necessary to estimate the actual shear modulus from the tests on shear. At a vertical pressure of 3.45 MPa (500 psi) the average shear stiffness of the first three bearings when tested in the longitudinal direction $0°$ is 1.278 MN/m which with an average area of $0.140 m^2$ and a thickness of rubber of 99 mm implies a shear modulus of 0.904 MPa (131 psi) — considerably larger than the nominal modulus from the fabricator. This use of the longitudinal tests to provide an estimate of the modulus is warranted by the fact that this case will have the least influence of the roll-off from the unbonded end condition.

A steel reinforced isolator with this shear modulus and this area of rubber thickness would, if compressibility effects are ignored, have an effective compression modulus E_c (Eq. 2.10) of $3738 MN/m^2$. When compressibility is taken into account the effective modulus is considerably reduced as given by Eq. (2.33). To estimate λ we use K=2000 MPa (290,000 psi) giving $\lambda = 5.3$, and from Eq. (2.33) we have $1150 MN/m^2$. The average measured value $563 MN/m^2$, can be used to deduce the effect of the extensibility of the carbon fiber reinforcement. For this purpose we now turn to Eq. (2.31) and assume that $\lambda = 5.3$. From the results we have $E_c/K = 0.28$ and from the equation we determine that $(\lambda + \mu)^{\frac{1}{2}} = 3.7$, implying $\mu = 8.4$. When the known values of the various parameters are inserted into the definition of μ we finally obtain the estimate of E_f as 14000 MPa.

Unfortunately there was no equipment in the test laboratory to directly measure the modulus of the carbon fiber sheet, nor has the fabricator provided a value. The result is somewhat lower than others quoted for carbon/epoxy sheets and the reason is not clear, but the sheets appear to be a very poor quality fiber with actual fiber constituting only 20–25%. The rest are holes, and the portion of the thickness that is fiber cannot be determined from visual analysis. It is certainly possible that the quality of the reinforcing could be improved but it is clear that this poor quality sheet is adequate for these bearings. An effective modulus E_c of $563 MN/m^2$ at an average pressure of 3.45 MPa implies a vertical vibrational frequency of 20 Hz, which is more than necessary in any isolation application. The conclusion is that although the fiber appears to be of very low quality, and presumably low-cost, it has sufficient stiffness and strength for application to low-cost isolators.

One significant if qualitative observation from the test program is that the most likely source of damage to an isolator is debonding when it is loaded across a saw-cut surface. This factor will be addressed in future development.

5 Conclusions

The test results show that the concept of a strip isolator reinforced with carbon fiber is viable. Because the isolator can be made in long, wide sheets and cut to the required width, the cost of the isolator can be reduced to a level that is acceptable for low-priced public housing. The tests also show that loading in the direction of the strip across a cut surface is not good, that the cut surface tends to be a source of delamination. In practice this should not be a problem, since the width of the manufactured sheet will be used as the length of the strip isolator and the ends will be finished ends and not cut. Loading in the transverse direction (90º), where the edges are cut, is not so severe because the rolling of the strip tends to produce lower forces in this direction. The most vulnerable direction of loading is at 45º, which appears to put a very distorted pattern of displacement on the isolator. For this reason it may be advisable to use either a better cutting method such as a water jet that will leave a smoother finished surface than a steel saw, or to finish the edge by a cold bonded surface layer.

The carbon fiber appeared to be very poor quality. The fibers were laid out in only two directions and in a woven sheet with many gaps. Nevertheless, the isolators still functioned acceptably. It would be possible to make a much better isolator with a better quality carbon fiber at little increase in cost.

The unresolved issue in the test program is that of overall system behavior, namely, can an isolation system made of strip isolators laid out in an orthogonal grid protect a masonry wall superstructure above. Isolators loaded in the longitudinal direction stiffen with increasing displacement and those loaded across the strip will soften with displacement above a certain threshold level. This poses the question of whether the unbalanced shear be accommodated by the wall system. Further research is needed to study this effect might and best be undertaken by testing a fiber-isolated masonry block house model on a large shake table.

It is important to recall that the benefit of isolation is achieved primarily through the ratio of the isolated period of the building to its fixed-base period. For a constant velocity spectrum, the base shear of the fixed-base building is reduced by this factor when the same building is isolated. A masonry wall structure will have an extremely short fixed-base period, in the range of 0.10 sec. A reduction by a factor of 10 can be obtained with an isolation period of 1 sec, which is not difficult to obtain. In fact, the code formula for isolation system displacement, which has remained unchanged throughout all versions of seismic isolation codes in the U.S. since the earliest in 1986, would predict a displacement of 15 cm. (6 in.) for a 1.5 sec period system. The isolators in our study tested to displacements of 15 cm. (6 in.) and more. However, if larger displacements are needed, the tests showed that stacking two isolators on top of each other was possible and would allow even larger displacements.

A shake table test using a full-size masonry block house would help clarify details of access across the isolation interface, the disadvantages, if any, of not having the bottom floor slab on the grade isolated, and the extent to which a concrete tie strip is needed between the isolators and the block wall. When these remaining uncertainties are resolved, this promising new technology can be implemented in many highly seismic areas in the developing world.

References

International Conference of Building Officials. 1997. Earthquake regulations for seismic isolated structures. *Uniform Building Code,* Appendix Chapter 16. Whittier, Calif.: ICBO.

Rocard Y. 1937. Note sur le calcul des propriétés élastique des supports en caoutchouc adhérent. *J. de Physique et de Radium* 8:197.

Gent A. N., and P. B. Lindley. 1959. The compression of bonded rubber blocks. In *Proceedings Institution of Mechanical Engineers* 173(3): 111–17.

Gent A. N., and Meinecke E. A. 1970. Compression, bending and shear of bonded rubber blocks. *Polymer Engineering and Science* 10(2): 48–53.

Appendix

The complete set of hysteresis loops for all tests carried out on the fiber-reinforced isolators is contained in this appendix.

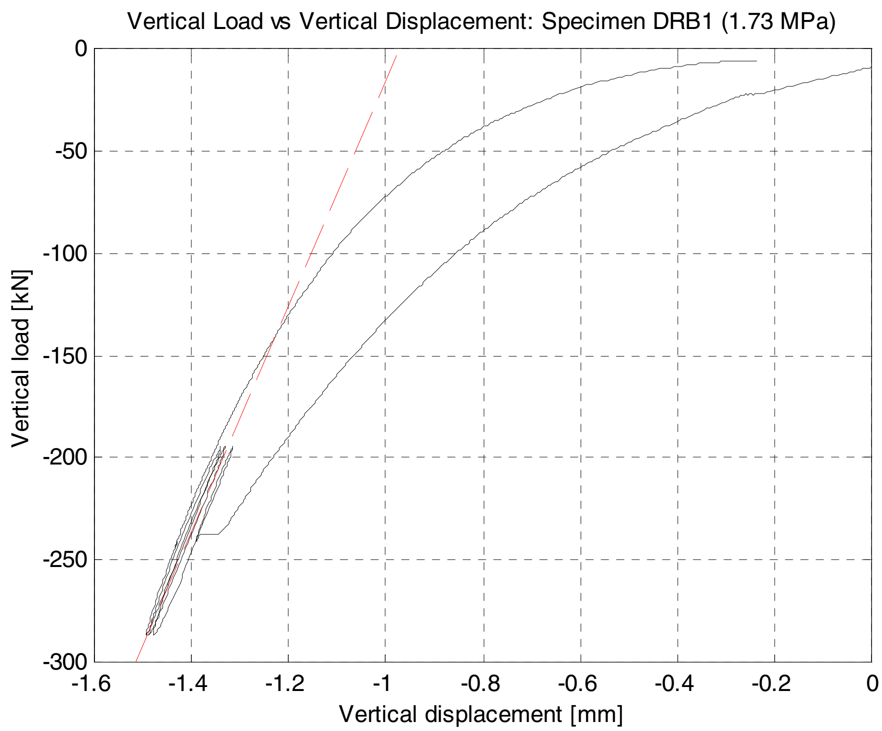

Figure A.1. Vertical test results for DRB1 with 1.73 MPa vertical pressure

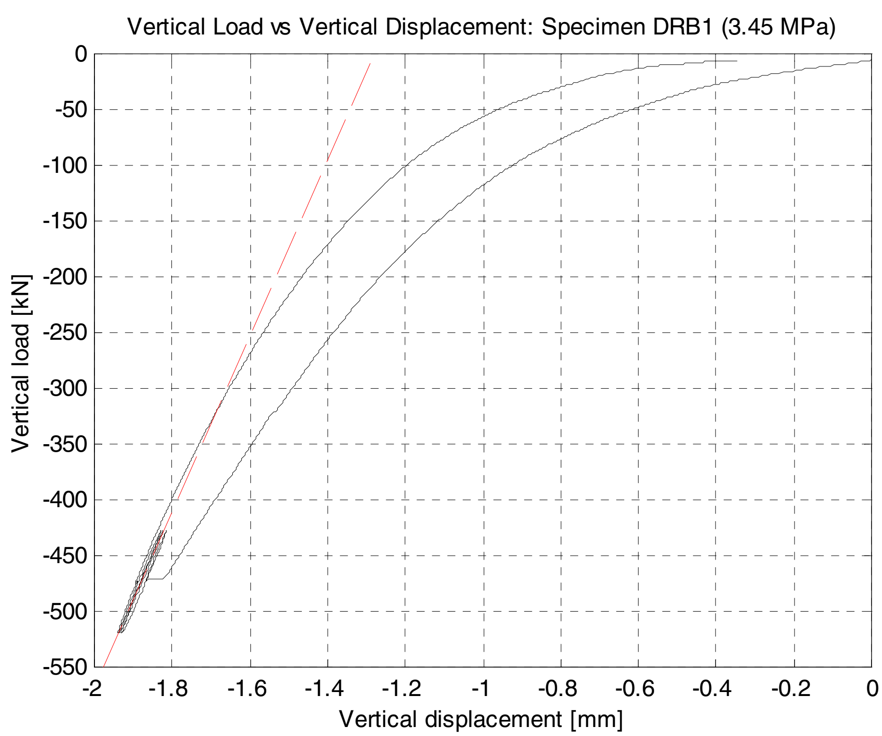

Figure A.2. Vertical test results for DRB1 with 3.45 MPa vertical pressure

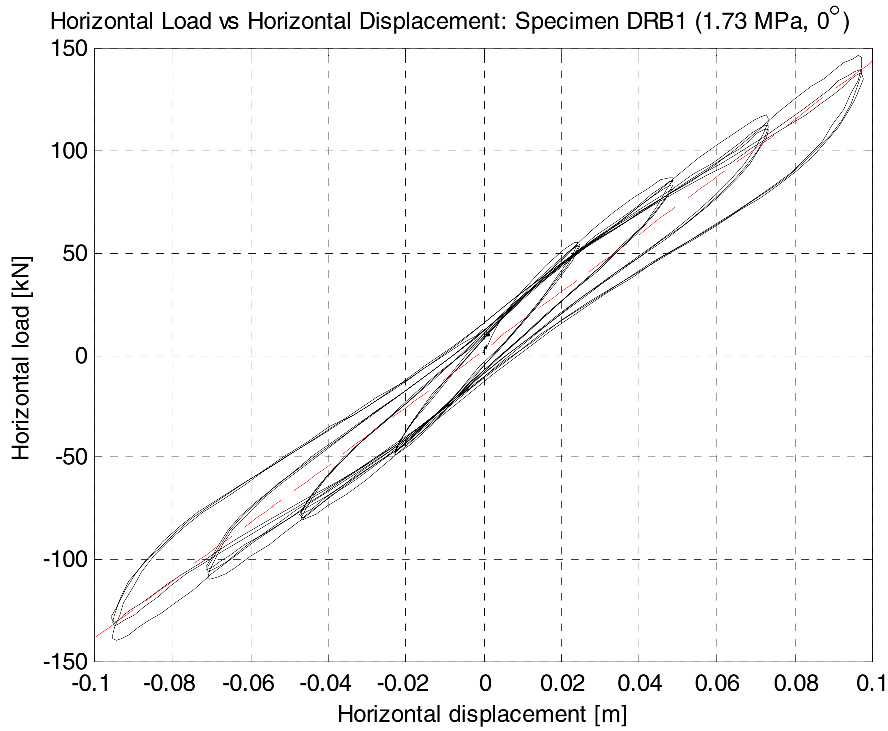

Figure A.3. Horizontal test results for DRB1 with 1.73 MPa vertical pressure (0°)

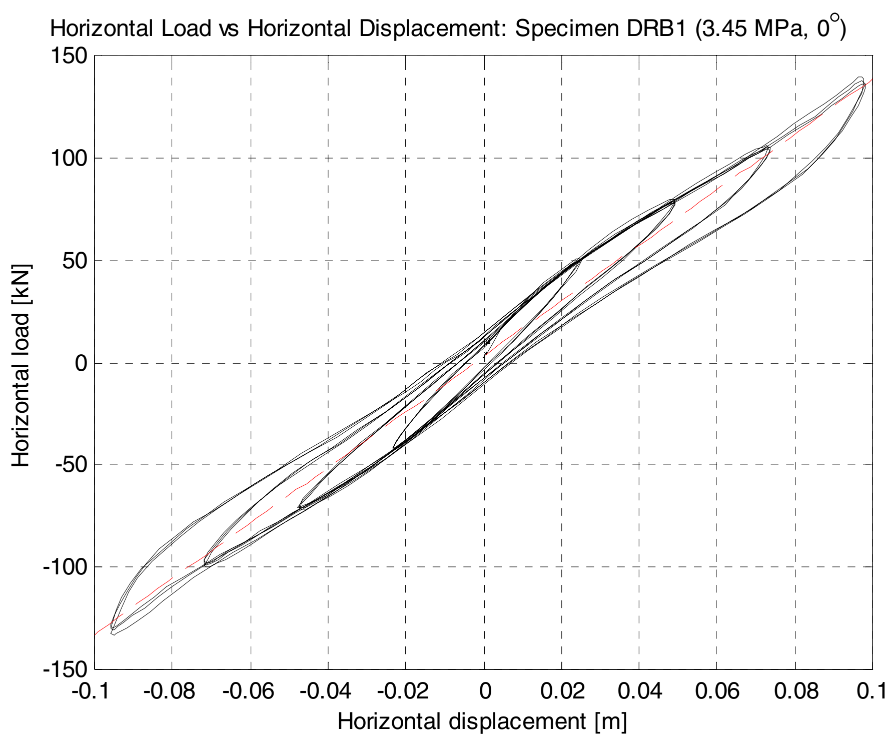

Figure A.4. Horizontal test results for DRB1 with 3.45 MPa vertical pressure (0°)

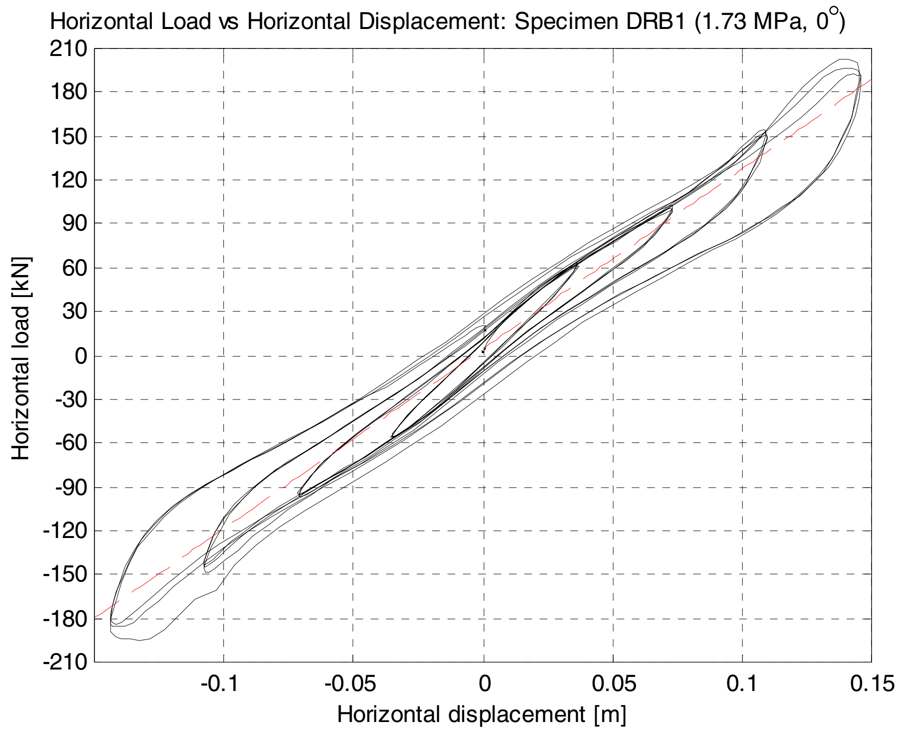

Figure A.5. Horizontal test results for DRB1 with 1.73 MPa vertical pressure (0°)

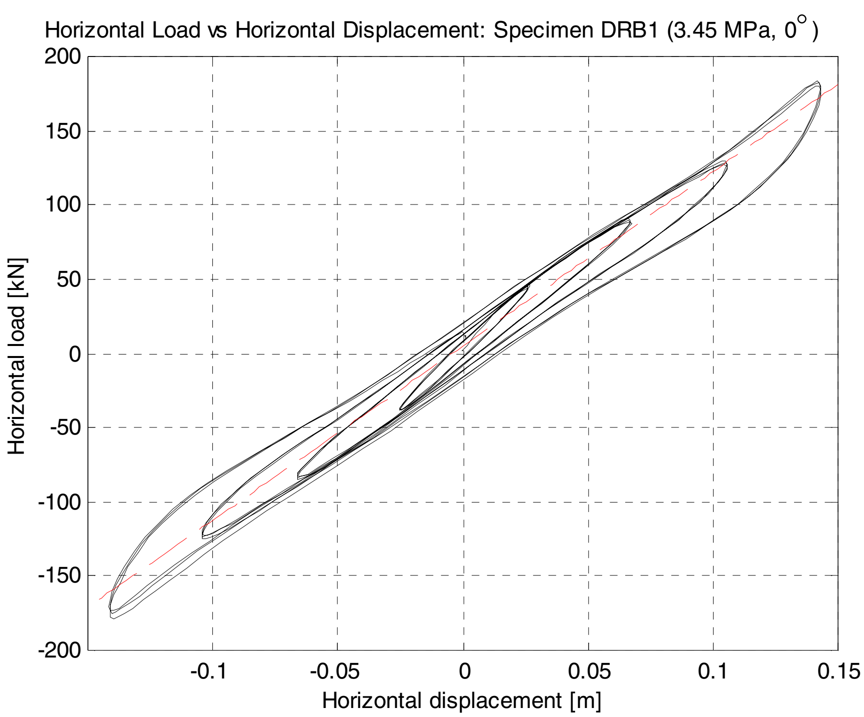

Figure A.6. Horizontal test results for DRB1 with 3.45 MPa vertical pressure (0°)

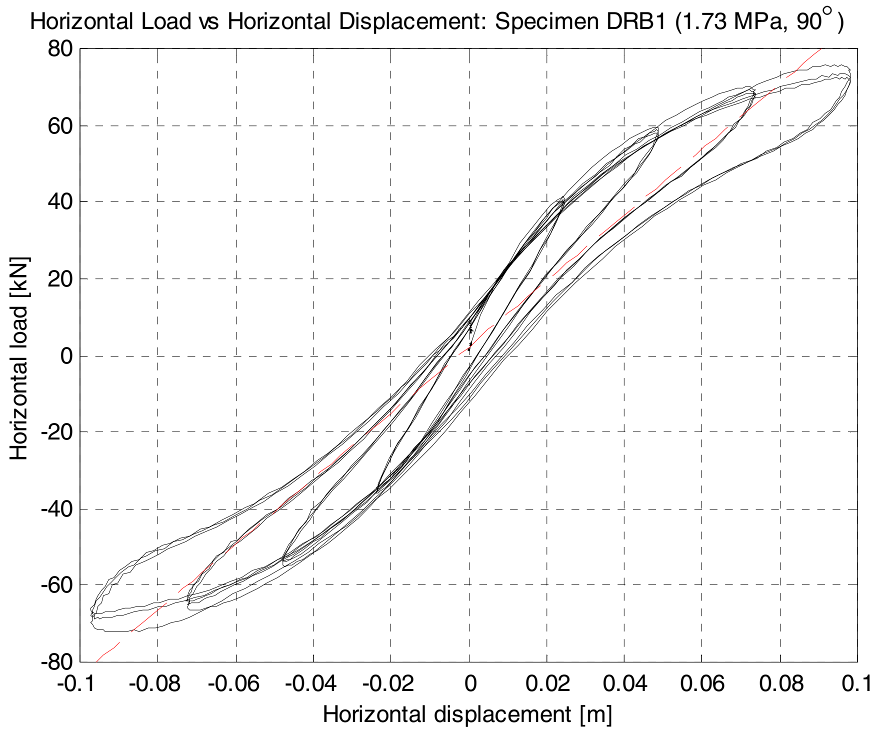

Figure A.7. Horizontal test results for DRB1 at 1.73 MPa vertical pressure (90°)

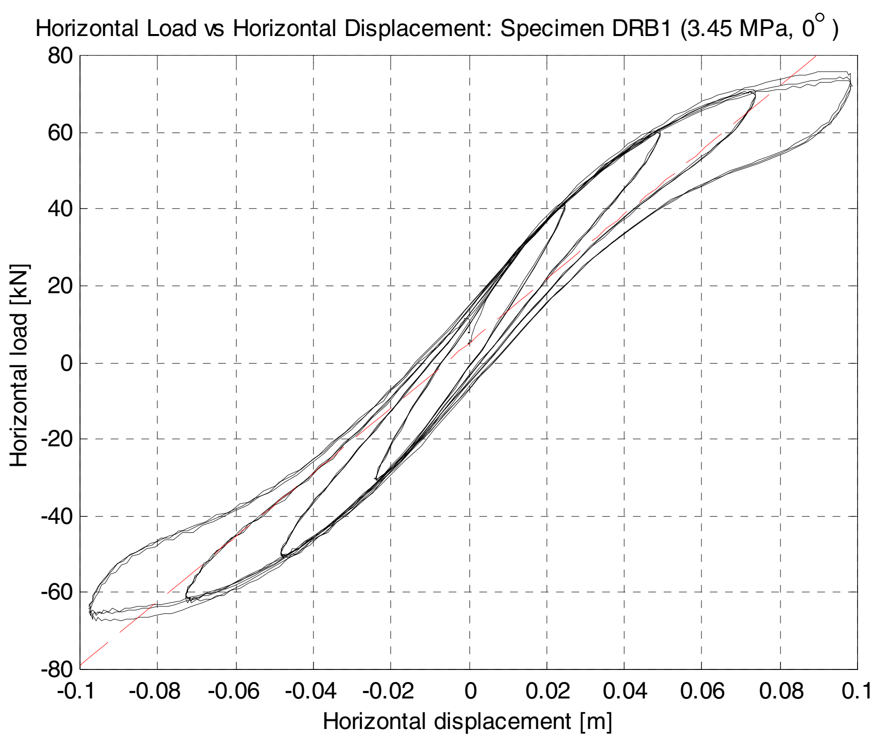

Figure A.8. Horizontal test results for DRB1 at 3.45 MPa vertical pressure (90°)

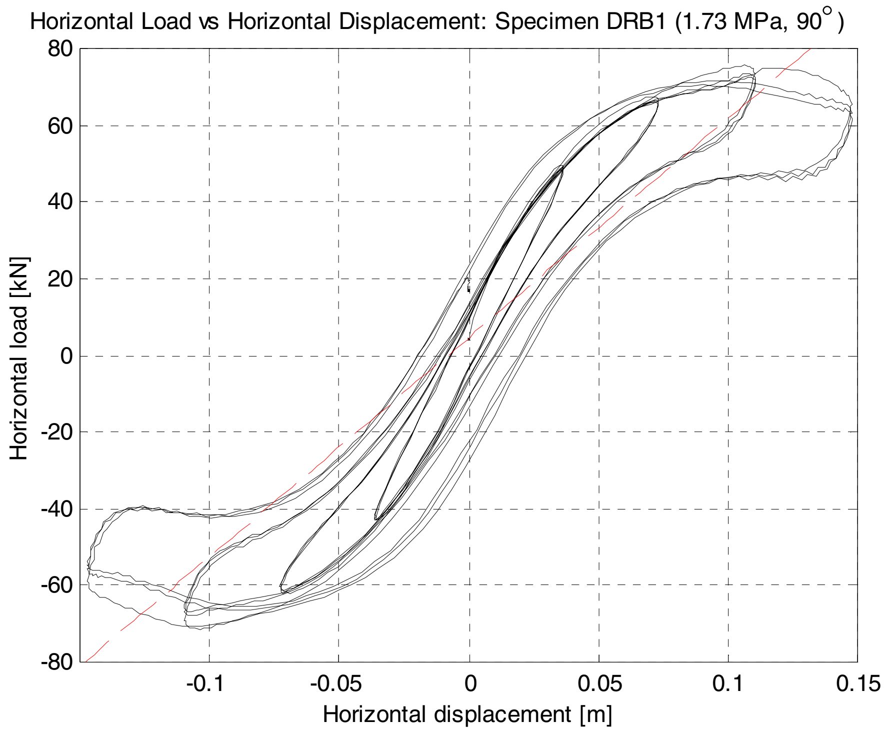

Figure A.9. Horizontal test results for DRB1 at 1.73 MPa vertical pressure (90°)

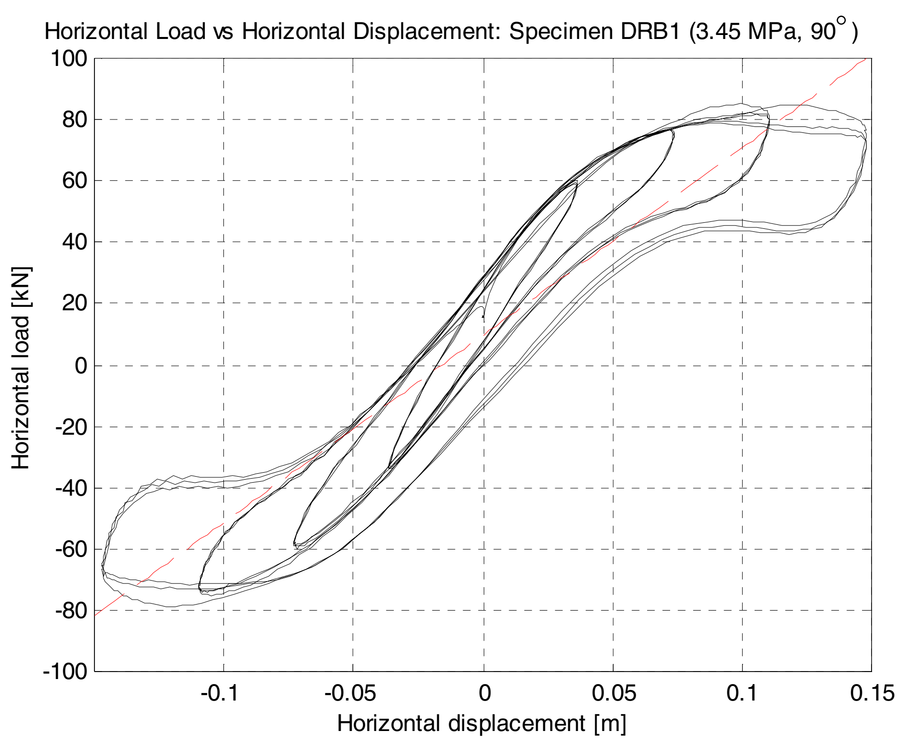

Figure A.10. Horizontal test results for DRB1 at 3.45 MPa vertical pressure (90°)

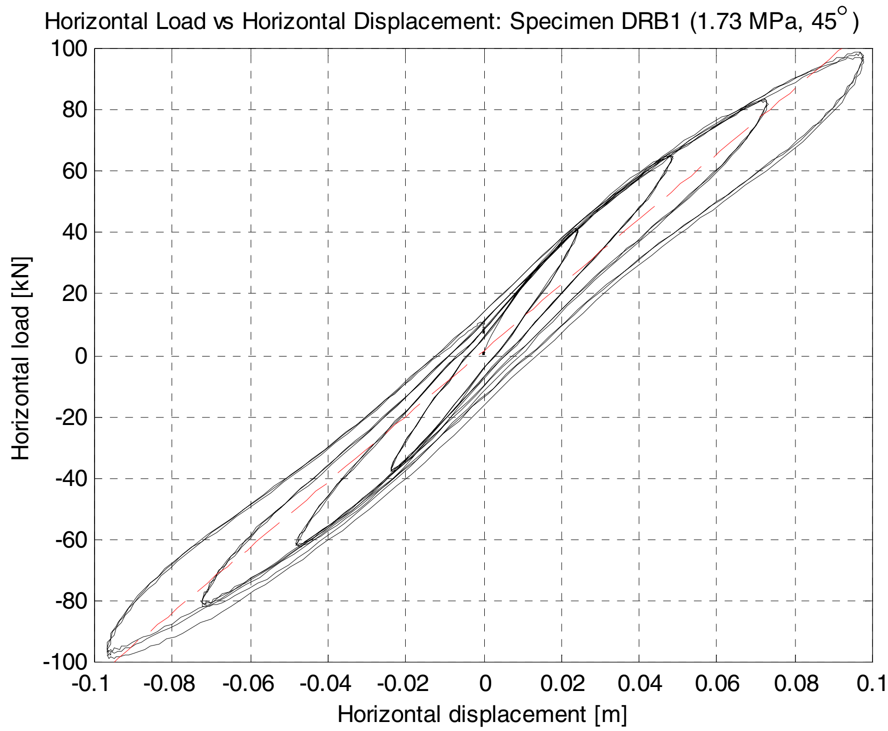

Figure A.11. Horizontal test results for DRB1 at 1.73 MPa vertical pressure (45°)

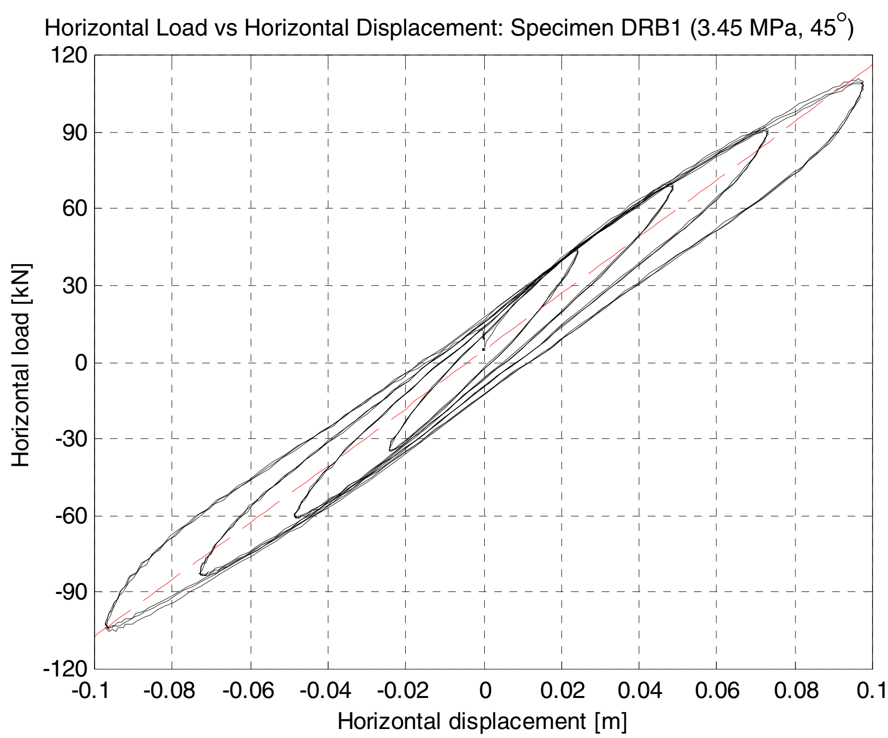

Figure A.12. Horizontal test results for DRB1 at 3.45 MPa vertical pressure (45°)

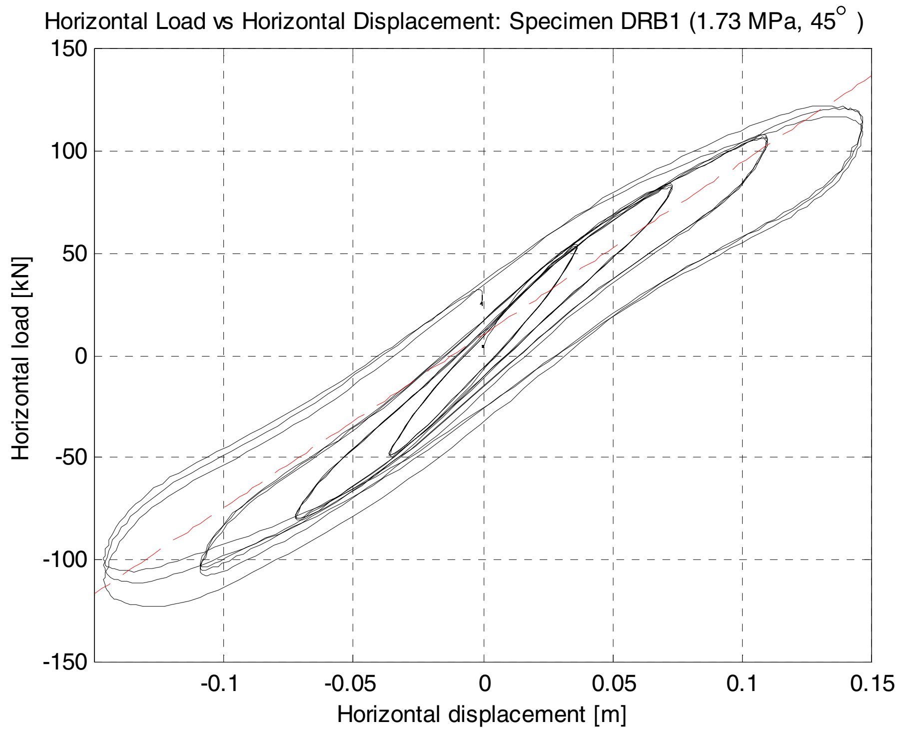

Figure A.13. Horizontal test results for DRB1 at 1.73 MPa vertical pressure (45°)

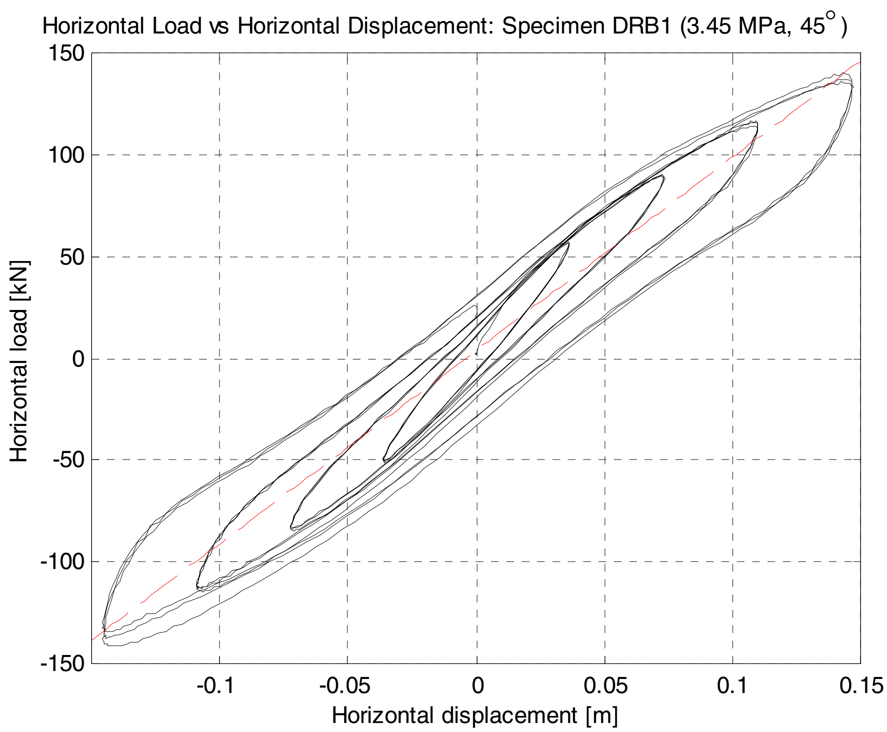

Figure A.14. Horizontal test results for DRB1 at 3.45 MPa vertical pressure (45°)

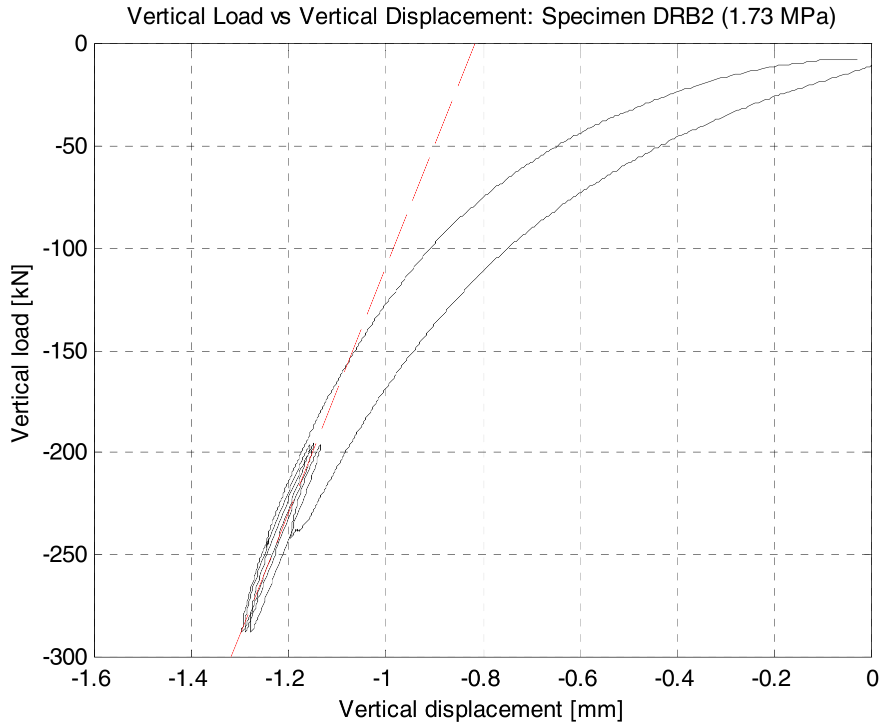

Figure A.15. Vertical test results for DRB2 with 1.73 MPa vertical pressure

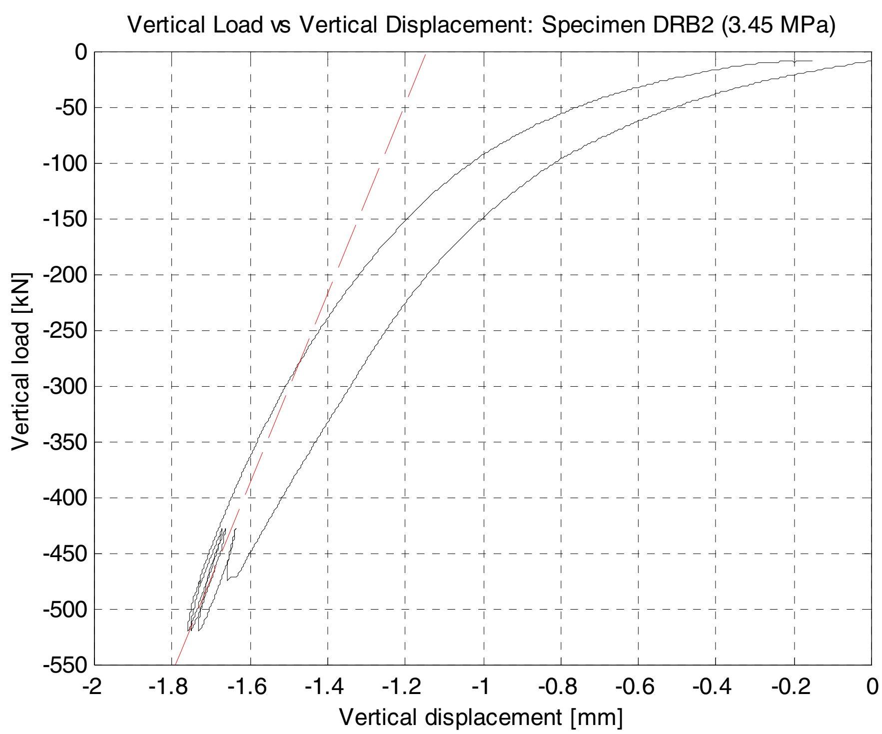

Figure A.16. Vertical test results for DRB2 with 3.45 MPa vertical pressure

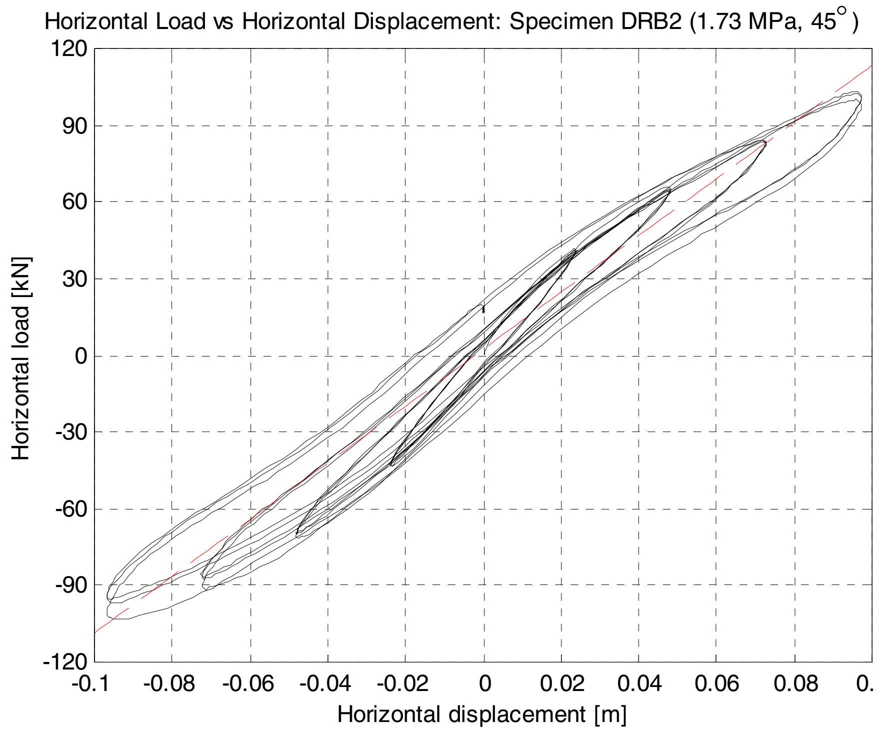

Figure A.17. Horizontal test results for DRB2 at 1.73 MPa vertical pressure (45°)

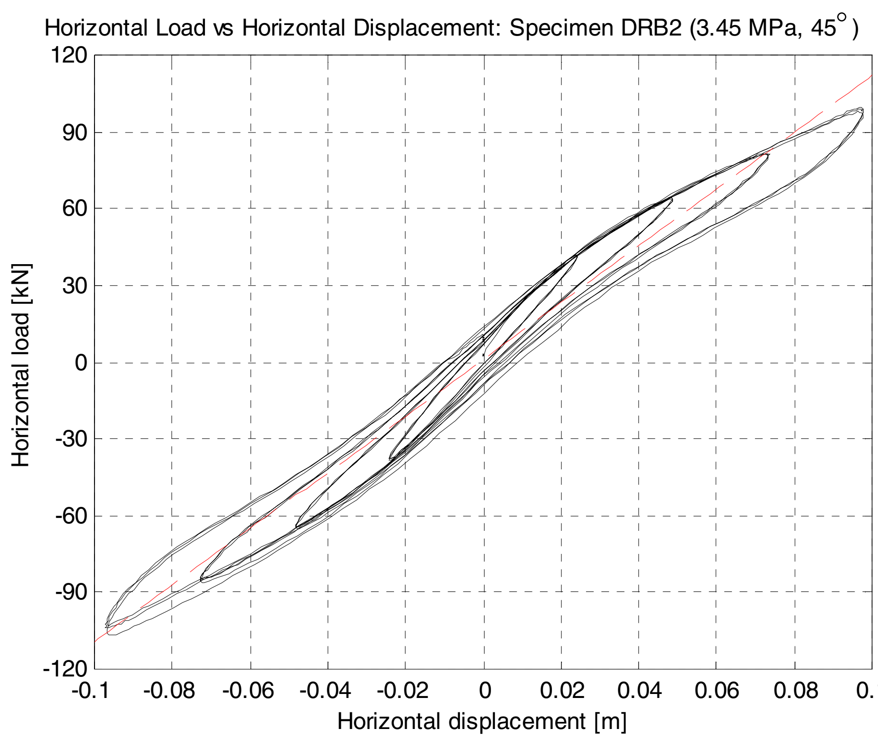

Figure A.18. Horizontal test results for DRB2 at 3.45 MPa vertical pressure (45°)

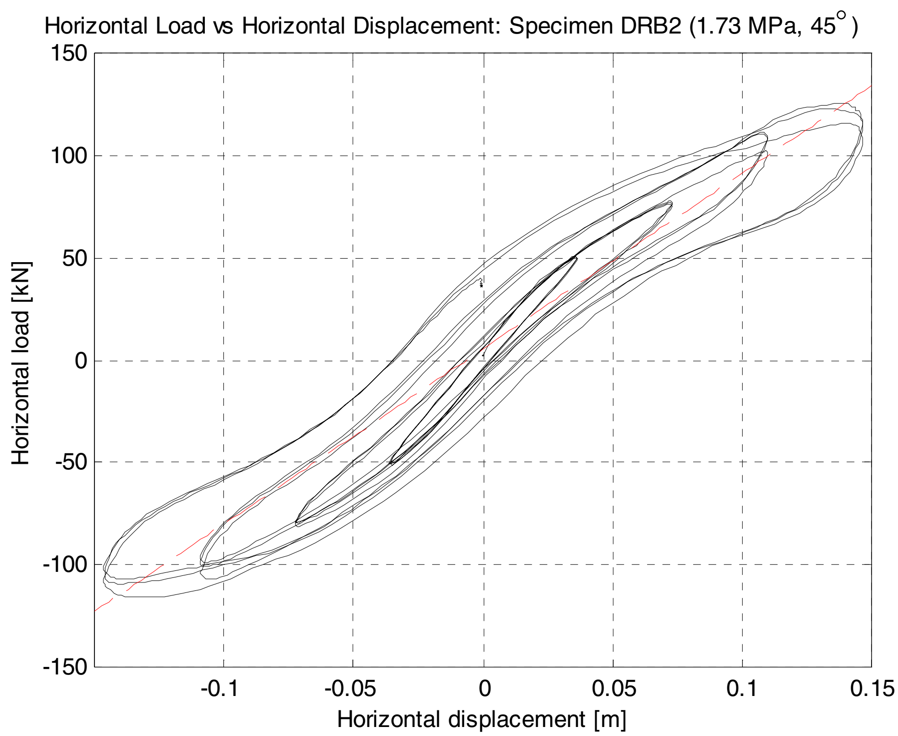

Figure A.19. Horizontal test results for DRB2 at 1.73 MPa vertical pressure (45°)

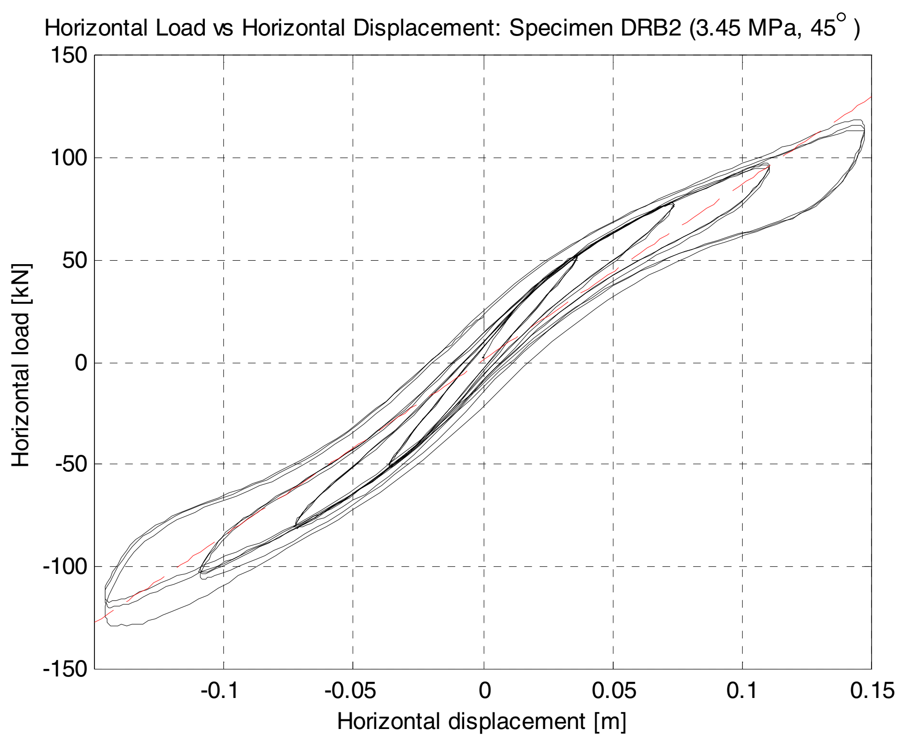

Figure A.20. Horizontal test results for DRB2 at 3.45 MPa vertical pressure (45°)

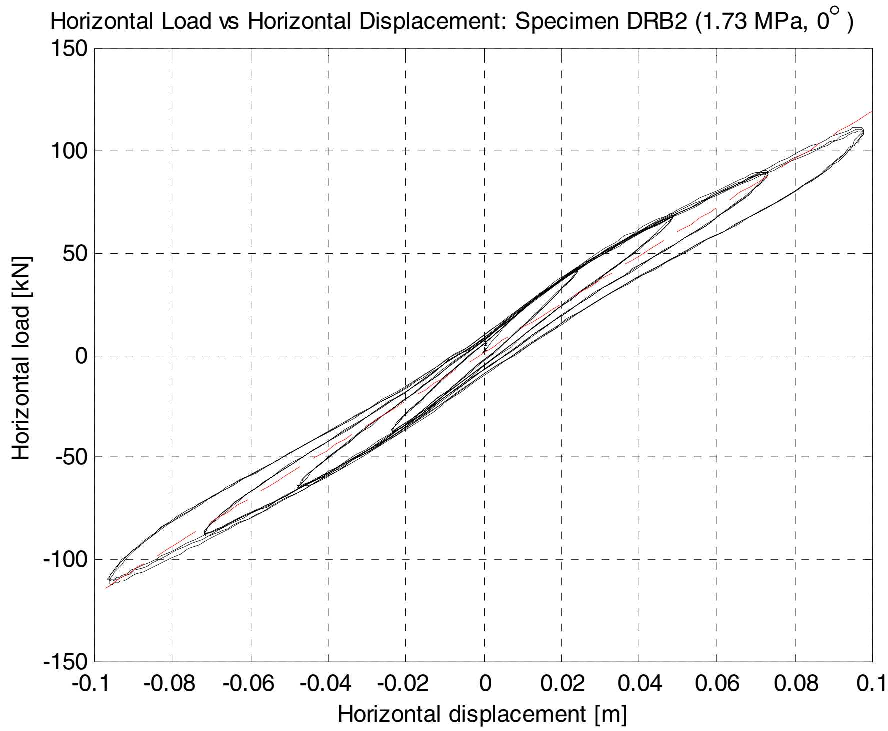

Figure A.21. Horizontal test results for DRB2 with 1.73 MPa vertical pressure (0°)

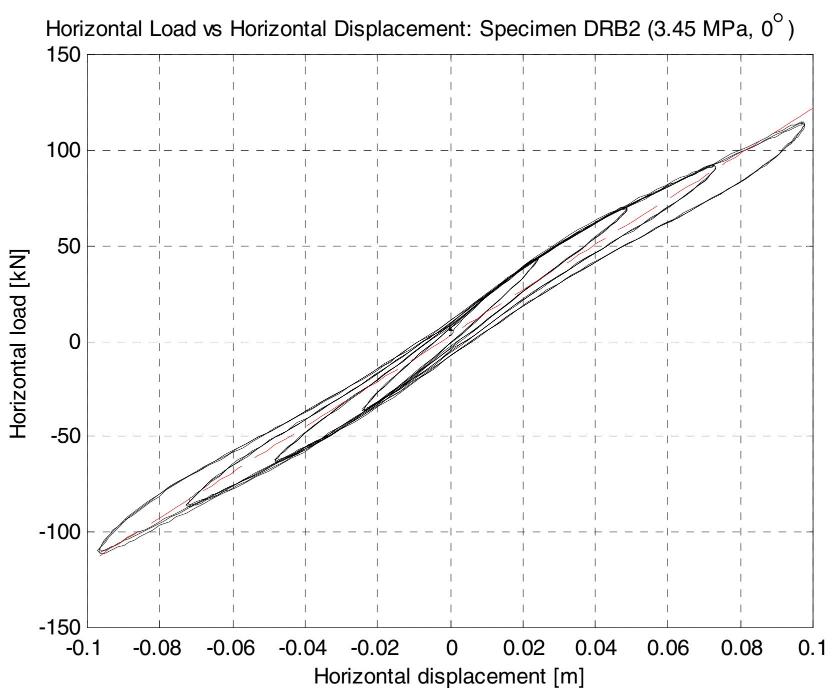

Figure A.22. Horizontal test results for DRB2 with 3.45 MPa vertical pressure (0°)

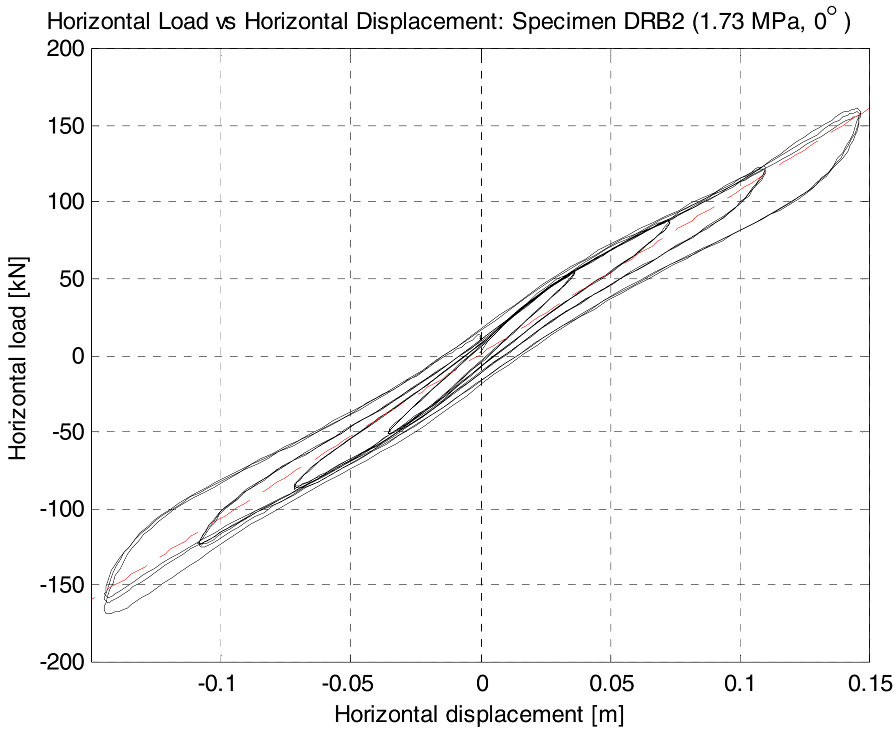

Figure A.23. Horizontal test results for DRB2 with 1.73 MPa vertical pressure (0°)

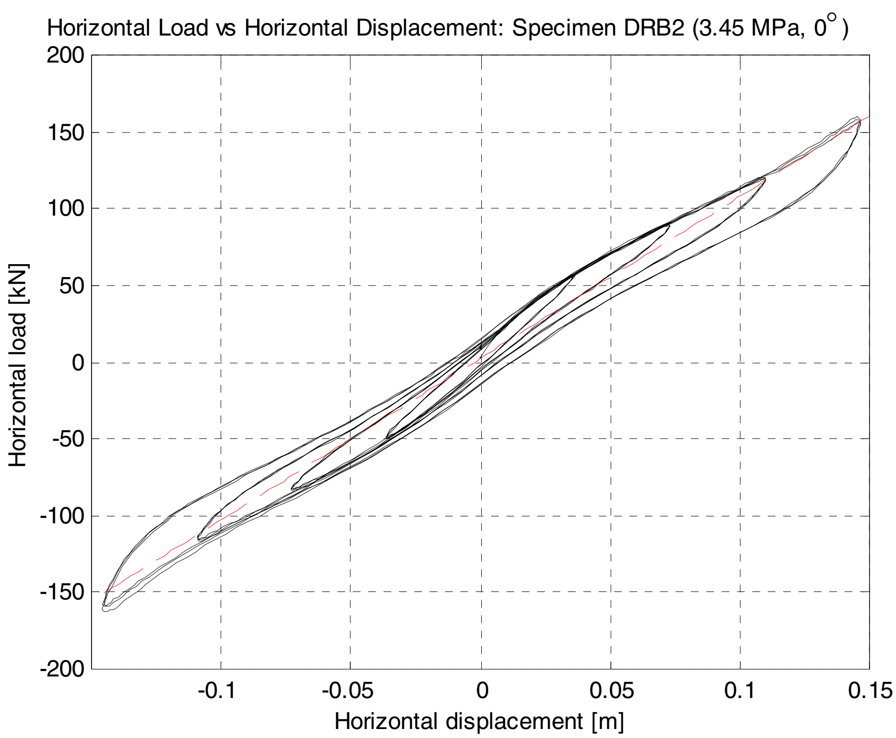

Figure A.24. Horizontal test results for DRB2 with 3.45 MPa vertical pressure (0°)

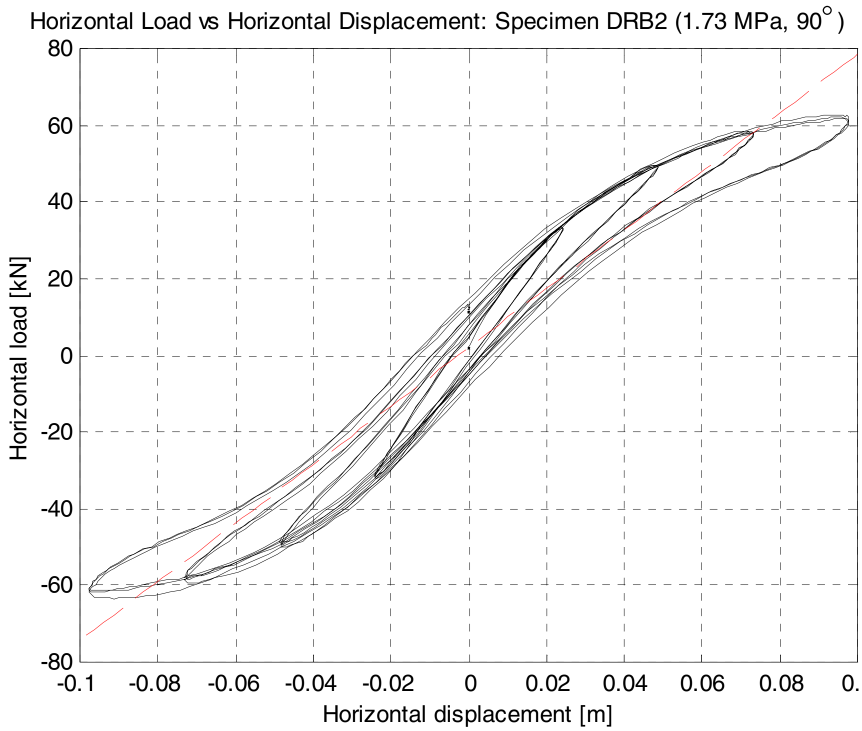

Figure A.25. Horizontal test results for DRB2 at 1.73 MPa vertical pressure (90°)

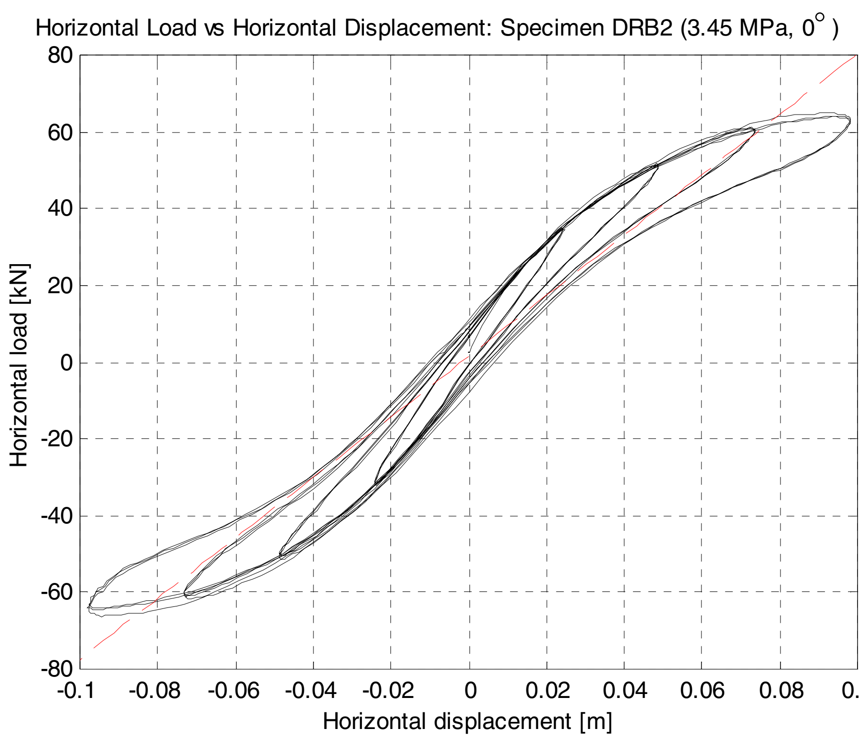

Figure A.26. Horizontal test results for DRB2 at 3.45 MPa vertical pressure (90°)

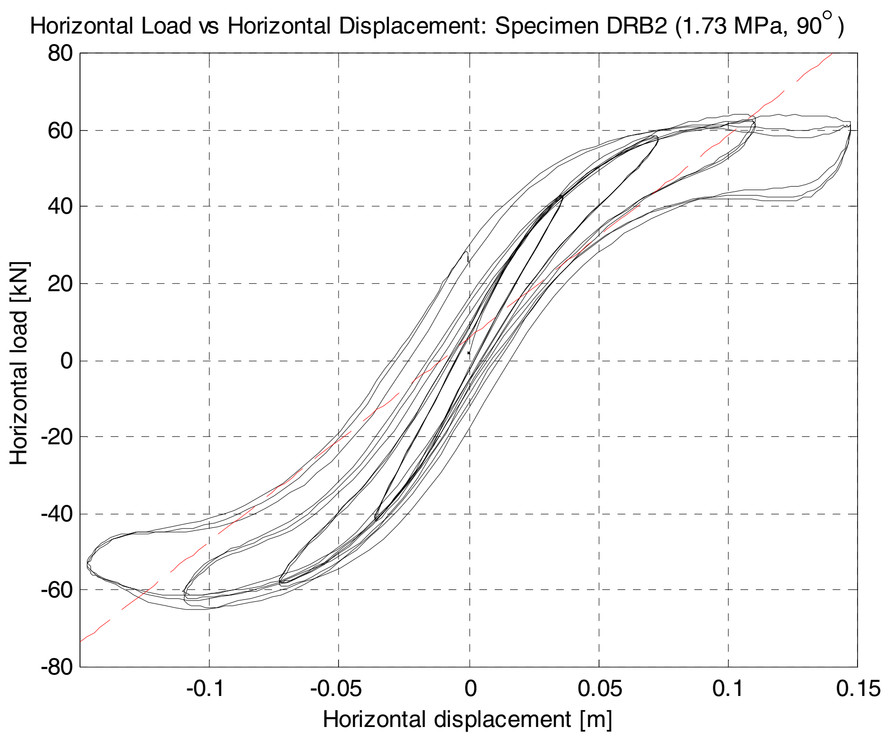

Figure A.27. Horizontal test results for DRB2 at 1.73 MPa vertical pressure (90°)

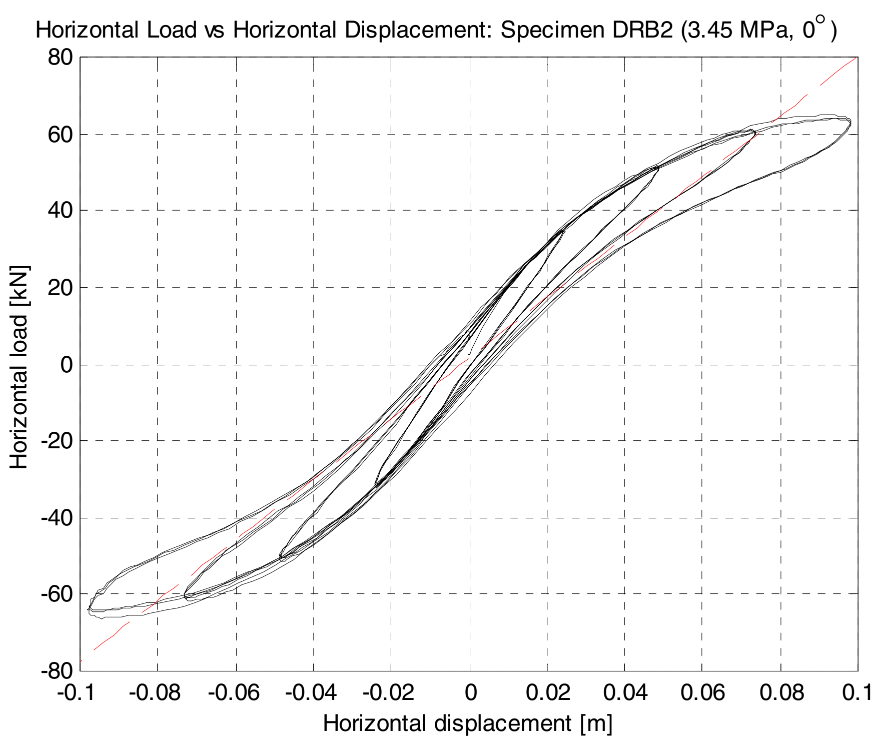

Figure A.28. Horizontal test results for DRB2 at 3.45 MPa vertical pressure (90°)

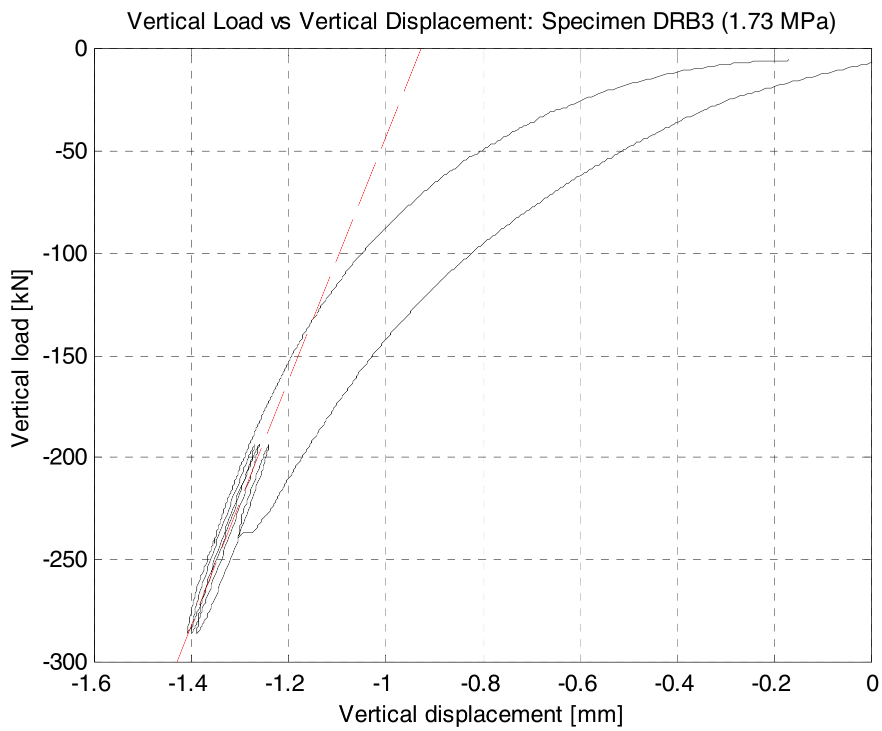

Figure A.29. Vertical test results for DRB3 with 1.73 MPa vertical pressure

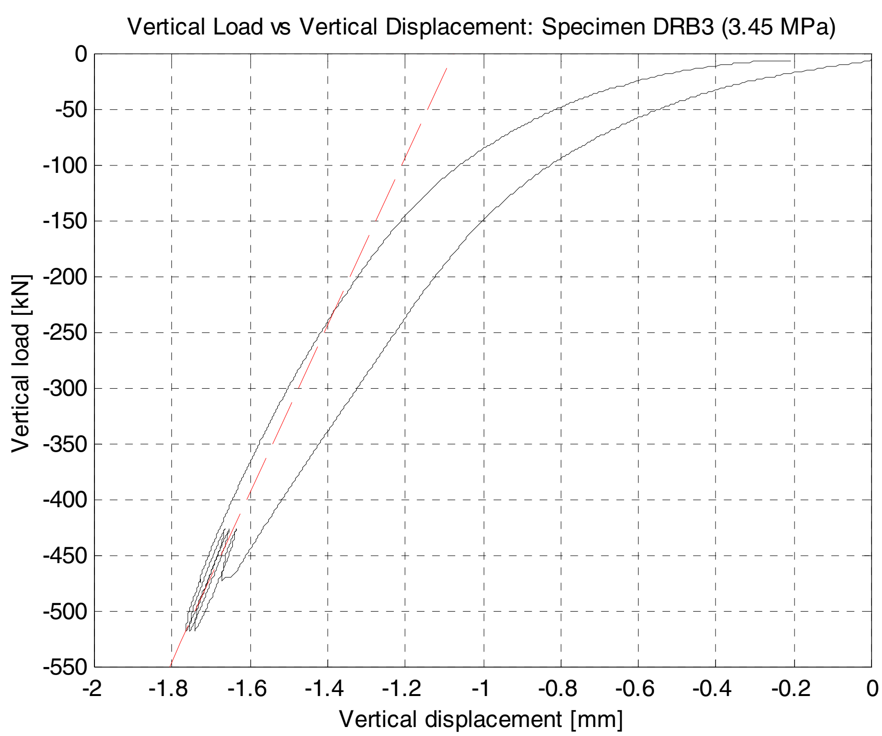

Figure A.30. Vertical test results for DRB3 with 3.45 MPa vertical pressure

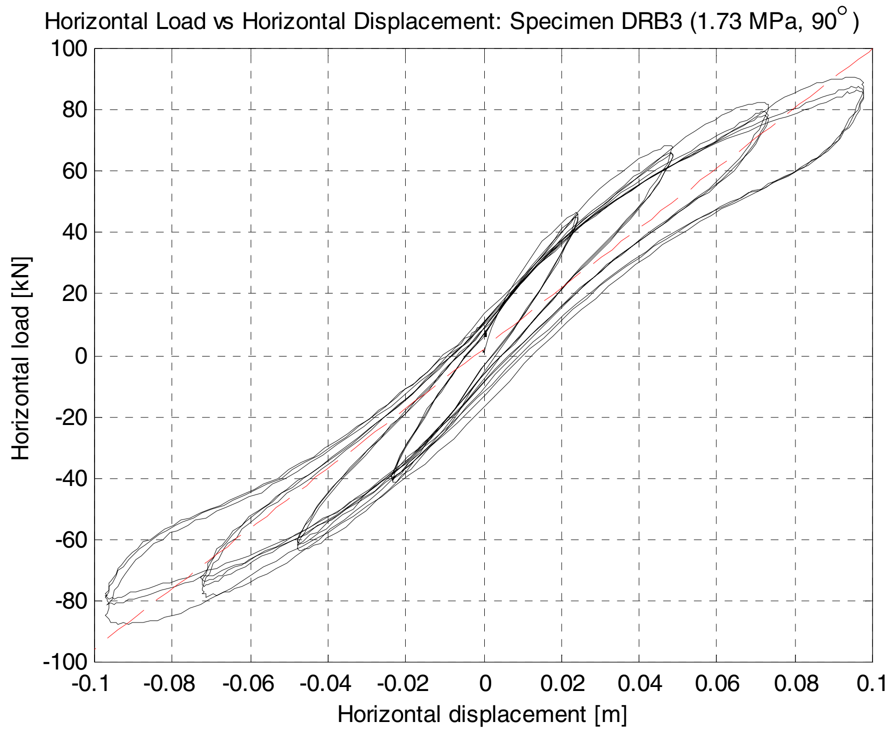

Figure A.31. Horizontal test results for DRB3 at 1.73 MPa vertical pressure (90°)

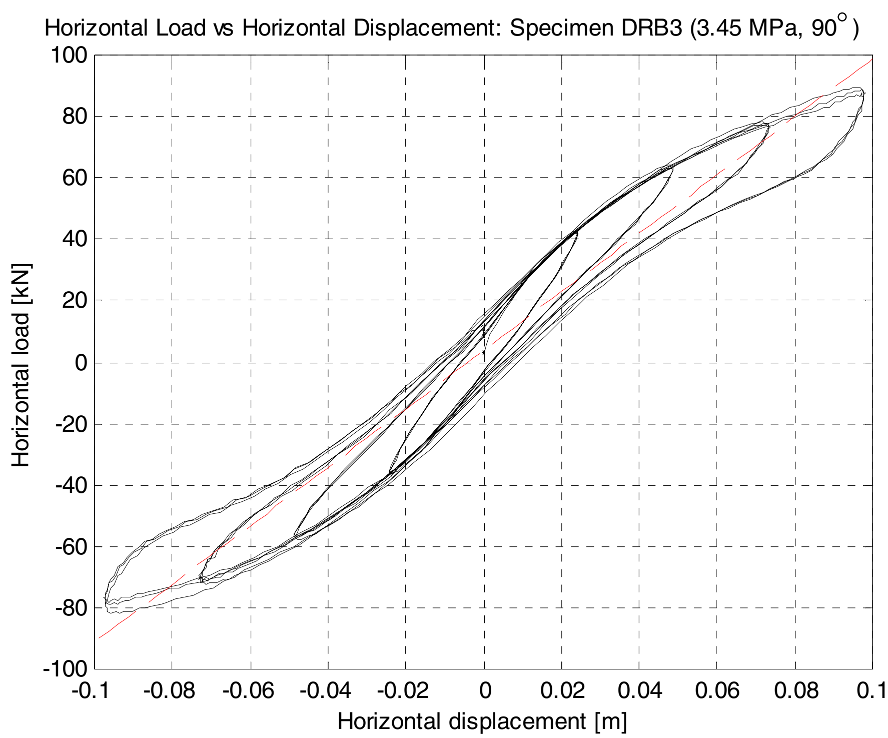

Figure A.32. Horizontal test results for DRB3 at 3.45 MPa vertical pressure (90°)

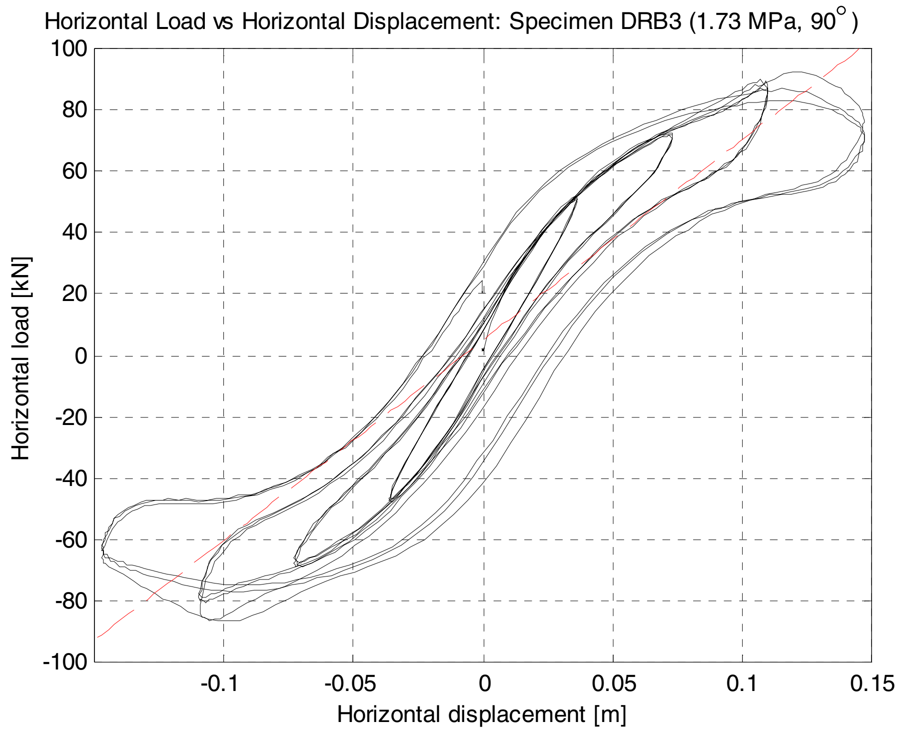

Figure A.33. Horizontal test results for DRB3 at 1.73 MPa vertical pressure (90°)

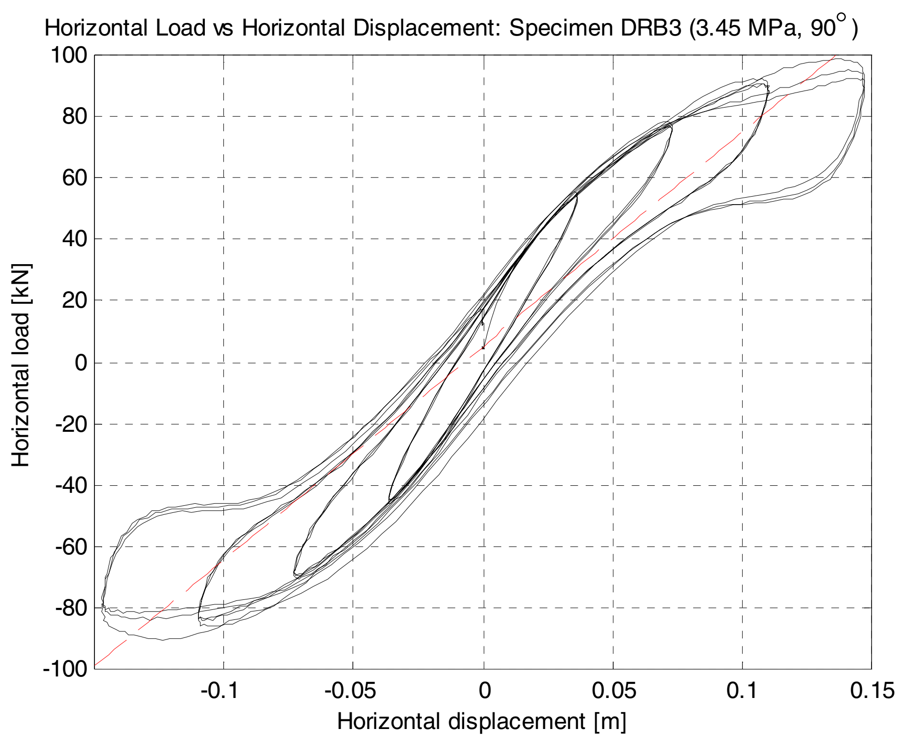

Figure A.34. Horizontal test results for DRB3 at 3.45 MPa vertical pressure (90°)

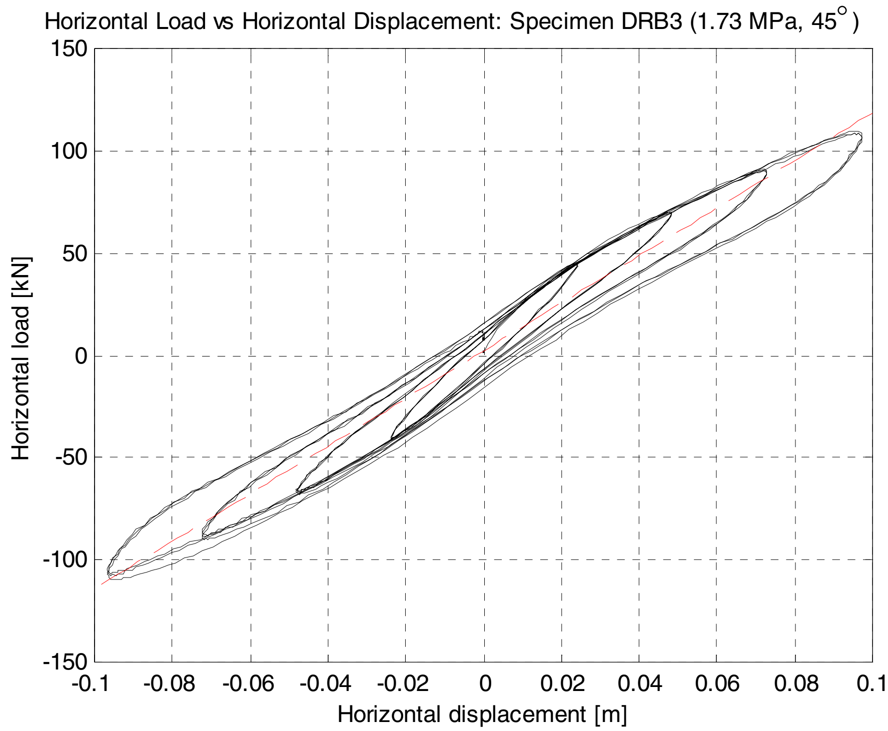

Figure A.35. Horizontal test results for DRB3 at 1.73 MPa vertical pressure (45°)

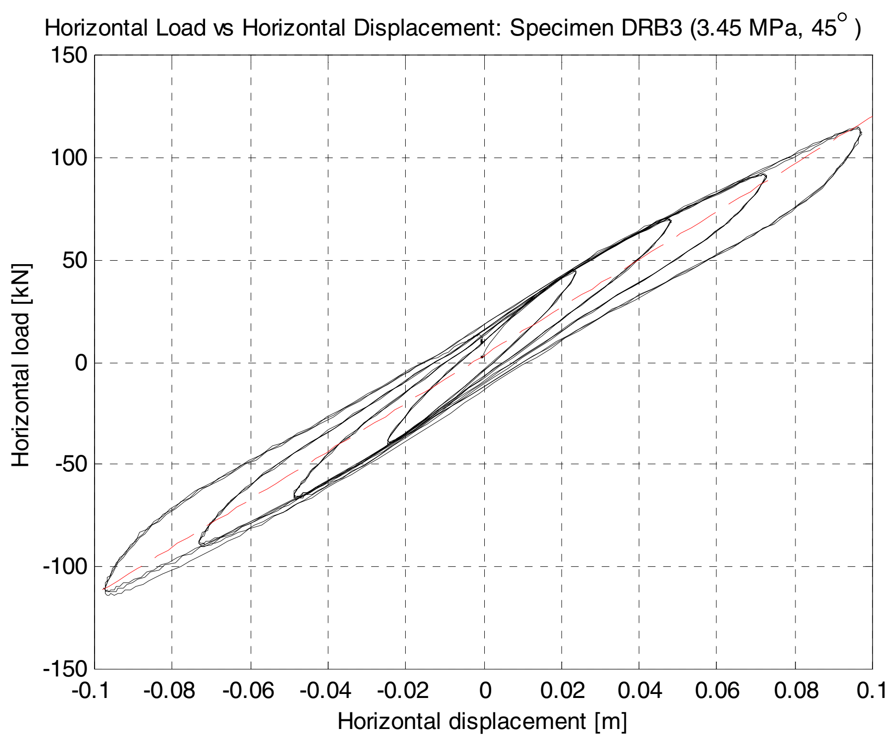

Figure A.36. Horizontal test results for DRB3 with 3.45 MPa vertical pressure (45°)

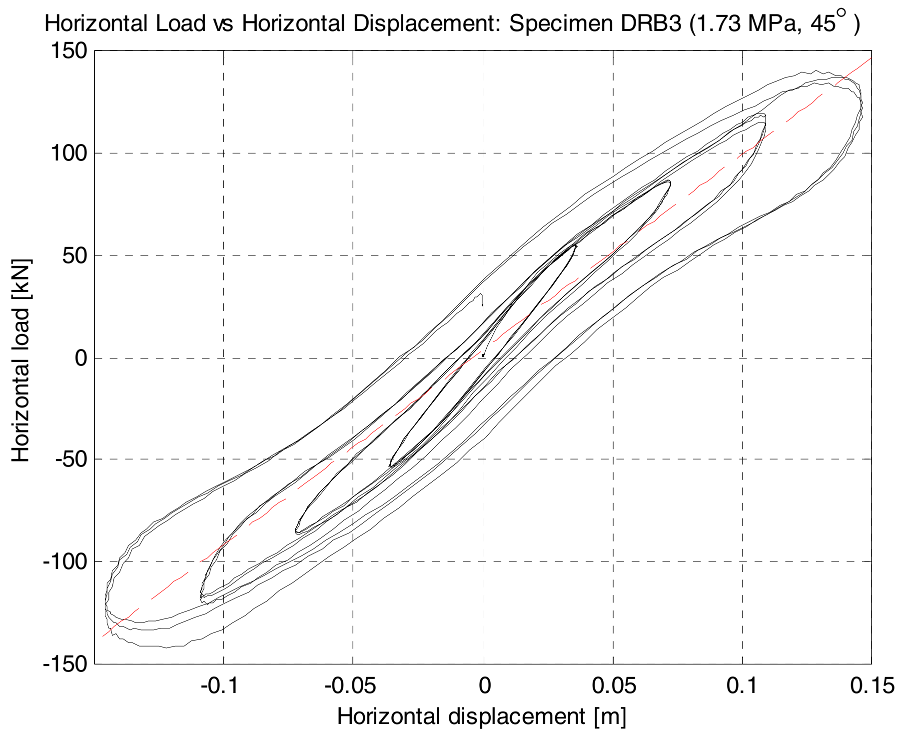

Figure A.37. Horizontal test results for DRB3 with 1.73 MPa vertical pressure (45°)

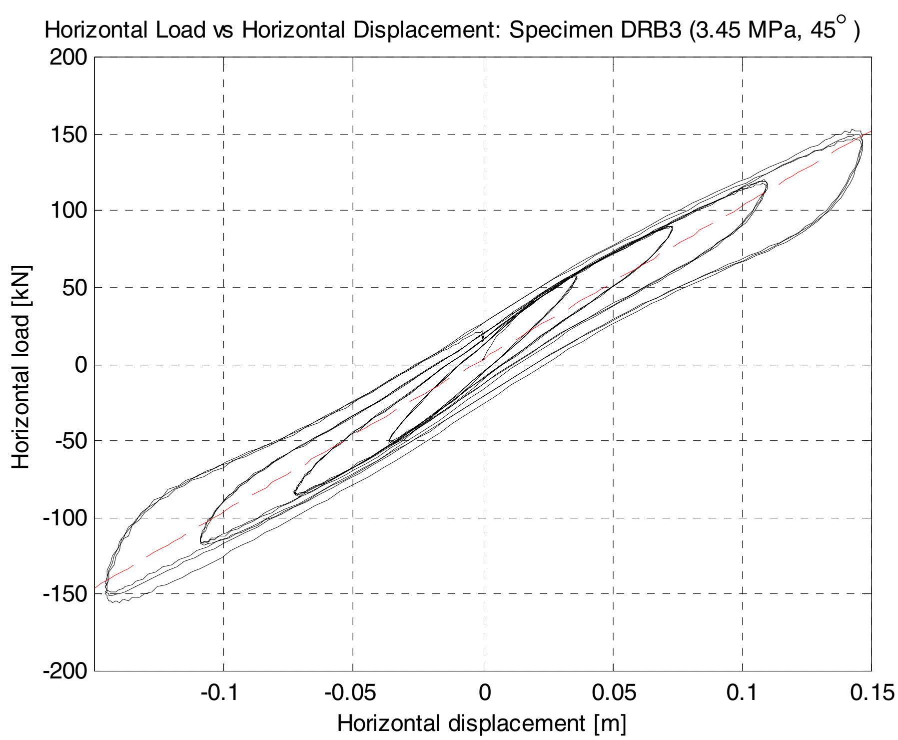

Figure A.38. Horizontal test results for DRB3 with 3.45 MPa vertical pressure (45°)

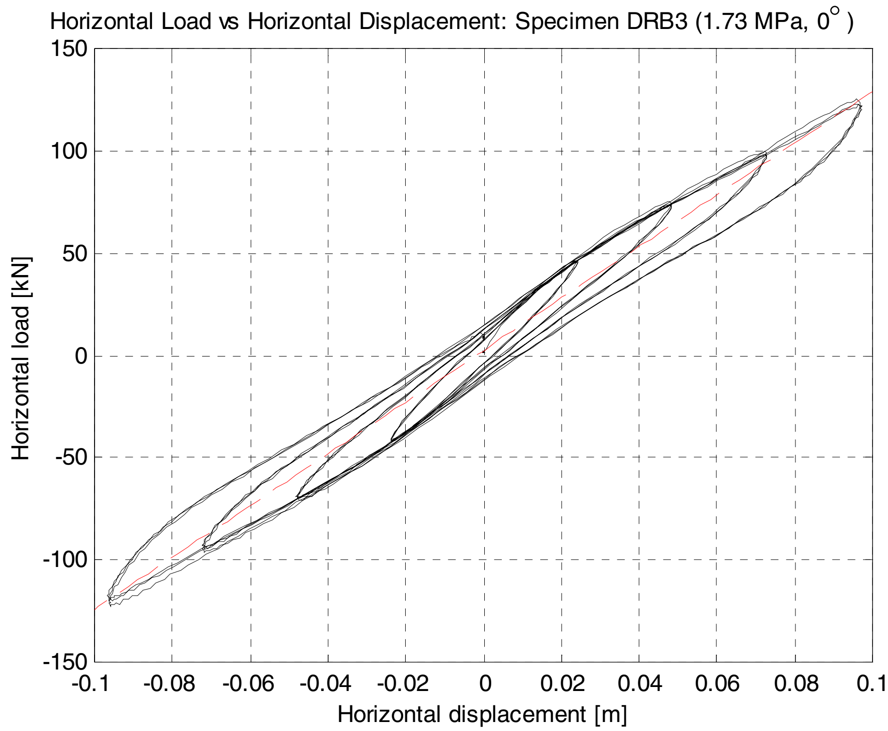

Figure A.39. Horizontal test results for DRB3 with 1.73 MPa vertical pressure (0°)

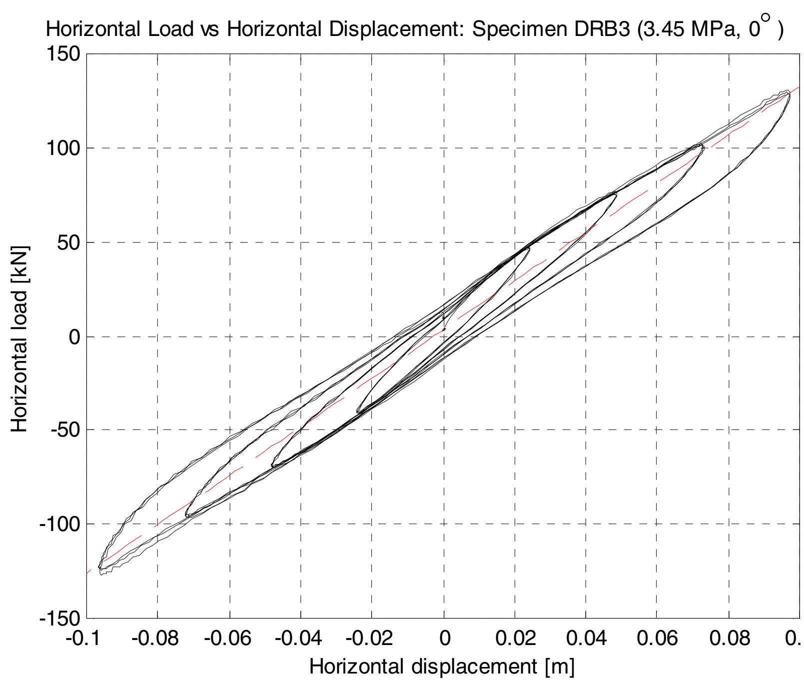

Figure A.40. Horizontal test results for DRB3 with 3.45 MPa vertical pressure (0°)

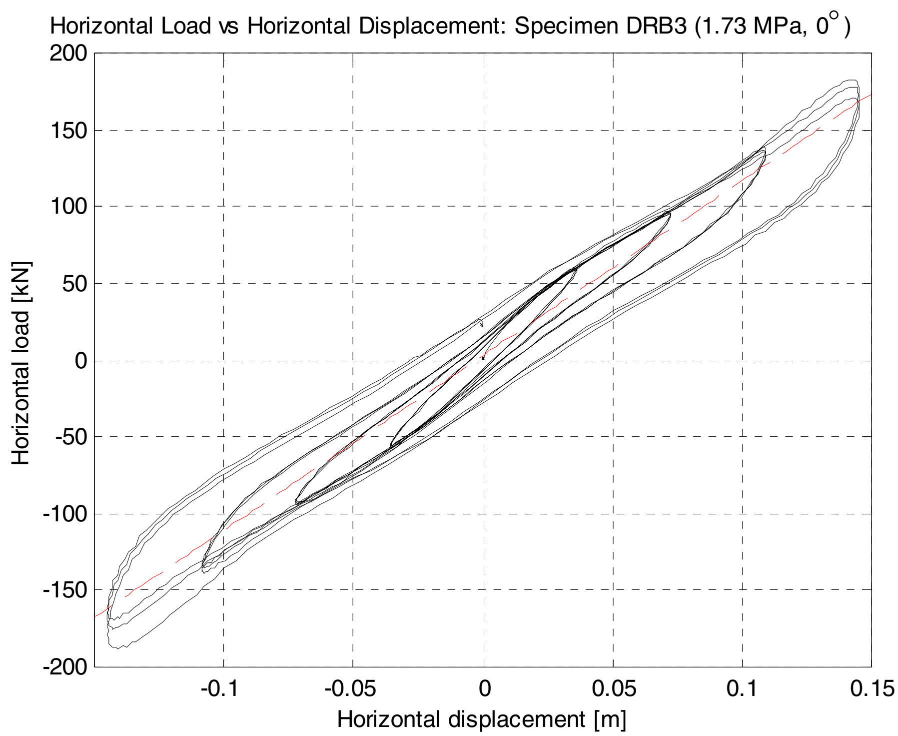

Figure A.41. Horizontal test results for DRB3 with 1.73 MPa vertical pressure (0°)

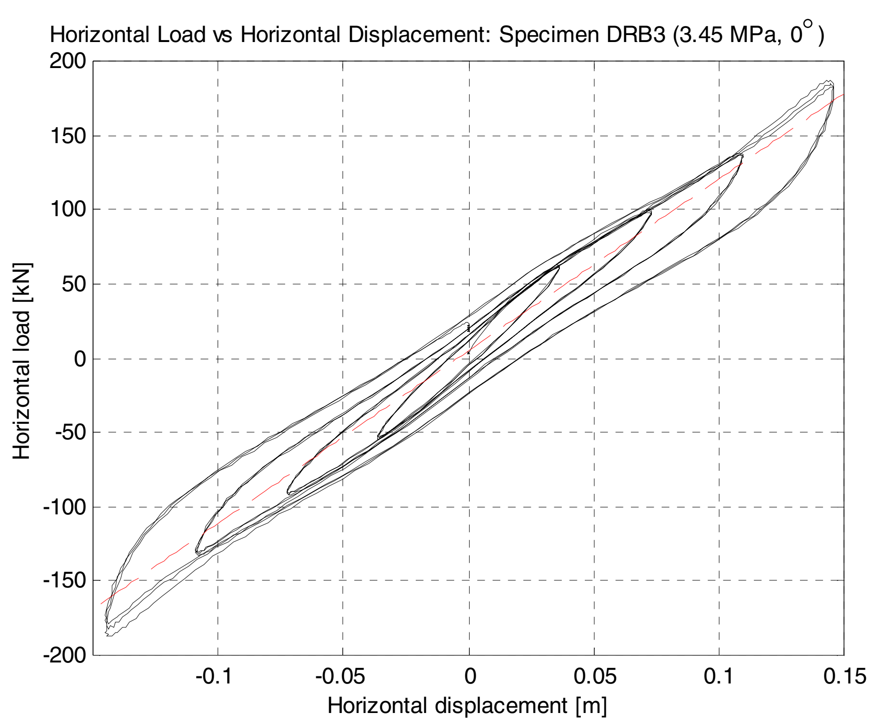

Figure A.42. Horizontal test results for DRB3 with 3.45 MPa vertical pressure (0°)

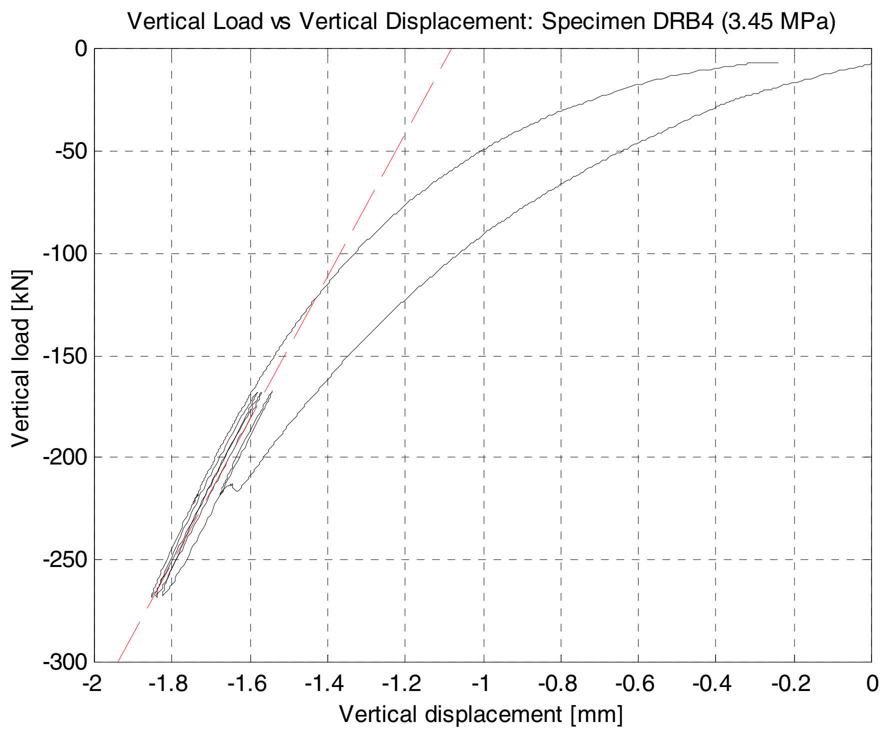

Figure A.43. Vertical test results for DRB4 with 3.45 MPa vertical pressure

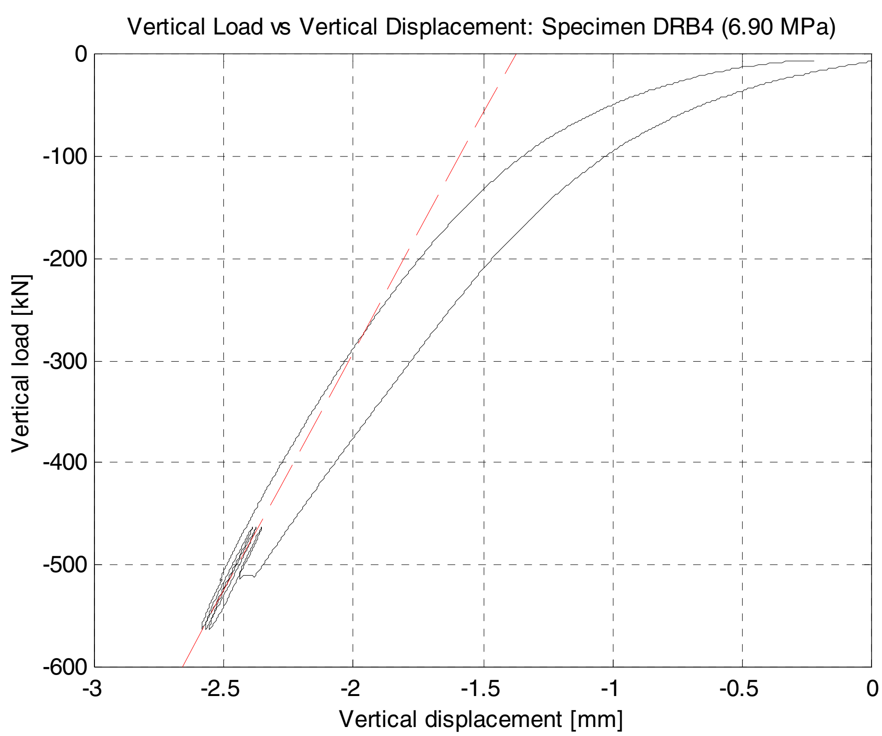

Figure A.44. Vertical test results for DRB4 with 6.90 MPa vertical pressure

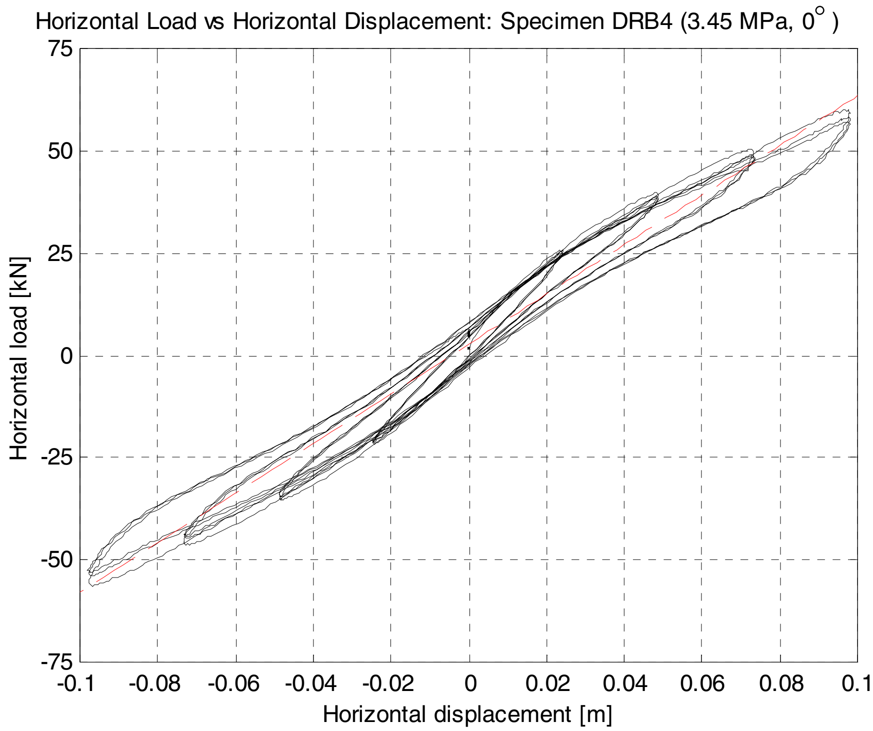

Figure A.45. Horizontal test results for DRB4 with 3.45 MPa vertical pressure (0°)

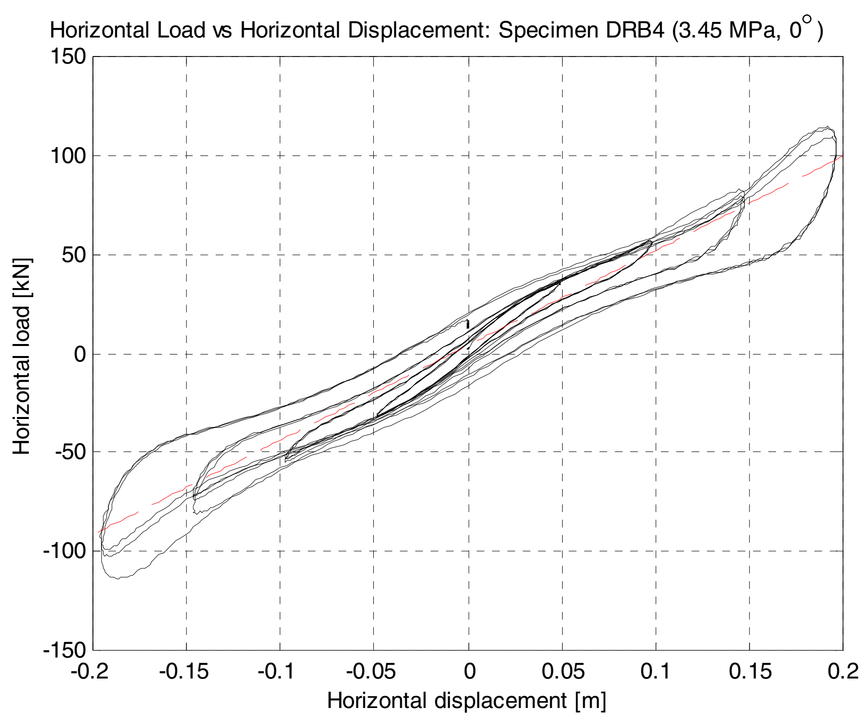

Figure A.46. Horizontal test results for DRB4 with 3.45 MPa vertical pressure (0°)

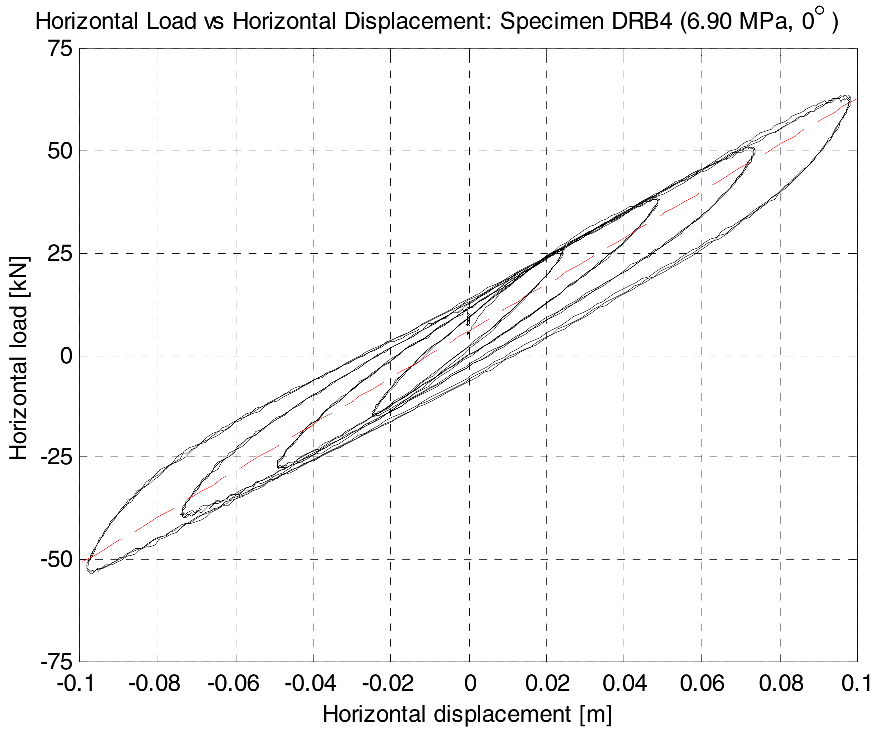

Figure A.47. Horizontal test results for DRB4 with 6.90 MPa vertical pressure (0°)

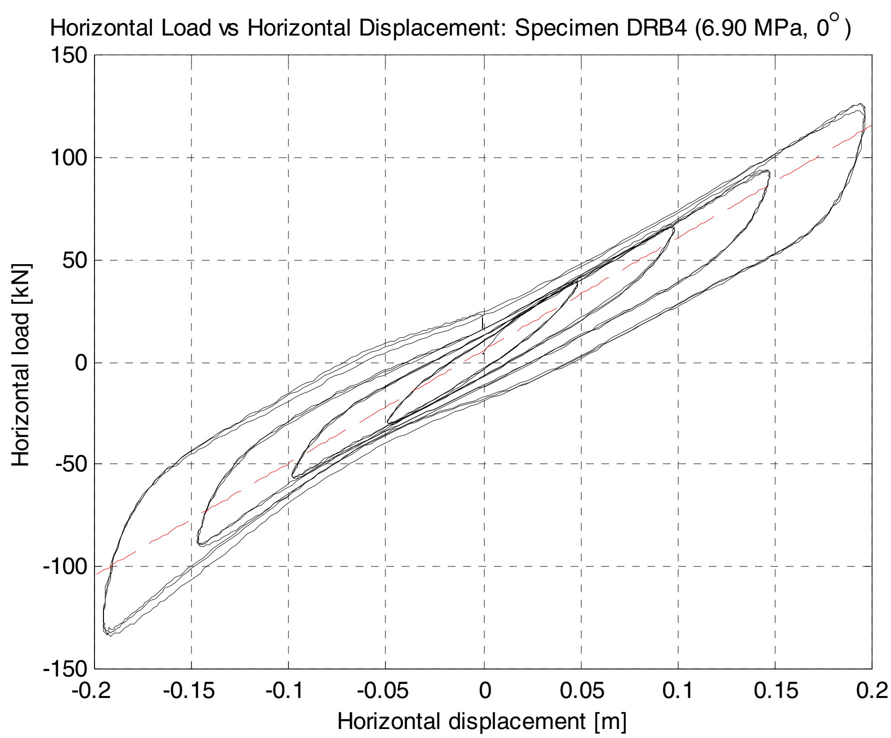

Figure A.48. Horizontal test results for DRB4 with 6.90 MPa vertical pressure (0°)

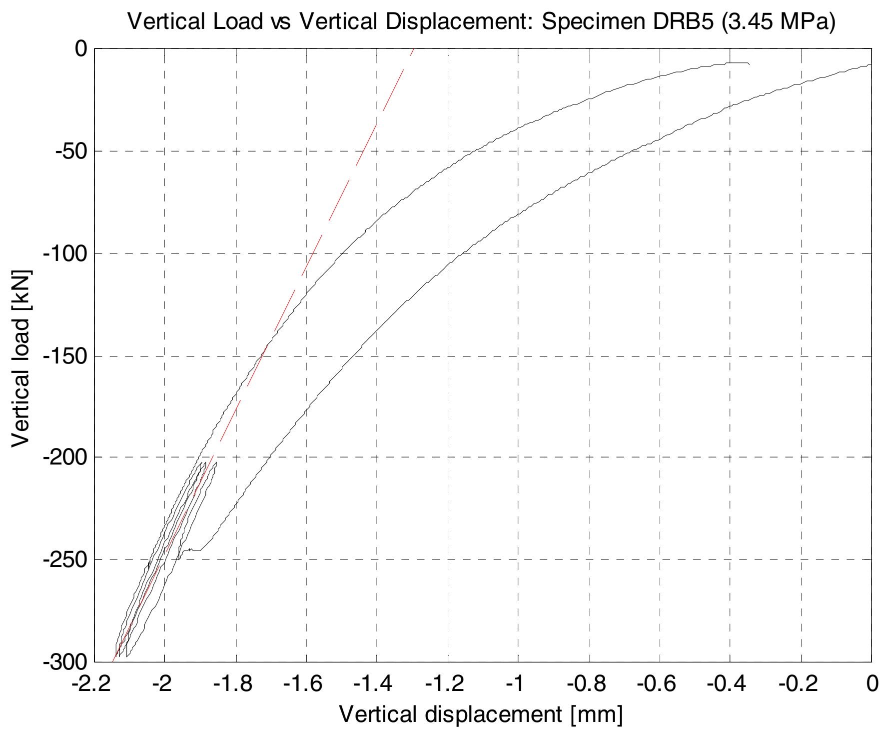

Figure A.49. Vertical test results for DRB5 with 3.45 MPa vertical pressure

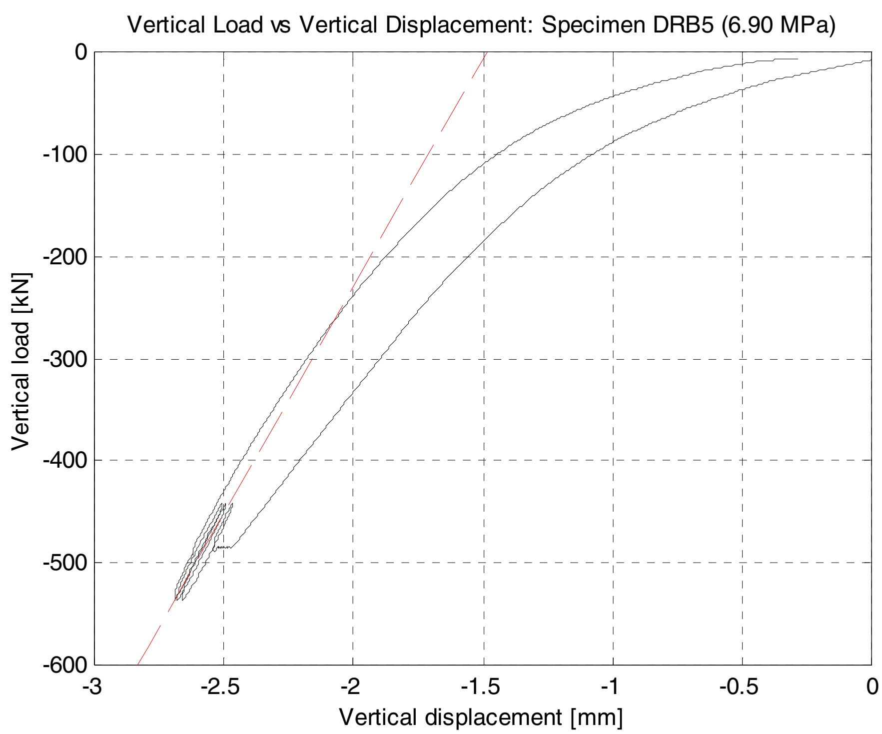

Figure A.50. Vertical test results for DRB5 with 6.90 MPa vertical pressure

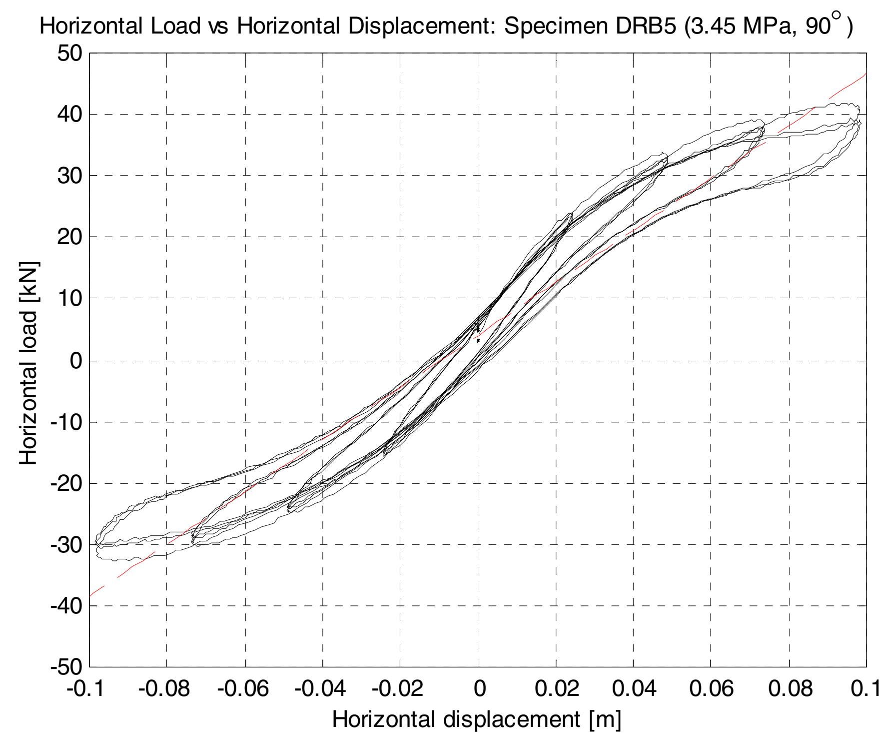

Figure A.51. Horizontal test results for DRB5 at 3.45 MPa vertical pressure (90°)

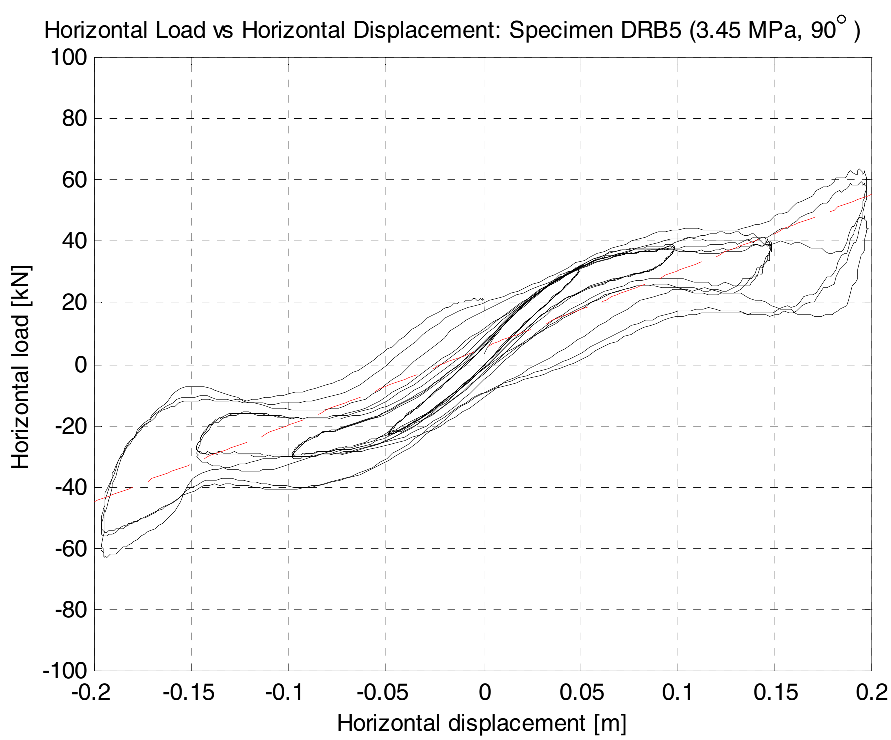

Figure A.52. Horizontal test results for DRB5 at 3.45 MPa vertical pressure (90°)

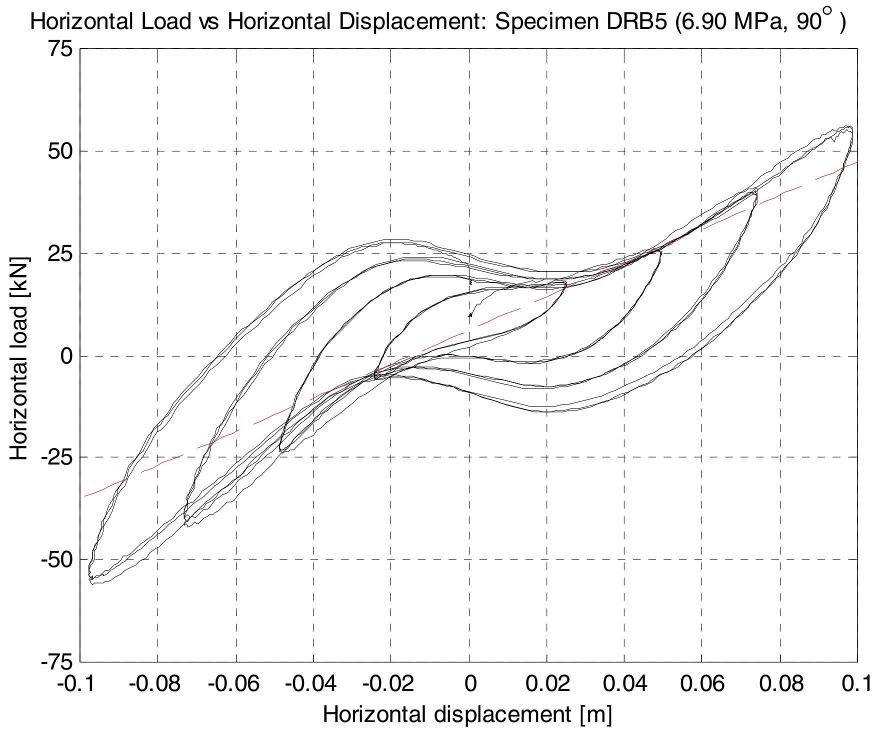

Figure A.53. Horizontal test results for DRB5 at 6.90 MPa vertical pressure (90°)

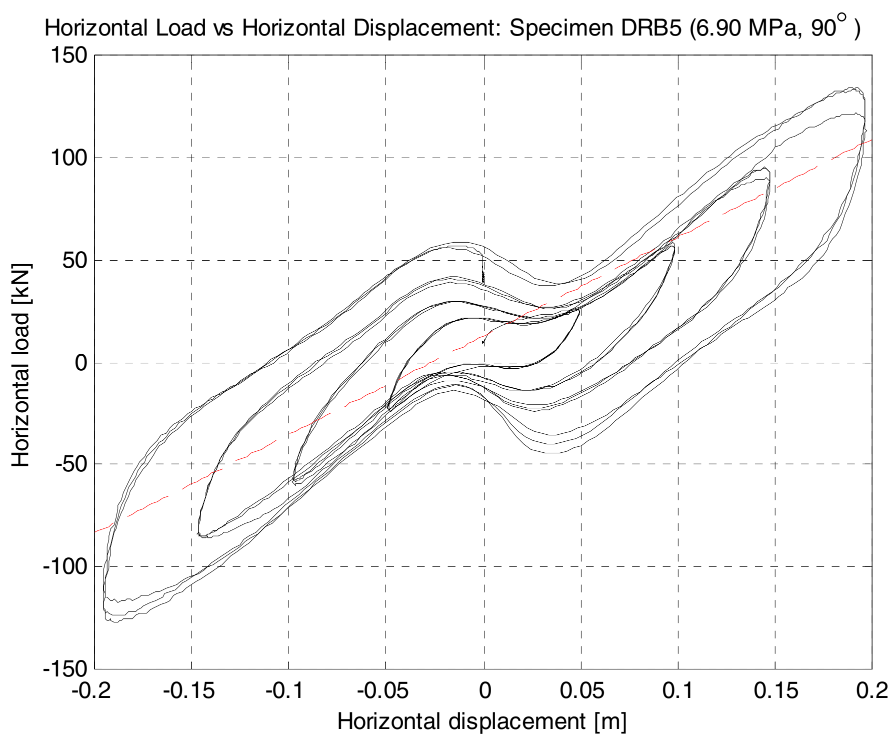

Figure A.54. Horizontal test results for DRB5 at 6.90 MPa vertical pressure (90°)

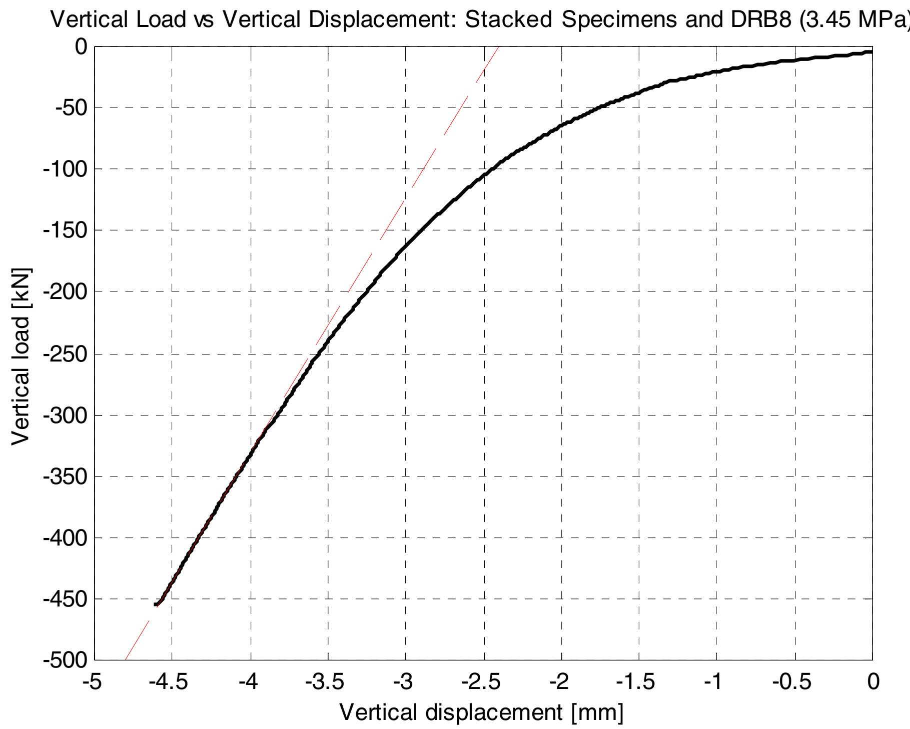

Figure A.55. Vertical test results for original specimen (183mm x 755mm x105) and DRB8 with 3.45 MPa vertical pressure

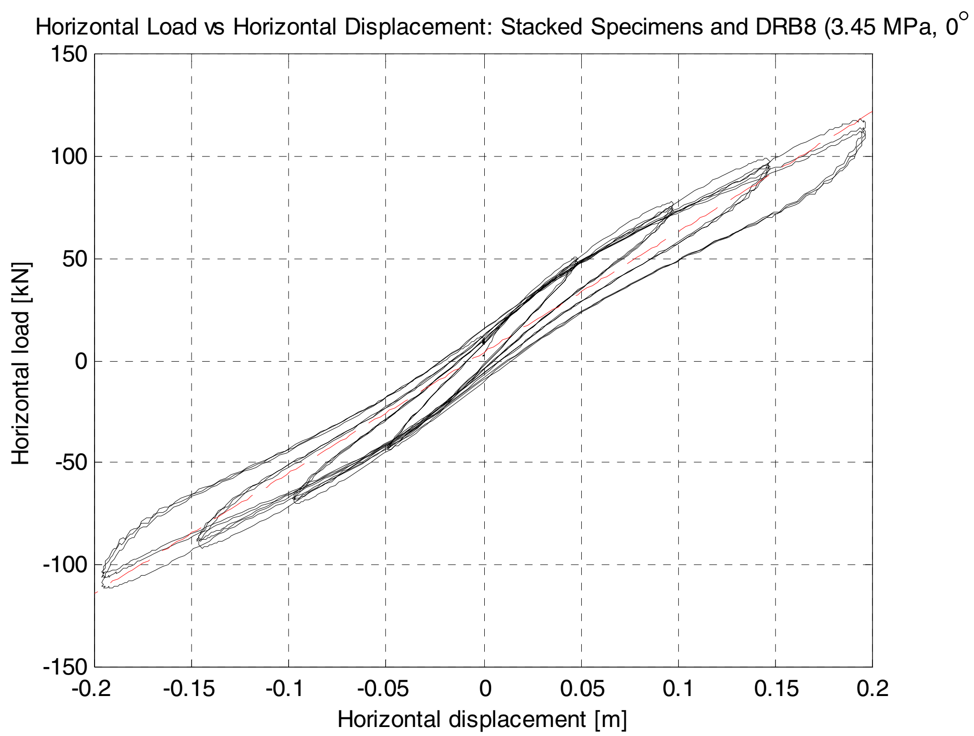

Figure A.56. Horizontal test results for original specimen (183mm x 755mm x105) and DRB8 with 3.45 MPa vertical pressure

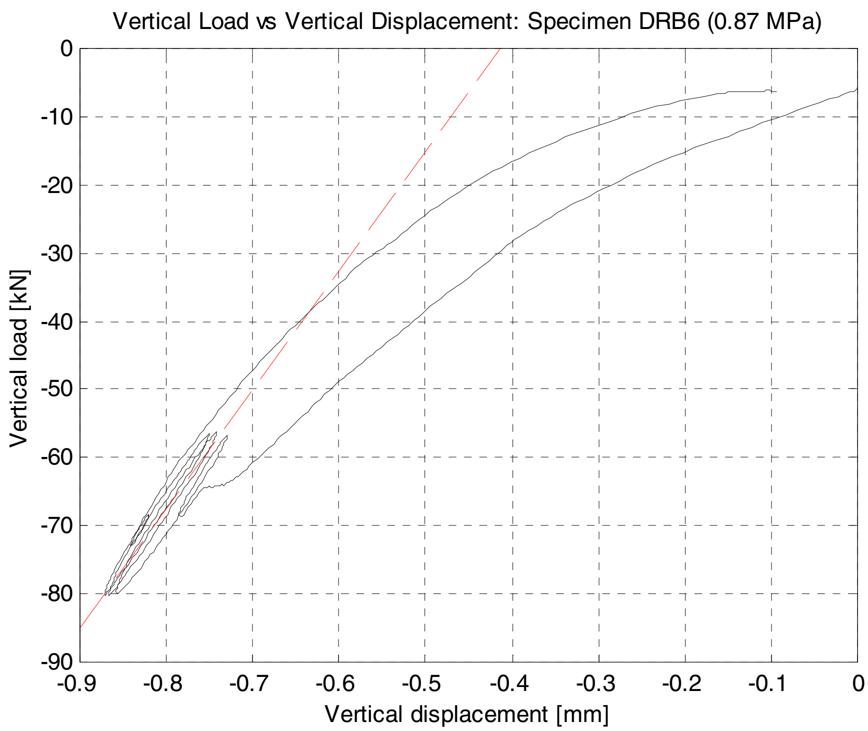

Figure A.57. Vertical test results for DRB6 with 0.87 MPa vertical pressure

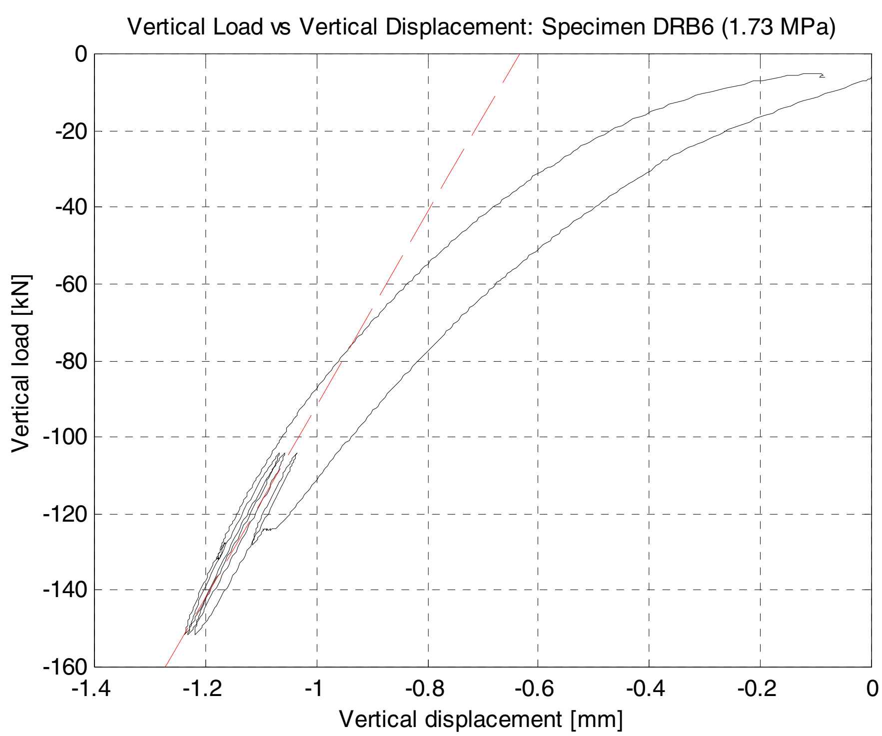

Figure A.58. Vertical test results for DRB6 with 1.73 MPa vertical pressure

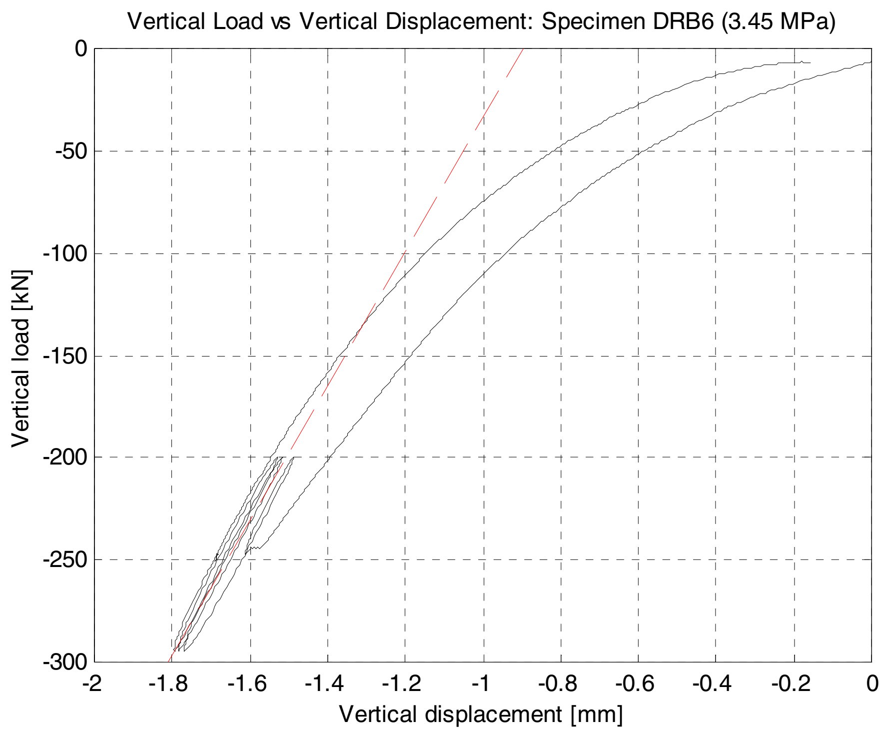

Figure A.59. Vertical test results for DRB6 with 3.45 MPa vertical pressure

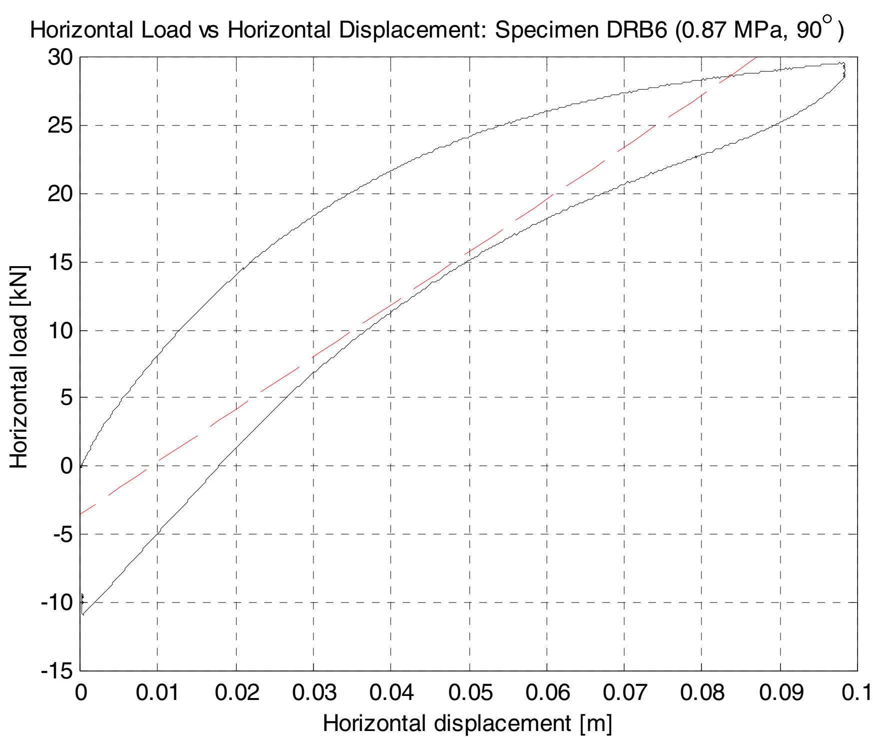

Figure A.60. Horizontal test results for DRB6 with 0.87 MPa vertical pressure (90°)

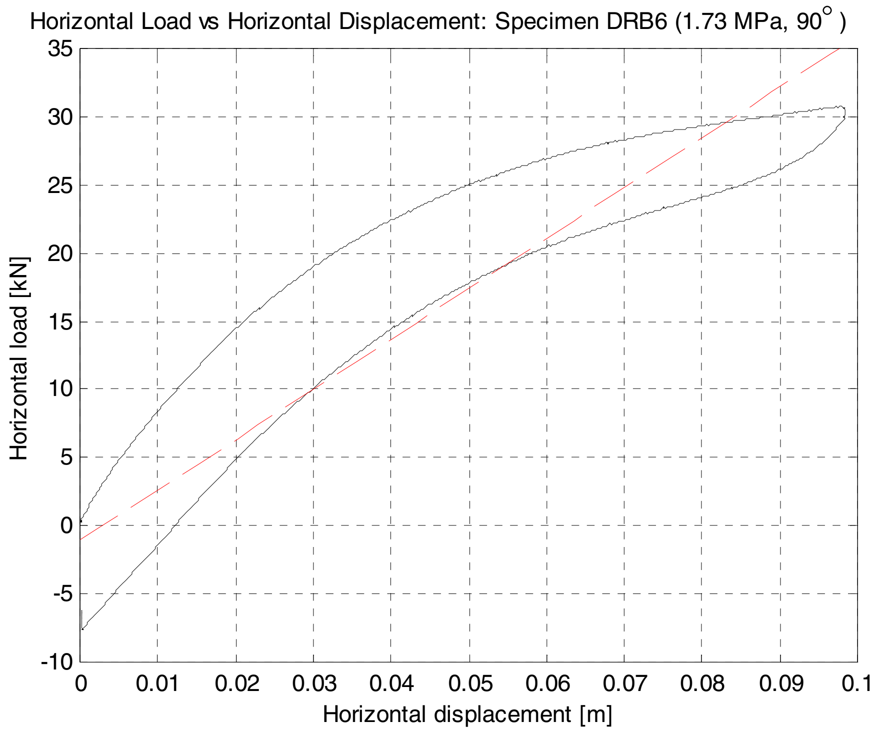

Figure A.61. Horizontal test results for DRB6 at 1.73 MPa vertical pressure (90°)

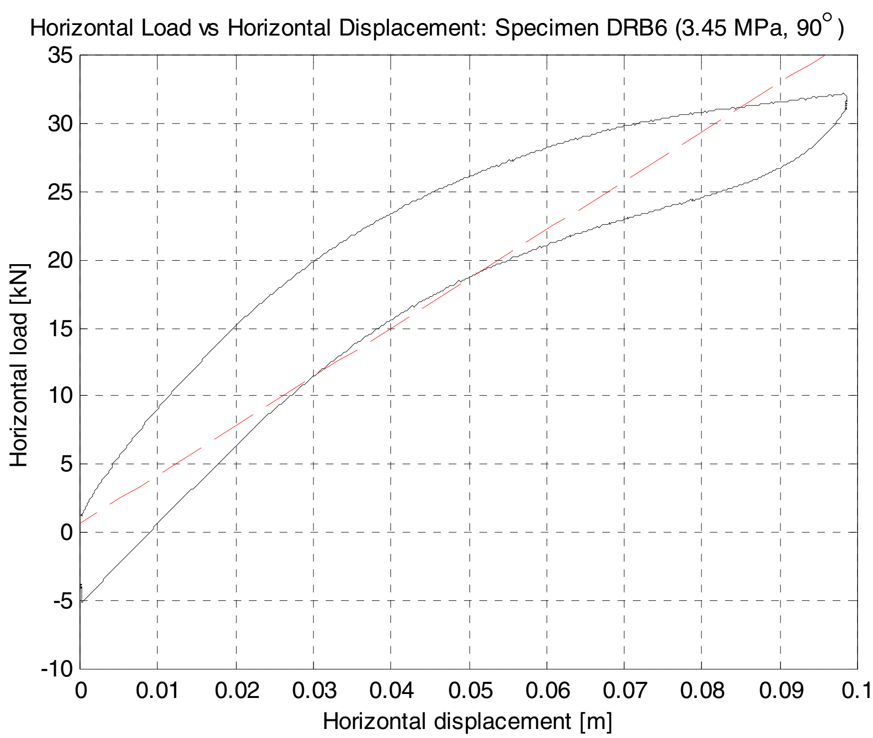

Figure A.62. Horizontal test results for DRB6 at 3.45 MPa vertical pressure (90°)

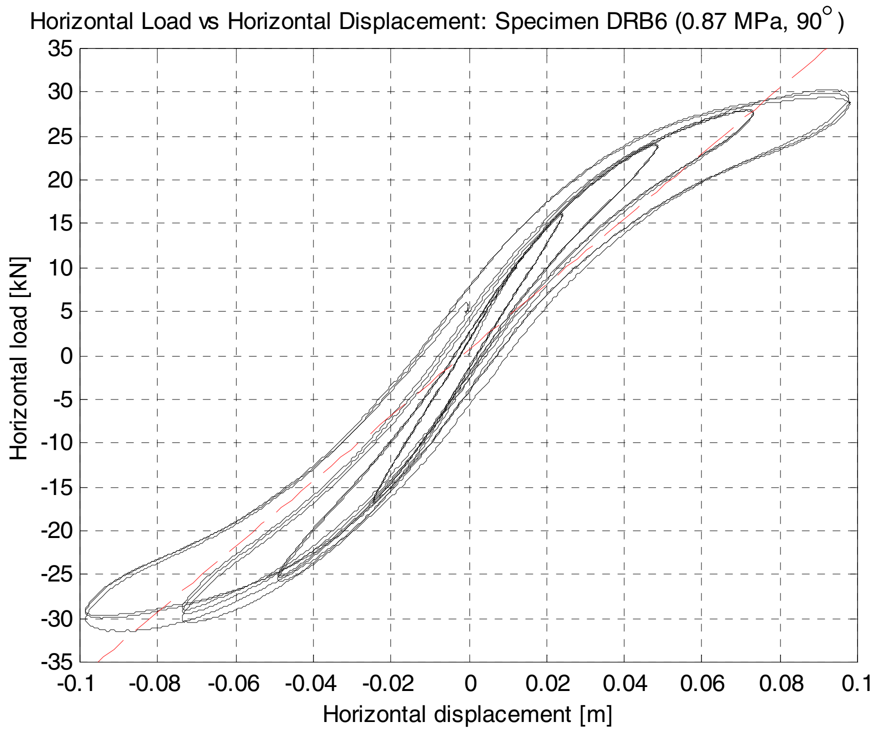

Figure A.63. Horizontal test results for DRB6 at 0.87 MPa vertical pressure (90°)

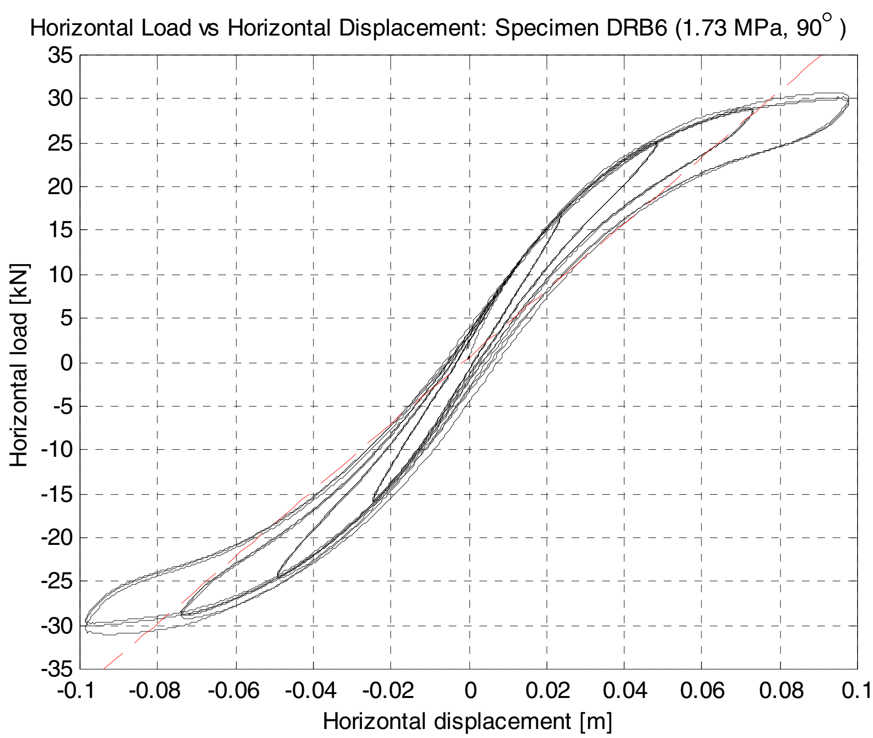

Figure A.64. Horizontal test results for DRB6 at 1.73 MPa vertical pressure (90°)

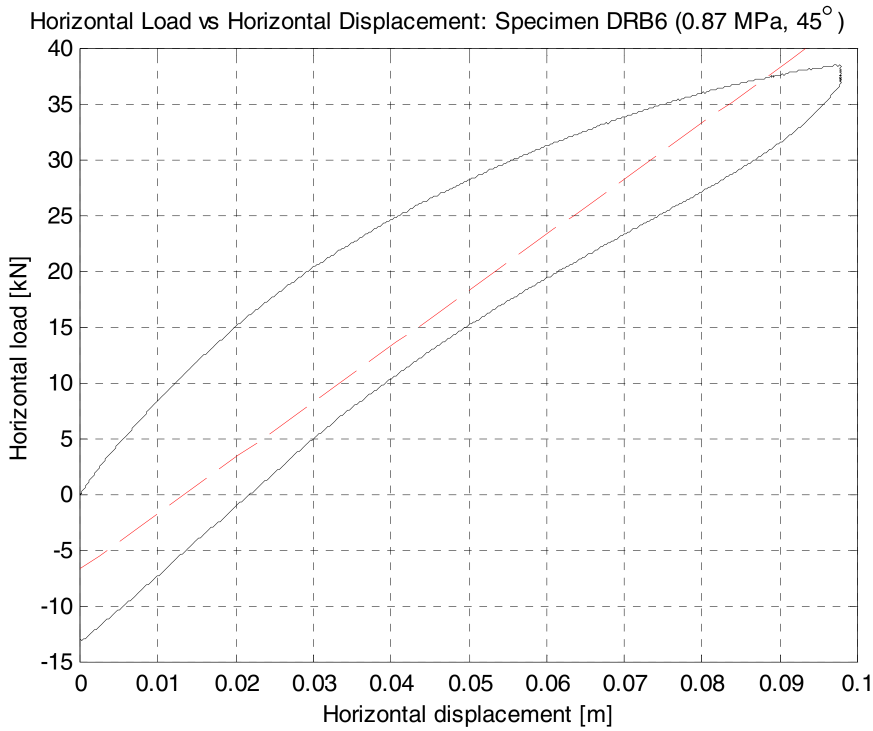

Figure A.65. Horizontal test results for DRB6 with 0.87 MPa vertical pressure (45°)

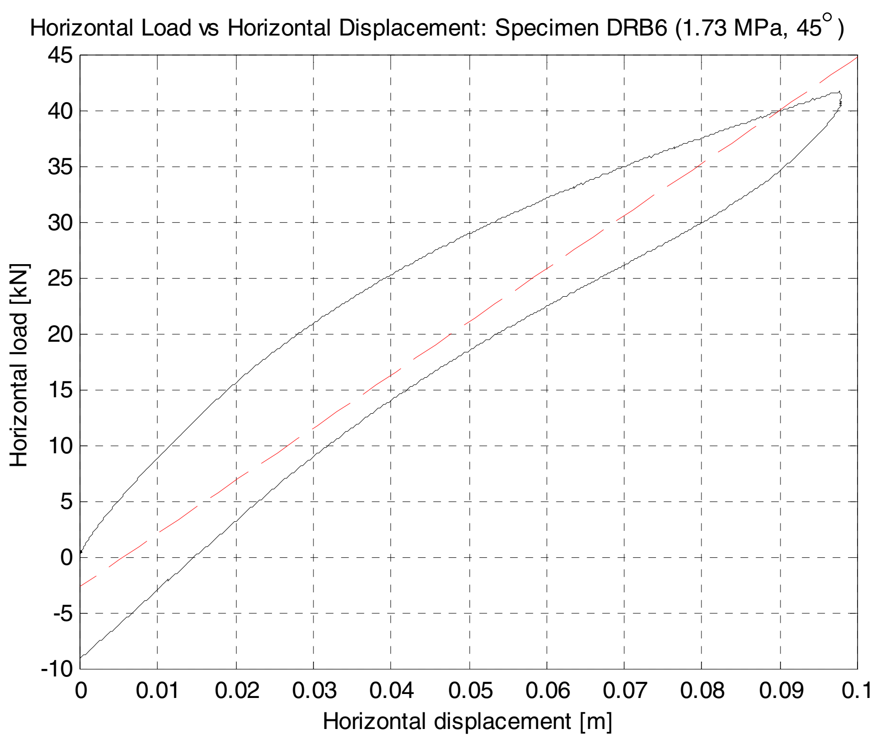

Figure A.66. Horizontal test results for DRB6 with 1.73 MPa vertical pressure (45°)

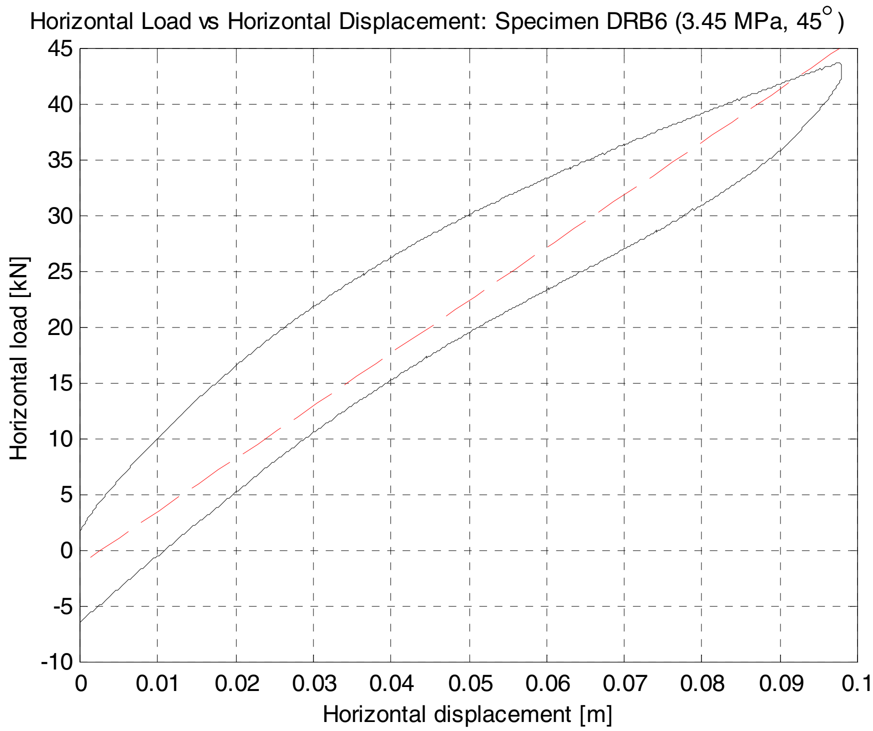

Figure A.67. Horizontal test results for DRB6 with 3.45 MPa vertical pressure (45°)

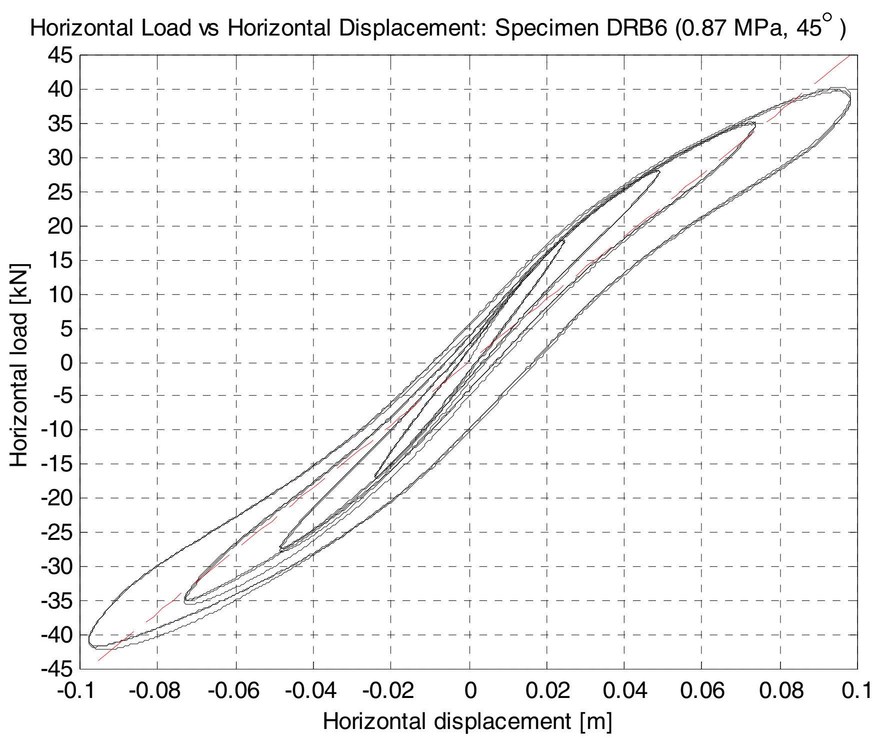

Figure A.68. Horizontal test results for DRB6 with 0.87 MPa vertical pressure (45°)

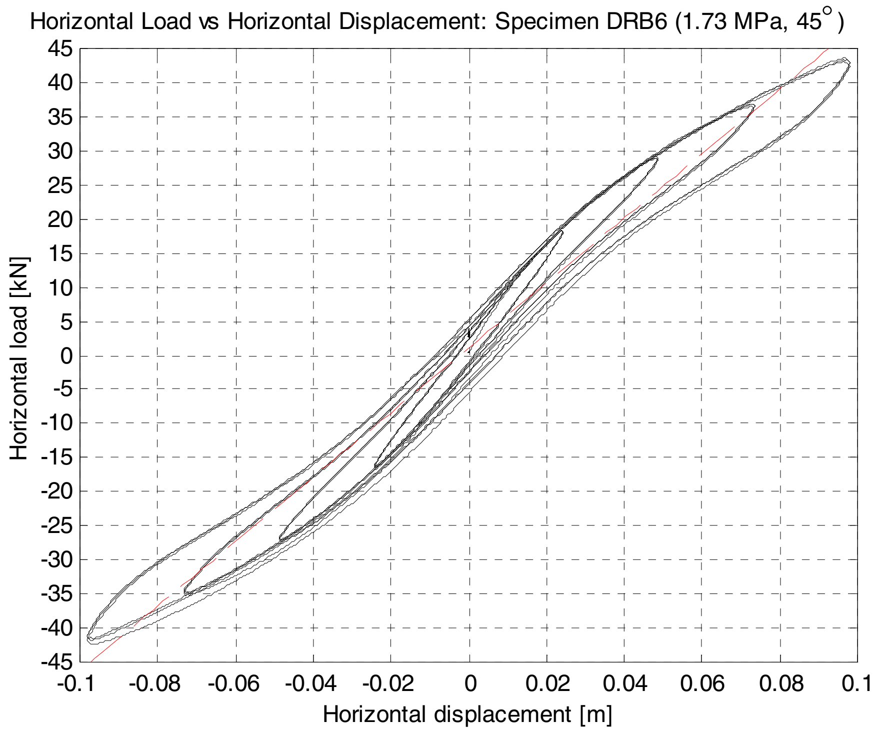

Figure A.69. Horizontal test results for DRB6 with 1.73 MPa vertical pressure (45°)

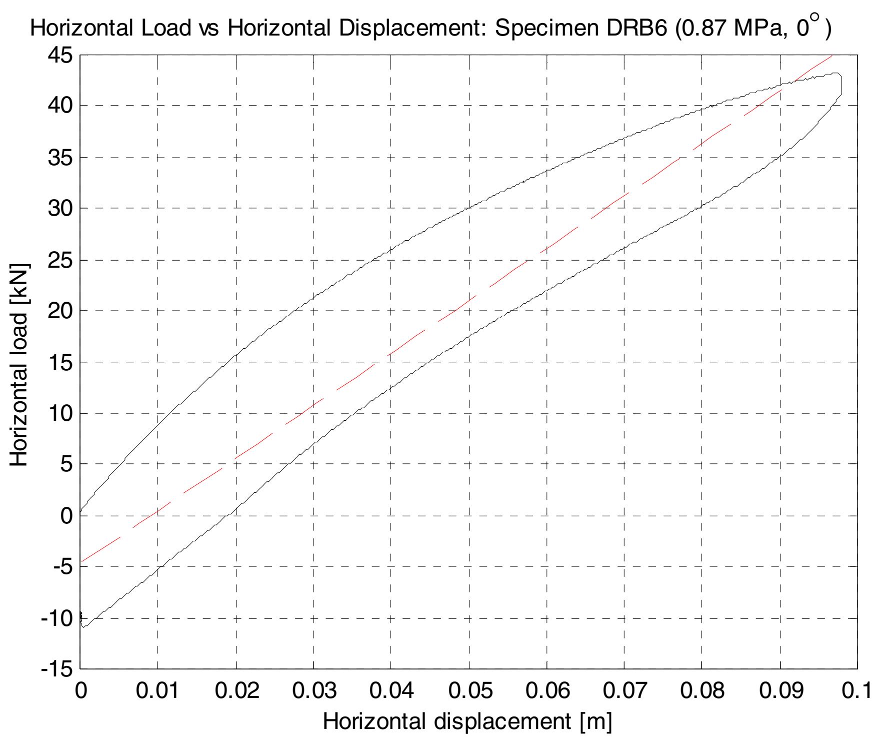

Figure A.70. Horizontal test results for DRB6 with 0.87 MPa vertical pressure (0°)

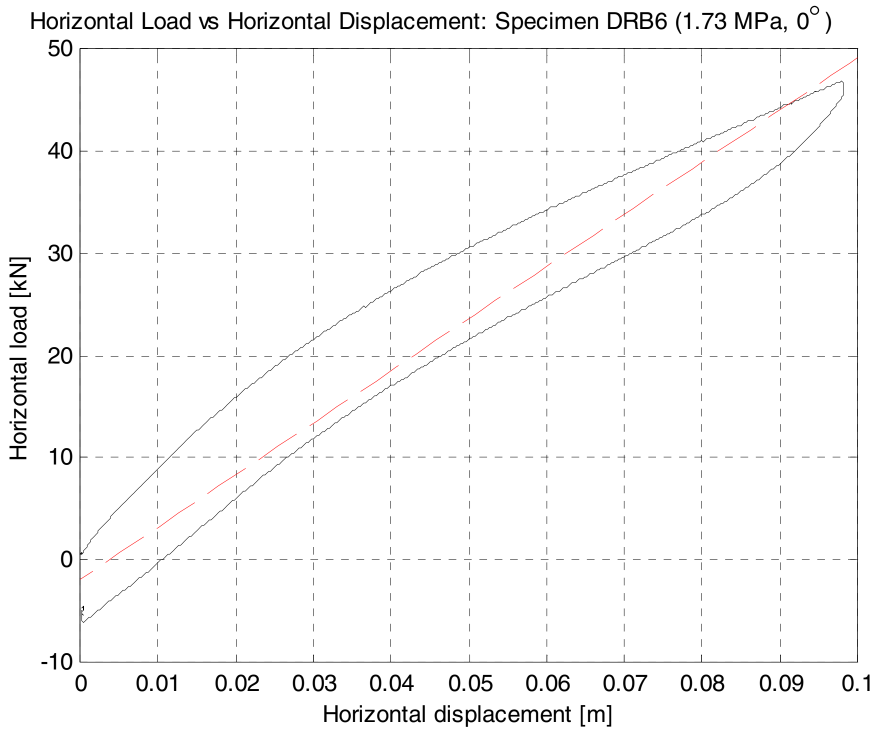

Figure A.71. Horizontal test results for DRB6 with 1.73 MPa vertical pressure (0°)

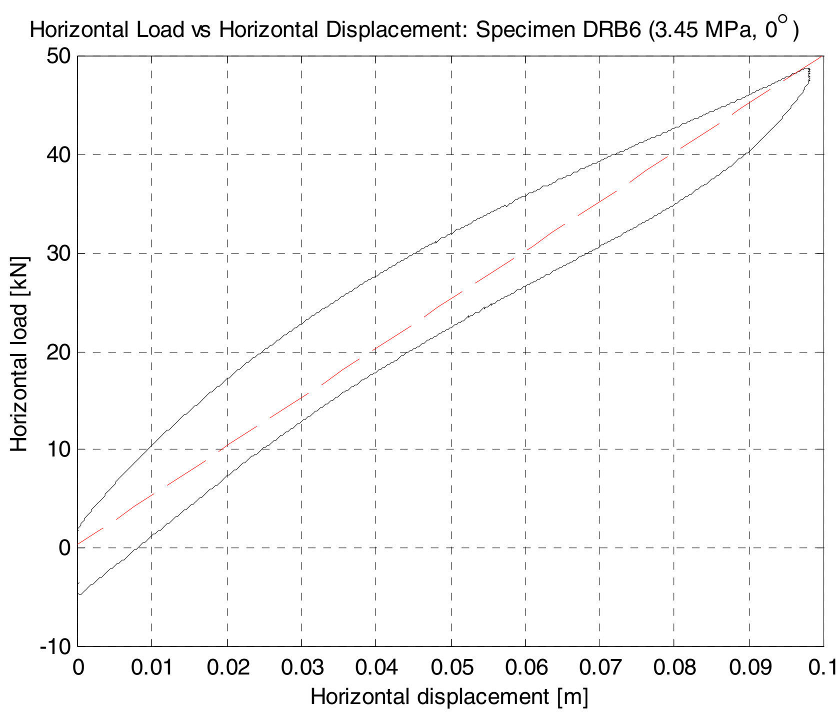

Figure A.72. Horizontal test results for DRB6 with 3.45 MPa vertical pressure (0°)

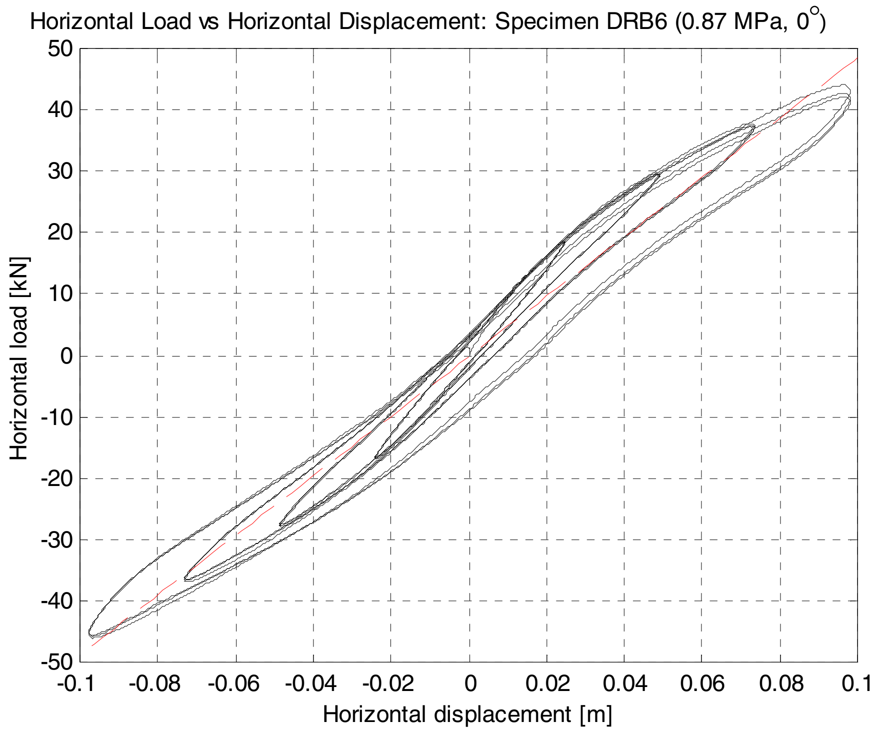

Figure A.73. Horizontal test results for DRB6 with 0.87 MPa vertical pressure (0°)

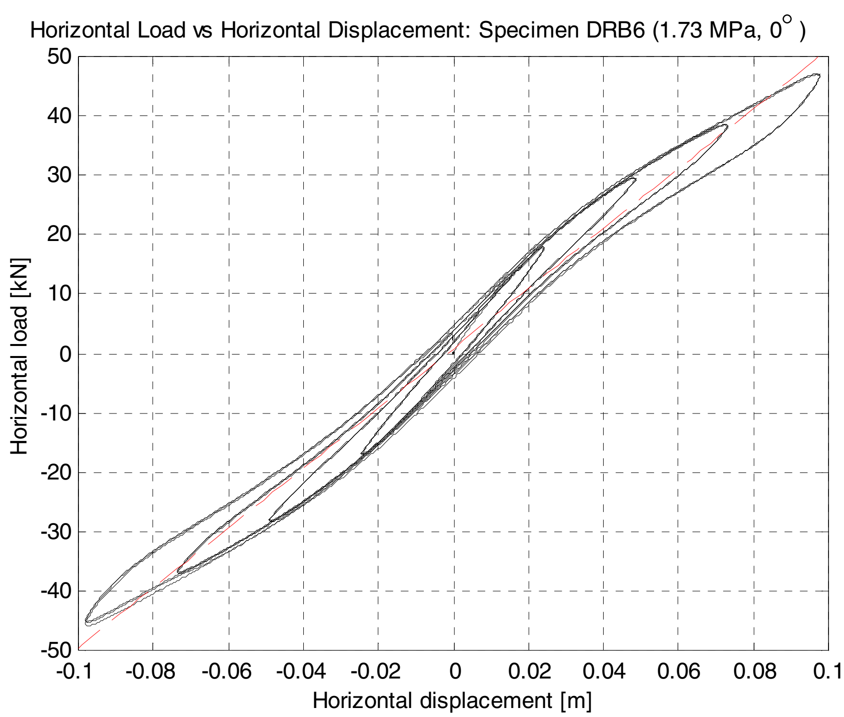

Figure A.74. Horizontal test results for DRB6 with 1.73 MPa vertical pressure (0°)

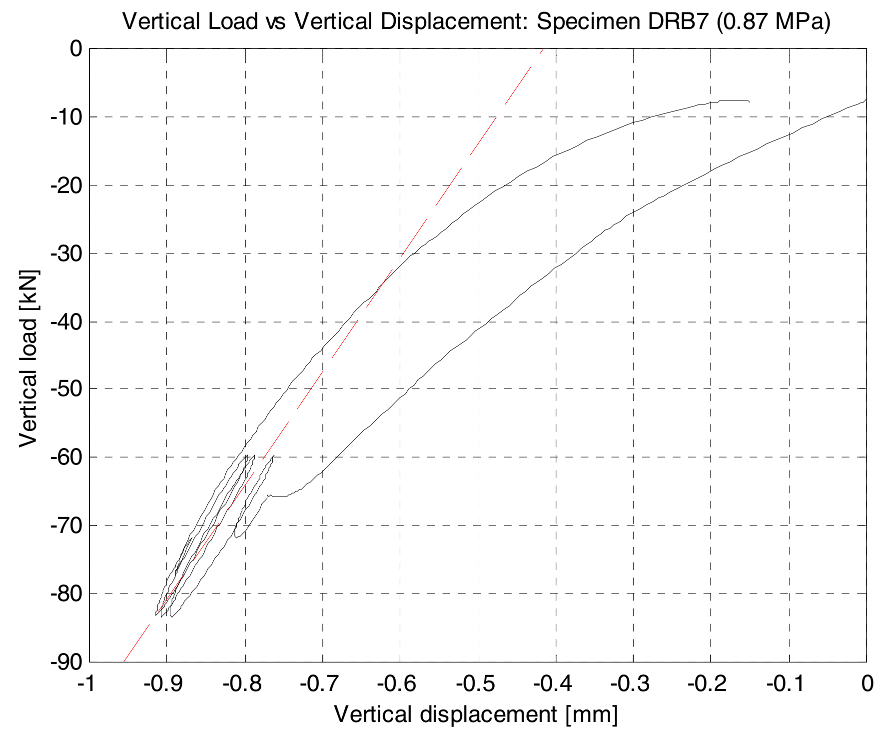

Figure A.75. Vertical test results for DRB7 with 0.87 MPa vertical pressure

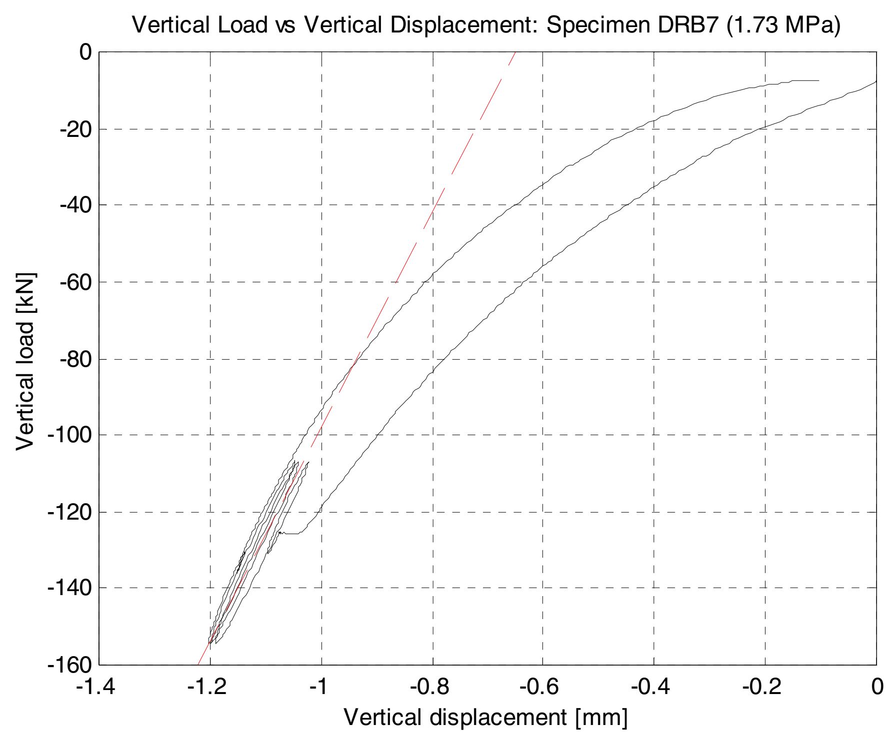

Figure A.76. Vertical test results for DRB7 with 1.73 MPa vertical pressure

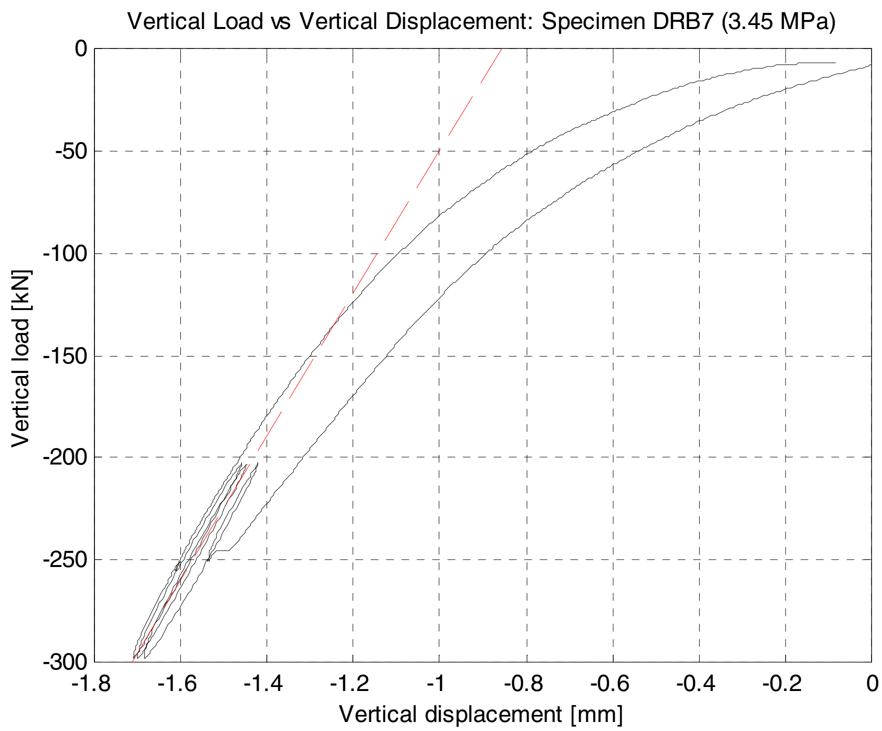

Figure A.77. Vertical test results for DRB7 with 3.45 MPa vertical pressure

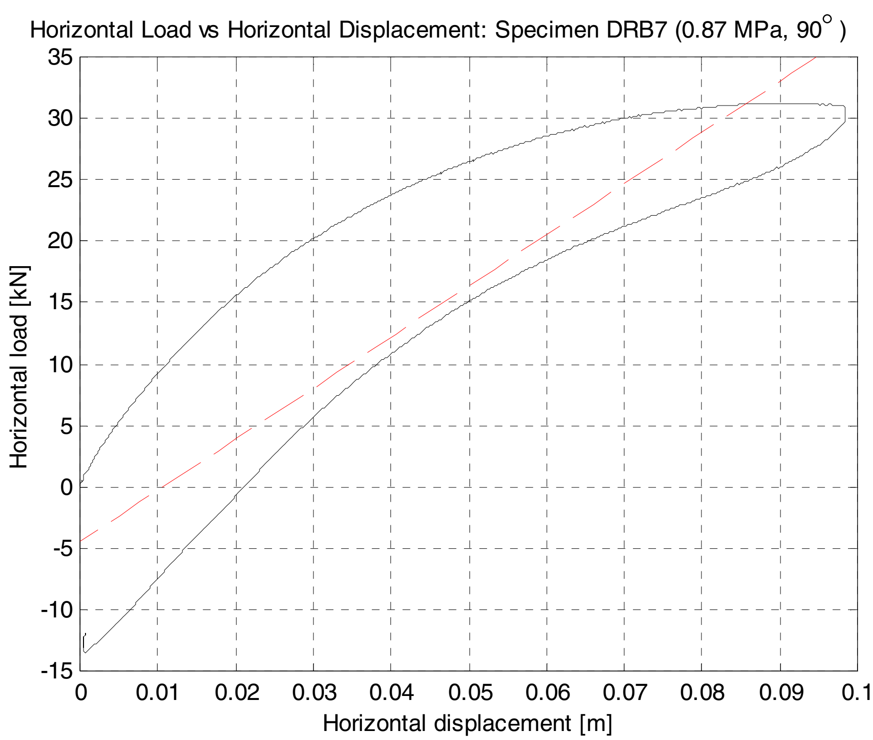

Figure A.78. Horizontal test results for DRB6 with 0.87 MPa vertical pressure (90°)

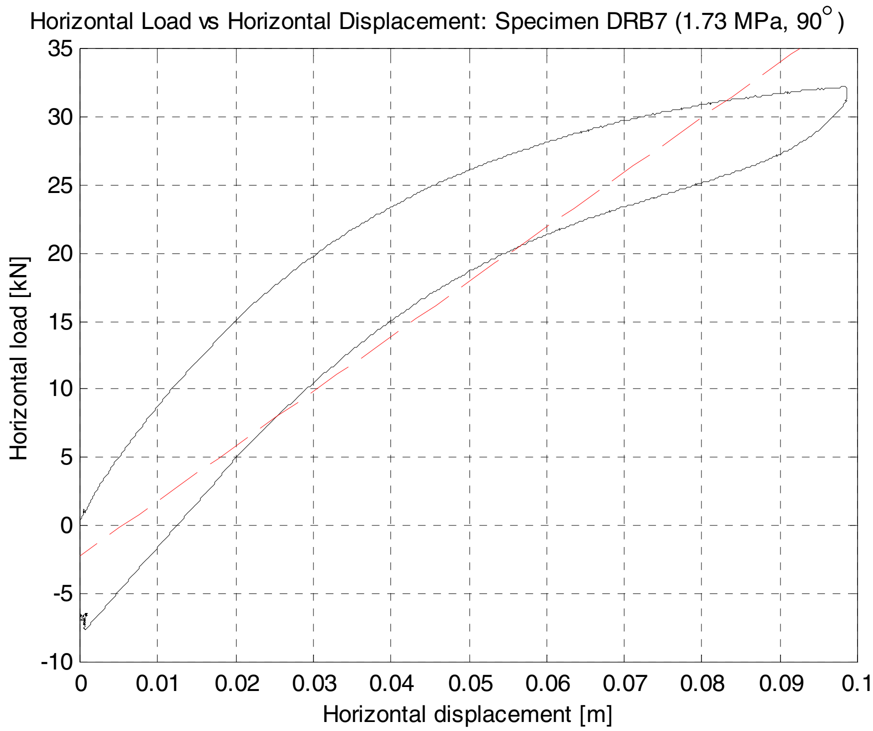

Figure A.79. Horizontal test results for DRB7 with 1.73 MPa vertical pressure (90°)

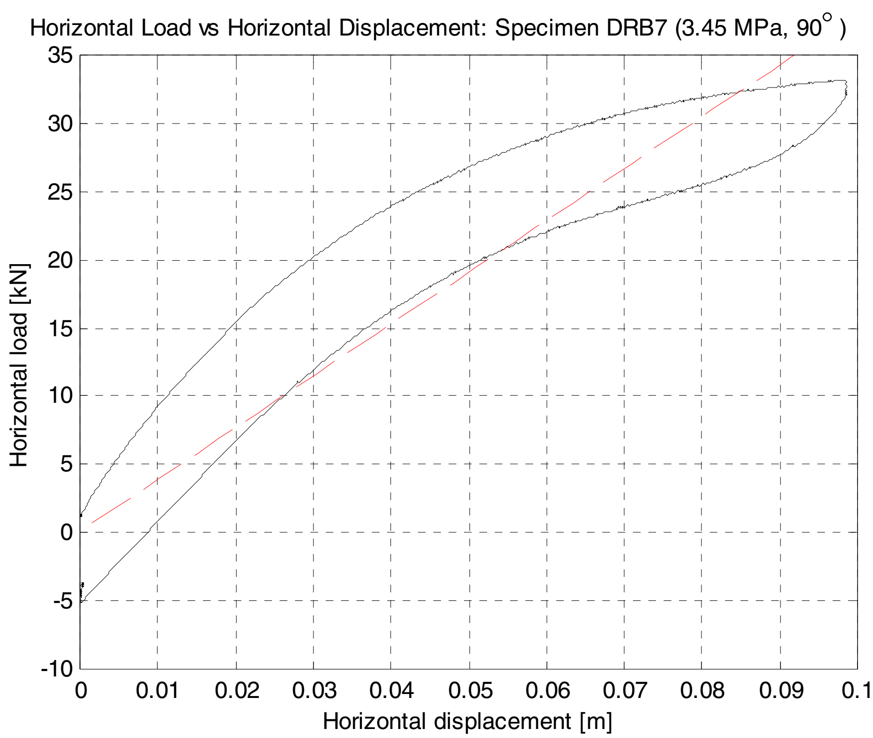

Figure A.80. Horizontal test results for DRB7 with 3.45 MPa vertical pressure (90°)

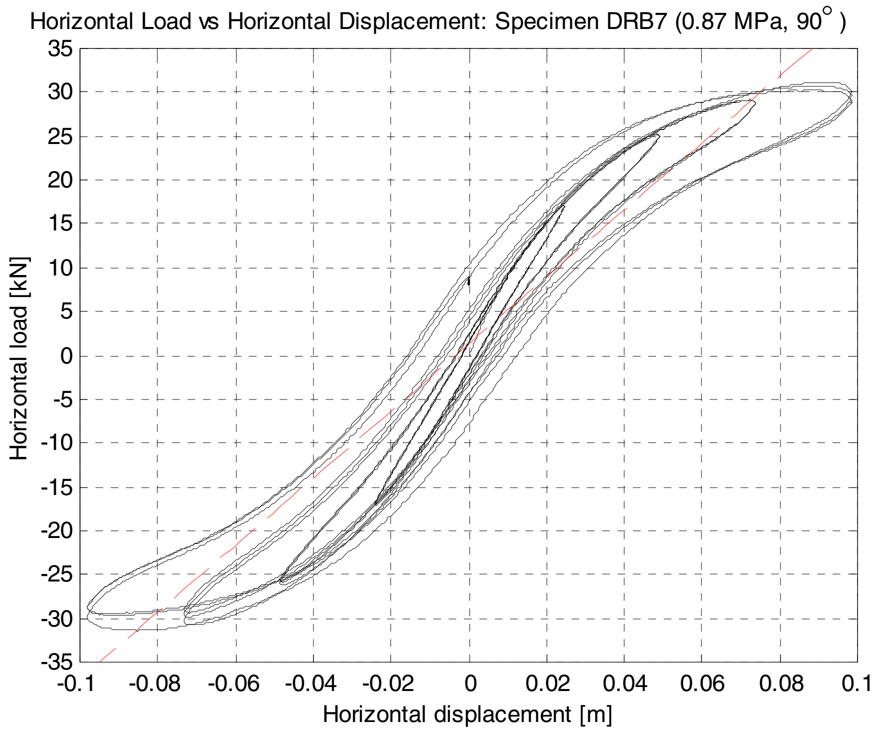

Figure A.81. Horizontal test results for DRB7 with 0.87 MPa vertical pressure (90°)

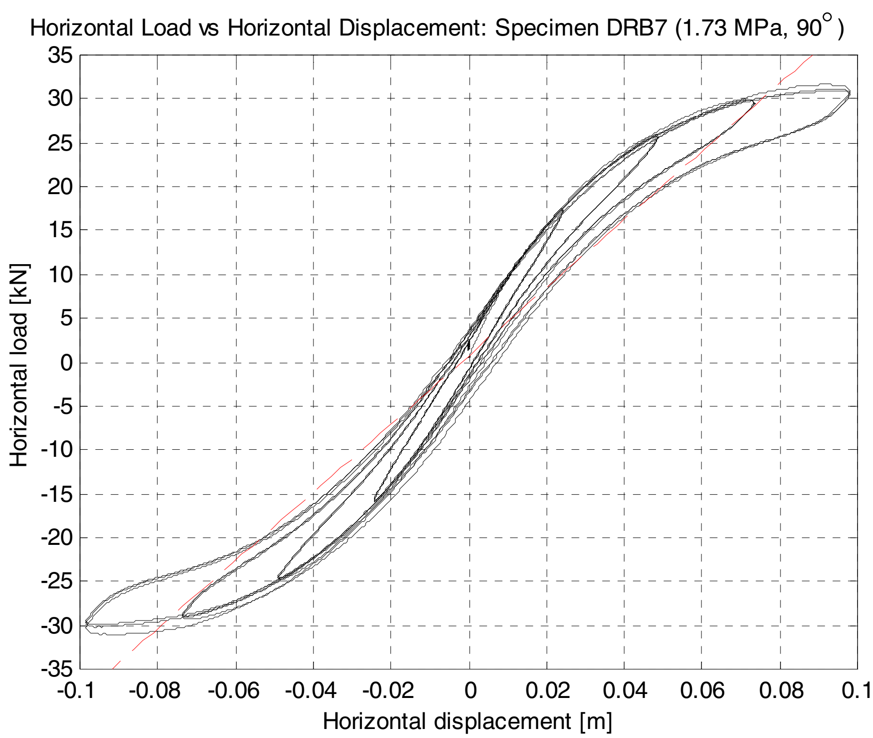

Figure A.82. Horizontal test results for DRB7 with 1.73 MPa vertical pressure (90°)

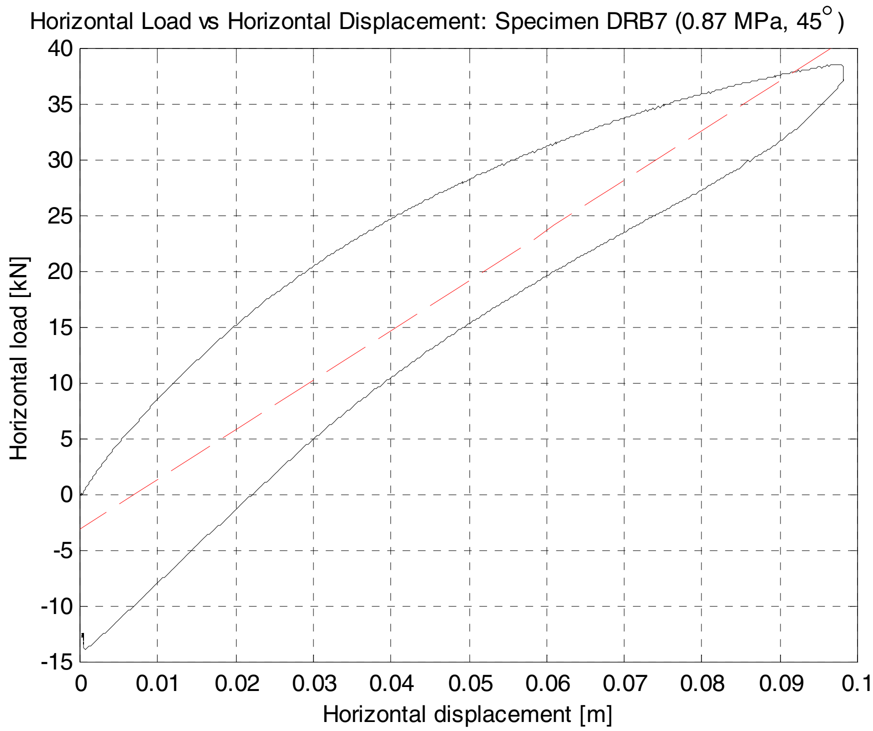

Figure A.83. Horizontal test results for DRB7 with 0.87 MPa vertical pressure (45°)

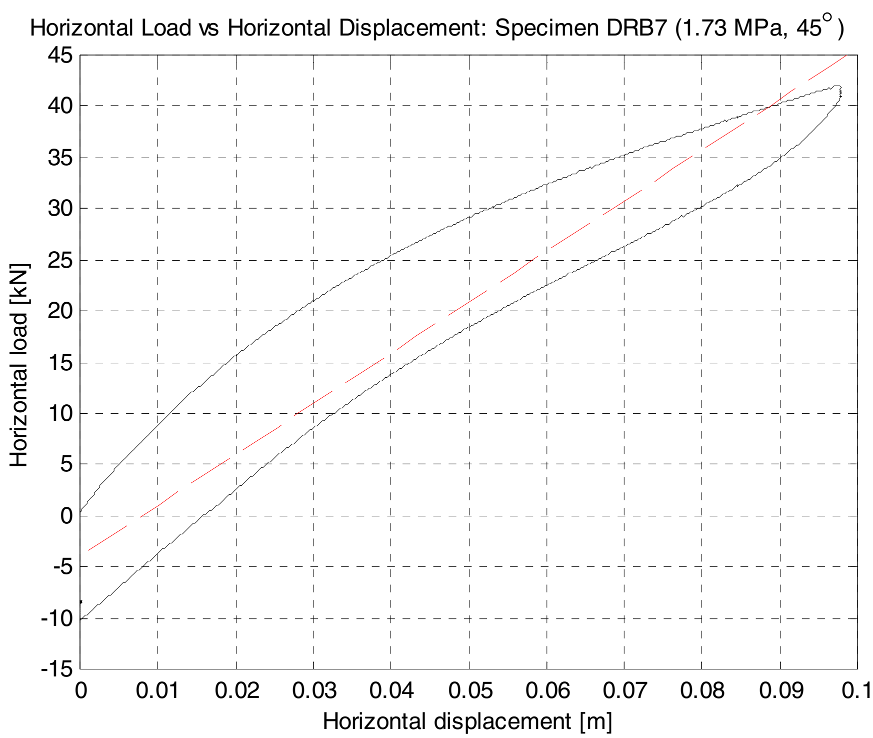

Figure A.84. Horizontal test results for DRB7 with 1.73 MPa vertical pressure (45°)

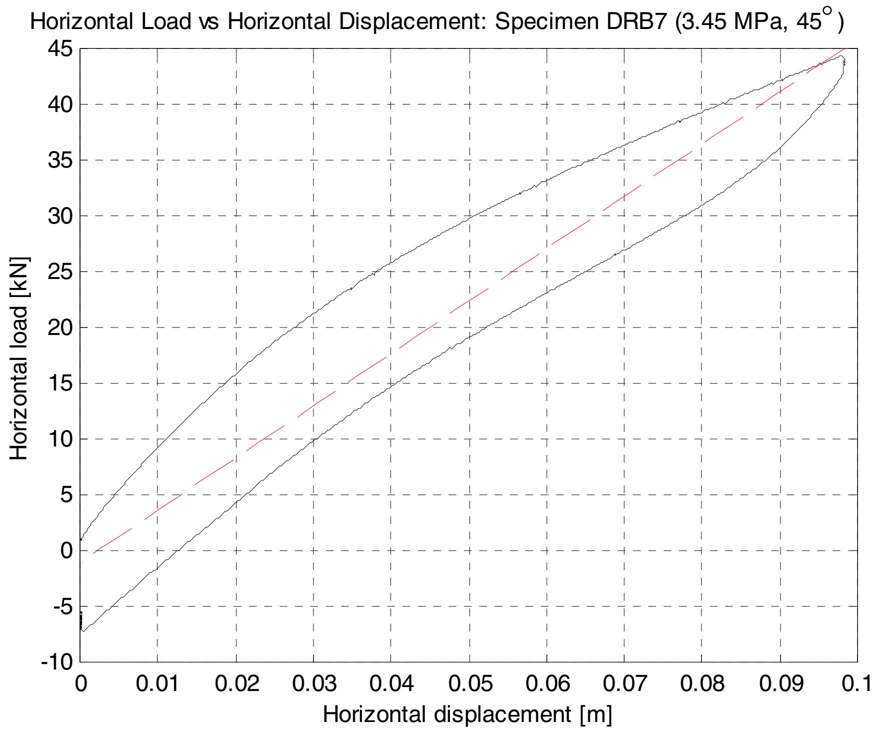

Figure A.85. Horizontal test results for DRB7 with 3.45 MPa vertical pressure (45°)

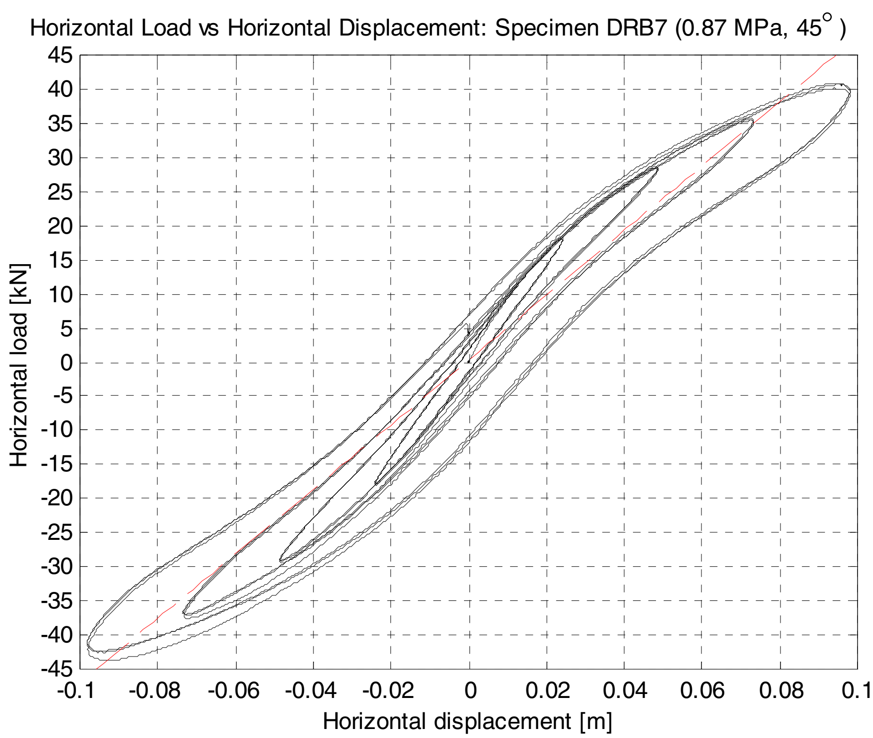

Figure A.86. Horizontal test results for DRB7 with 0.87 MPa vertical pressure (45°)

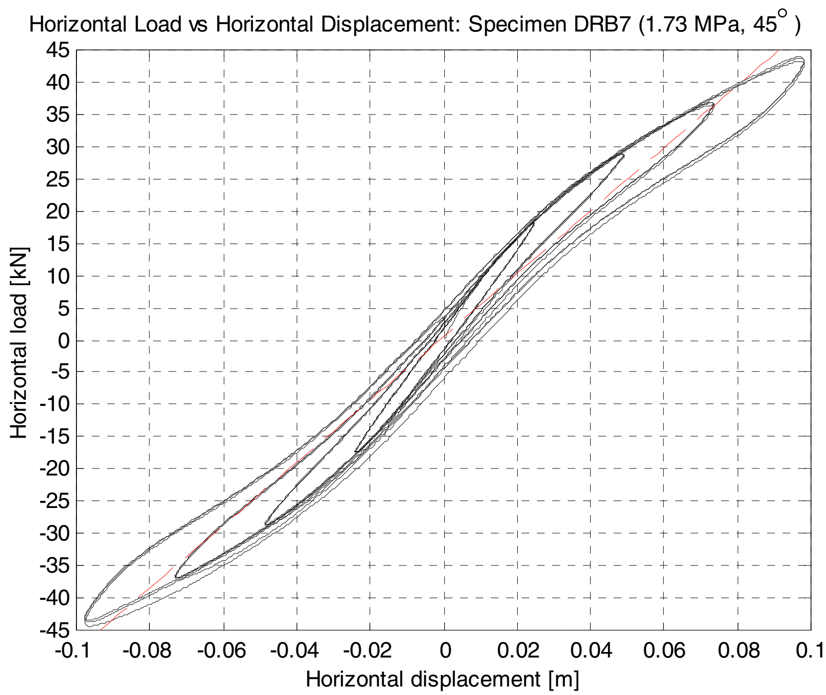

Figure A.87. Horizontal test results for DRB7 with 1.73 MPa vertical pressure (45°)

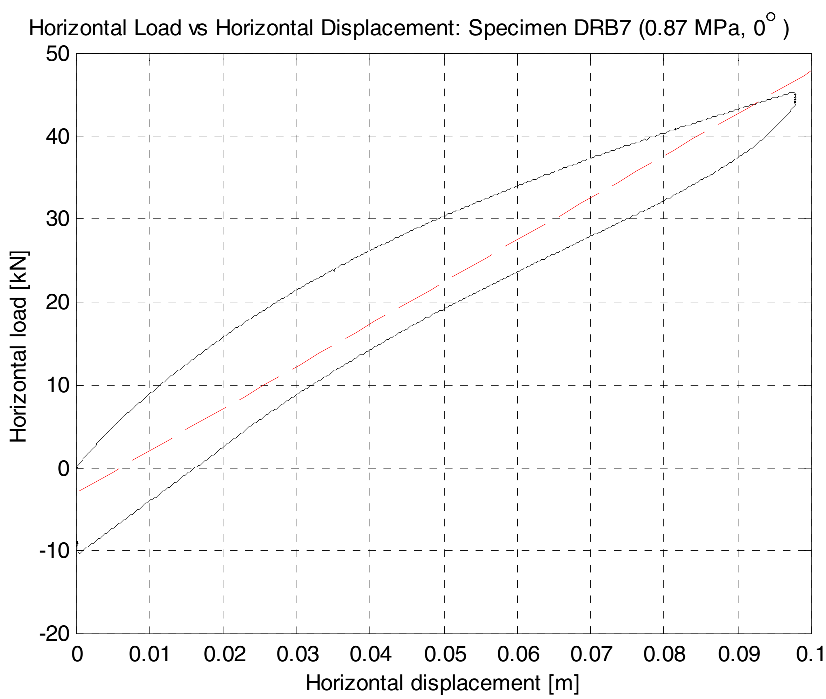

Figure A.88. Horizontal test results for DRB7 with 0.87 MPa vertical pressure (0°)

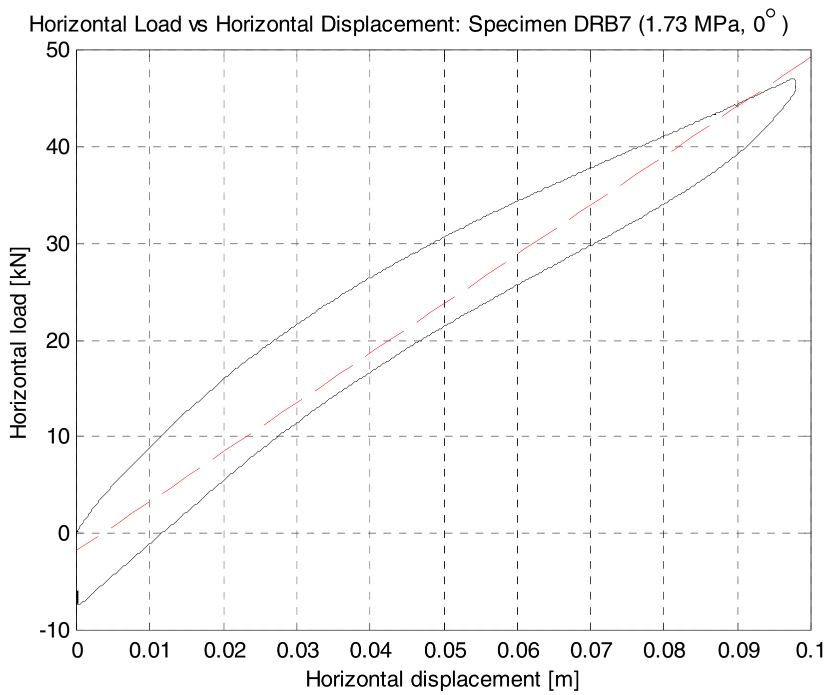

Figure A.89. Horizontal test results for DRB7 with 1.73 MPa vertical pressure (0°)

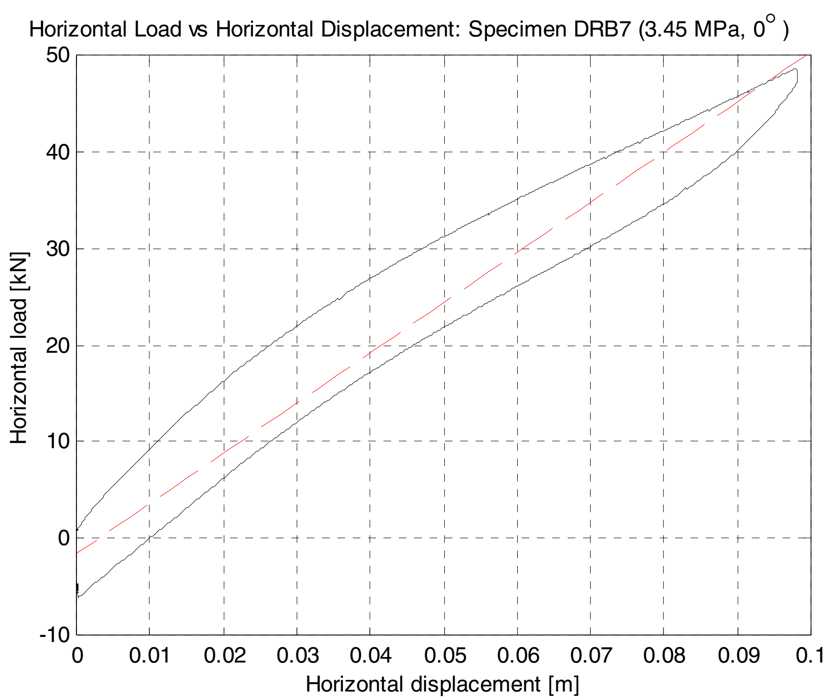

Figure A.90. Horizontal test results for DRB7 with 3.45 MPa vertical pressure (0°)

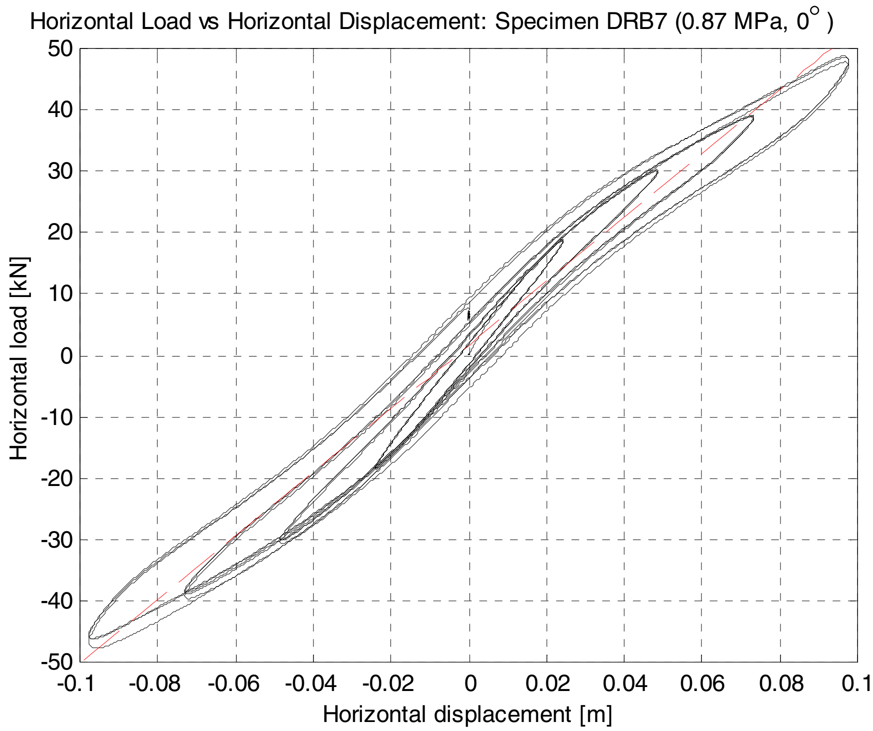

Figure A.91. Horizontal test results for DRB7 at 0.87 MPa vertical pressure (0°)

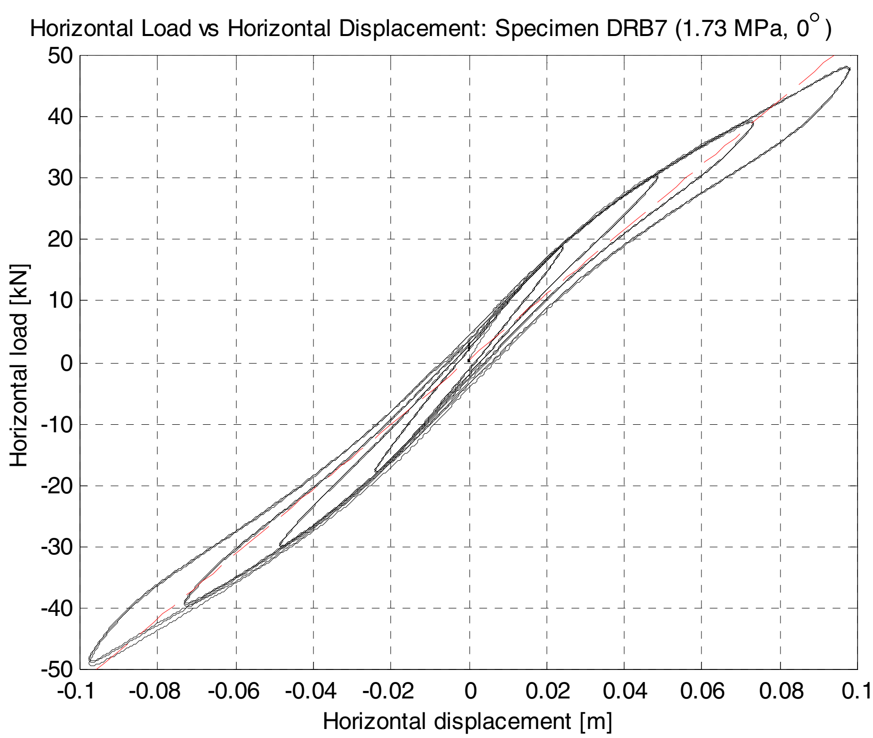

Figure A.92. Horizontal test results for DRB7 at 1.73 MPa vertical pressure (0°)

PEER REPORTS

PEER reports are available from the National Information Service for Earthquake Engineering (NISEE). To order PEER reports, please contact the Pacific Earthquake Engineering Research Center, 1301 South 46th Street, Richmond, California 94804-4698. Tel.: (510) 231-9468; Fax: (510) 231-9461.

PEER 2002/11 *Analytical and Experimental Study of Fiber-Reinforced Strip Isolators.* James M. Kelly and Shakhzod M. Takhirov. September 2002.

PEER 2002/08 *Component Testing, Stability Analysis and Characterization of Buckling-Restrained Unbonded Braces™.* Cameron Black, Nicos Makris, and Ian Aiken. September 2002.

PEER 2002/07 *Seismic Performance of Pile-Wharf Connections.* Charles W. Roeder, Robert Graff, Jennifer Soderstrom, and Jun Han Yoo. December 2001.

PEER 2002/06 *The Use of Benefit-Cost Analysis for Evaluation of Performance-Based Earthquake Engineering Decisions*. Richard O. Zerbe and Anthony Falit-Baiamonte. September 2001.

PEER 2002/05 *Guidelines, Specifications, and Seismic Performance Characterization of Nonstructural Building Components and Equipment*. André Filiatrault, Constantin Christopoulos, and Christopher Stearns. September 2001.

PEER 2002/03 *Investigation of Sensitivity of Building Loss Estimates to Major Uncertain Variables for the Van Nuys Testbed.* Keith A. Porter, James L. Beck, and Rustem V. Shaikhutdinov. August 2002.

PEER 2002/02 *The Third U.S.-Japan Workshop on Performance-Based Earthquake Engineering Methodology for Reinforced Concrete Building Structures*. July 2002.

PEER 2002/01 *Nonstructural Loss Estimation: The UC Berkeley Case Study. Mary C. Comerio and John C. Stallmeyer.* December 2001.

PEER 2001/16 *Statistics of SDF-System Estimate of Roof Displacement for Pushover Analysis of Buildings.* Anil K. Chopra, Rakesh K. Goel, and Chatpan Chintanapakdee. December 2001.

PEER 2001/15 *Damage to Bridges during the 2001 Nisqually Earthquake.* R. Tyler Ranf, Marc O. Eberhard, and Michael P. Berry. November 2001.

PEER 2001/14 *Rocking Response of Equipment Anchored to a Base Foundation.* Nicos Makris and Cameron J. Black. September 2001.

PEER 2001/13 *Modeling Soil Liquefaction Hazards for Performance-Based Earthquake Engineering.* Steven L. Kramer and Ahmed-W. Elgamal. February 2001.

PEER 2001/12 *Development of Geotechnical Capabilities in OpenSees.* Boris Jeremic. September 2001.

PEER 2001/11 *Analytical and Experimental Study of Fiber-Reinforced Elastomeric Isolators*. James M. Kelly and Shakhzod M. Takhirov. September 2001.

PEER 2001/10 *Amplification Factors for Spectral Acceleration in Active Regions.* Jonathan P. Stewart, Andrew H. Liu, Yoojoong Choi, and Mehmet B. Baturay. December 2001.

PEER 2001/09 *Ground Motion Evaluation Procedures for Performance-Based Design.* Jonathan P. Stewart, Shyh-Jeng Chiou, Jonathan D. Bray, Robert W. Graves, Paul G. Somerville, and Norman A. Abrahamson. September 2001.

PEER 2001/08 *Experimental and Computational Evaluation of Reinforced Concrete Bridge Beam-Column Connections for Seismic Performance*. Clay J. Naito, Jack P. Moehle, and Khalid M. Mosalam. Nover

PEER 2001/07 *The Rocking Spectrum and the Shortcomings of Design Guidelines.* Nicos Makris and Dimitrios Konstantinidis. August 2001.

PEER 2001/06 *Development of an Electrical Substation Equipment Performance Database for Evaluation of Equipment Fragilities*. Thalia Agnanos. April 1999.

PEER 2001/05 *Stiffness Analysis of Fiber-Reinforced Elastomeric Isolators.* Hsiang-Chuan Tsai and James M. Kelly. May 2001.

PEER 2001/04 *Organizational and Societal Considerations for Performance-Based Earthquake Engineering.* Peter J. May. April 2001.

PEER 2001/03 *A Modal Pushover Analysis Procedure to Estimate Seismic Demands for Buildings: Theory and Preliminary Evaluation.* Anil K. Chopra and Rakesh K. Goel. January 2001.

PEER 2001/02 *Seismic Response Analysis of Highway Overcrossings Including Soil-Structure Interaction.* Jian Zhang and Nicos Makris. March 2001.

PEER 2001/01 *Experimental Study of Large Seismic Steel Beam-to-Column Connections.* Egor P. Popov and Shakhzod M. Takhirov. November 2000.

PEER 2000/10 *The Second U.S.-Japan Workshop on Performance-Based Earthquake Engineering Methodology for Reinforced Concrete Building Structures.* March 2000.

PEER 2000/09 *Structural Engineering Reconnaissance of the August 17, 1999 Earthquake: Kocaeli (Izmit), Turkey.* Halil Sezen, Kenneth J. Elwood, Andrew S. Whittaker, Khalid Mosalam, John J. Wallace, and John F. Stanton. December 2000.

PEER 2000/08 *Behavior of Reinforced Concrete Bridge Columns Having Varying Aspect Ratios and Varying Lengths of Confinement.* Anthony J. Calderone, Dawn E. Lehman, and Jack P. Moehle. January 2001.

PEER 2000/07 *Cover-Plate and Flange-Plate Reinforced Steel Moment-Resisting Connections.* Taejin Kim, Andrew S. Whittaker, Amir S. Gilani, Vitelmo V. Bertero, and Shakhzod M. Takhirov. September 2000.

PEER 2000/06 *Seismic Evaluation and Analysis of 230-kV Disconnect Switches.* Amir S. J. Gilani, Andrew S. Whittaker, Gregory L. Fenves, Chun-Hao Chen, Henry Ho, and Eric Fujisaki. July 2000.

PEER 2000/05 *Performance-Based Evaluation of Exterior Reinforced Concrete Building Joints for Seismic Excitation.* Chandra Clyde, Chris P. Pantelides, and Lawrence D. Reaveley. July 2000.

PEER 2000/04 *An Evaluation of Seismic Energy Demand: An Attenuation Approach.* Chung-Che Chou and Chia-Ming Uang. July 1999.

PEER 2000/03 *Framing Earthquake Retrofitting Decisions: The Case of Hillside Homes in Los Angeles.* Detlof von Winterfeldt, Nels Roselund, and Alicia Kitsuse. March 2000.

PEER 2000/02 *U.S.-Japan Workshop on the Effects of Near-Field Earthquake Shaking.* Andrew Whittaker, ed. July 2000.

PEER 2000/01 *Further Studies on Seismic Interaction in Interconnected Electrical Substation Equipment.* Armen Der Kiureghian, Kee-Jeung Hong, and Jerome L. Sackman. November 1999.

PEER 1999/14 *Seismic Evaluation and Retrofit of 230-kV Porcelain Transformer Bushings*. Amir S. Gilani, Andrew S. Whittaker, Gregory L. Fenves, and Eric Fujisaki. December 1999.

PEER 1999/13 *Building Vulnerability Studies: Modeling and Evaluation of Tilt-up and Steel Reinforced Concrete Buildings.* John W. Wallace, Jonathan P. Stewart, and Andrew S. Whittaker, editors. December 1999.

PEER 1999/12 *Rehabilitation of Nonductile RC Frame Building Using Encasement Plates and Energy-Dissipating Devices.* Mehrdad Sasani, Vitelmo V. Bertero, James C. Anderson. December 1999.

PEER 1999/11 *Performance Evaluation Database for Concrete Bridge Components and Systems under Simulated Seismic Loads.* Yael D. Hose and Frieder Seible. November 1999.

PEER 1999/10 *U.S.-Japan Workshop on Performance-Based Earthquake Engineering Methodology for Reinforced Concrete Building Structures.* December 1999.

PEER 1999/09 *Performance Improvement of Long Period Building Structures Subjected to Severe Pulse-Type Ground Motions*. James C. Anderson, Vitelmo V. Bertero, and Raul Bertero. October 1999.

PEER 1999/08 *Envelopes for Seismic Response Vectors.* Charles Menun and Armen Der Kiureghian. July 1999.

PEER 1999/07 *Documentation of Strengths and Weaknesses of Current Computer Analysis Methods for Seismic Performance of Reinforced Concrete Members.* William F. Cofer. November 1999.

PEER 1999/06 *Rocking Response and Overturning of Anchored Equipment under Seismic Excitations.* Nicos Makris and Jian Zhang. November 1999.

PEER 1999/05 *Seismic Evaluation of 550 kV Porcelain Transformer Bushings.* Amir S. Gilani, Andrew S. Whittaker, Gregory L. Fenves, and Eric Fujisaki. October 1999.

PEER 1999/04 *Adoption and Enforcement of Earthquake Risk-Reduction Measures.* Peter J. May, Raymond J. Burby, T. Jens Feeley, and Robert Wood.

PEER 1999/03 *Task 3 Characterization of Site Response General Site Categories*. Adrian Rodriguez-Marek, Jonathan D. Bray, and Norman Abrahamson. February 1999.

PEER 1999/02 *Capacity-Demand-Diagram Methods for Estimating Seismic Deformation of Inelastic Structures: SDF Systems*. Anil K. Chopra and Rakesh Goel. April 1999.

PEER 1999/01 *Interaction in Interconnected Electrical Substation Equipment Subjected to Earthquake Ground Motions.* Armen Der Kiureghian, Jerome L. Sackman, and Kee-Jeung Hong. February 1999.

PEER 1998/08 *Behavior and Failure Analysis of a Multiple-Frame Highway Bridge in the 1994 Northridge Earthquake.* Gregory L. Fenves and Michael Ellery. December 1998.

PEER 1998/07 *Empirical Evaluation of Inertial Soil-Structure Interaction Effects.* Jonathan P. Stewart, Raymond B. Seed, and Gregory L. Fenves. November 1998.

PEER 1998/06 *Effect of Damping Mechanisms on the Response of Seismic Isolated Structures.* Nicos Makris and Shih-Po Chang. November 1998.

PEER 1998/05 *Rocking Response and Overturning of Equipment under Horizontal Pulse-Type Motions.* Nicos Makris and Yiannis Roussos. October 1998.

PEER 1998/04 *Pacific Earthquake Engineering Research Invitational Workshop Proceedings, May 14–15, 1998: Defining the Links between Planning, Policy Analysis, Economics and Earthquake Engineering.* Mary Comerio and Peter Gordon. September 1998.

PEER 1998/03 *Repair/Upgrade Procedures for Welded Beam to Column Connections.* James C. Anderson and Xiaojing Duan. May 1998.

PEER 1998/02 *Seismic Evaluation of 196 kV Porcelain Transformer Bushings.* Amir S. Gilani, Juan W. Chavez, Gregory L. Fenves, and Andrew S. Whittaker. May 1998.

PEER 1998/01 *Seismic Performance of Well-Confined Concrete Bridge Columns.* Dawn E. Lehman and Jack P. Moehle. December 2000.